Caste differentiation in *Cardiocondyla obscurior*

DISSERTATION ZUR ERLANGUNG DES

DOKTORGRADES DER NATURWISSENSCHAFTEN (DR. RER. NAT.)

DER FAKULTÄT FÜR BIOLOGIE UND VORKLINISCHE MEDIZIN

DER UNIVERSITÄT REGENSBURG

vorgelegt von

Tobias Wallner

(geb. Weichselgartner)

aus Aachen

im Jahr 2021

Das Promotionsgesuch wurde eingereicht am: 07.07.2021

Die Arbeit wurde angeleitet von:
PD Dr. Jan Oettler

Unterschrift:

_____

Tobias Wallner

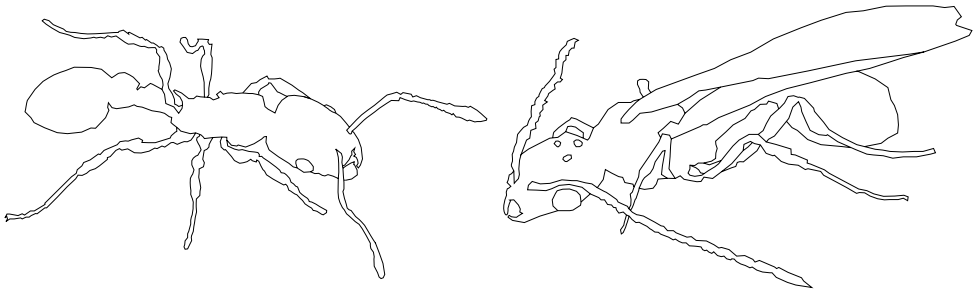

“Ants have the most complicated social organization on earth next to humans.”
E. O. Wilson

TABLE OF CONTENTS

1 ABSTRACT

In ants reproductive division of labor is a key feature of eusociality and is facilitated by the development of morphological distinct castes. In the myrmicine ant *Cardiocondyla obscurior* queens monopolize reproduction while workers are sterile and have no reproductive power. This extreme form of worker sterility is only found in 11 out of 283 genera. The species is proposed as a model for phenotypic plasticity and late larval stages have been studied with regard to imaginal wing disc development and gene expression. In this thesis, the development of queen and worker embryos and larvae is described in more detail.

A visual marker to separate queen from worker castes during development is described, presumably urate depositions (Chapter 4). We found the same visual marker in four additional *Cardiocondyla* species, but not in 50 other ant species spanning the ant phylogeny.

The visual distinction between the castes allowed to reconstruct ovarian development in queens, showing differences to other insects. One of these differences is the active elongation process of the ovarioles from the initial gonadal cell cluster (Chapter 4). Further, the embryogenesis of *C. obscurior* is characterized in five embryonic stages, showing similarities to the long-germ-type development in holometabolous insects (Chapter 5).

Lastly, a model is presented how caste in *C. obscurior* is determined (Chapter 6). This occurs during the third embryonic stage and involves the interaction of the homeotic gene *Abd-B* and the sex differentiation gene *doublesex* (*dsx*). The interplay of the sex-specific isoforms of *dsx* with *Abd-B* ensure that the somatic gonadal precursor cells (SGPs), necessary for gonad formation, localize at the correct posterior segment. The mis-localization of SGPs results in the development of sterile workers.

Taken together, this thesis lays the basis for understanding caste determination and differentiation in the ant *Cardiocondyla obscurior*.

2 ZUSAMMENFASSUNG

In Ameisen ist die reproduktive Arbeitsteilung ein Schlüsselmoment der Eusozialität und wird durch die Entwicklung von morphologisch unterschiedlichen Kasten ermöglicht. In der Knotenameise *Cardiocondyla obscurior* monopolisieren Königinnen die Reproduktion, während Arbeiterinnen steril sind und keinen reproduktiven Einfluss haben. Diese extreme Art der Arbeiterinnensterilität findet sich lediglich in 11 von 283 Gattungen. Diese Spezies wird als Modell für phänotypische Plastizität vorgeschlagen und ihre späten Larvalstadien wurden in Bezug auf die Entwicklung der Flügelimaginalscheiben und Genexpression hin untersucht. In dieser Arbeit wird detailliert über die Entwicklung von Königinnen und Arbeiterinnen Embryonen und Larven berichtet.

Hier beschreiben wir ein sichtbares Merkmal, welches erlaubt Königinnen- von Arbeiterinnenkaste während ihrer Entwicklung zu unterscheiden (Kapitel 4). Dabei handelt es sich vermutlich um Uratablagerungen. Dasselbe Merkmal fanden wir in vier weiteren *Cardiocondyla* Spezies. Allerdings fehlte dieses in 50 weiteren Spezies in der Ameisenphylogenie.

Die sichtbare Unterscheidung der Kasten ermöglichte die Rekonstruktion der Entwicklung der Ovarien von Königinnen, welche Unterschiede zu anderen Insekten aufwies. Einer dieser Unterschiede ist der aktive Verlängerungsprozess der Ovariolen aus dem gonadalen Zellhaufen (Kapitel 4). Ferner ist die Embryogenese von *C. obscurior* in fünf Embryonalstadien eingeteilt, welche Ähnlichkeiten zur Langkeim Entwicklung in holometabolen Insekten aufzeigen (Kapitel 5).

Als letztes wird ein Model vorgestellt, welches die Kaste in *C. obscurior* determiniert (Kapitel 6). Dies geschieht während des dritten Embryonalstadiums und beinhaltet die Interaktion des homeotischen Genes *Abdominal-B* (*Abd-B*) und das Sexdifferenzierungsgen *doublesex* (*dsx*). Das Zwischenspiel der sex-spezifischen Isoformen von *dsx* und *Abd-B* erlaubt es den somatischen Gonadenvorläuferzellen (SGPs), welche wichtig sind für die Entwicklung der Gonaden, sich am richtigen posterior gelegenen Segment anzusiedeln. Eine Fehlansiedlung der SGPs resultiert in die Entwicklung von sterilen Arbeiterinnen.

Zusammenfassend legt diese Arbeit die Basis für das Verständnis von Kastendeterminierung und -differenzierung in der Ameise *Cardiocondyla obscurior*.

3 INTRODUCTION

3.1 LIVE-HISTORY AND REPRODUCTIVE CONSTRAINTS IN ANTS

Ants (Formicidae, Hymenoptera) are probably the most triumphant creatures in the animal kingdom. They have successfully dispersed all around the globe (e.g., deserts, forests, mountains), inhabiting almost all ecological niches and most of the climate zones. Ants make 15-20 % of the terrestrial animal biomass, in tropical regions even up to 25 % (Schultz, 2000). Therefore, it could be said that ants are the silent dominant of our planet.

The evolution of sociality in Hymenopterans facilitated their success as a predominant species, with eusociality being one of the most successful forms. Eusociality in social Hymenoptera is classically outlined by three definitions: a) cooperative brood care; b) reproductive division of labor; c) overlap of adult generations. This textbook definition of eusociality was initially defined for ground nesting halictid bees (*Halictidea*), which are considered primitively eusocial (Batra, 1966). Contrary to this "lower" or "primitive" form of eusociality in these halictid bees, "higher" eusocial Hymenoptera are additionally characterized by morphological distinct phenotypes. Depending on task and function this phenotypic plasticity can reach a high degree of specialization, for example soldiers and minor workers in *Pheidole* (Rajakumar et al., 2018) or in leaf cutter ants of the genus *Atta*, with its high variability in worker size (Wilson, 1980). This type of functional adaptation is also referred to as caste polyethism.

This "true social" or "eusocial" behavior is only applicable through altruism. Altruism requires reproductive division of labor, in particular worker sterility. In order to explain how worker sterility evolved and has been evolutionary stable since then, Hamilton depicted his theory of inclusive fitness. In it, helpers (sterile workers) gain indirect fitness by supporting the reproductive success of the individual that benefits (queen) (Hamilton, 1964a, 1964b). Complete worker sterility can therefore be seen as the highest grade of altruism. Even though worker sterility has evolved 50 million years ago, not only once but several times independently from each other, it can be found only in 13 genera of social Hymenoptera, including subfamilies of ponerine and myrmicine ants (Ronai et al., 2016).

In ants real worker sterility is found only in few species, so for example in *Pheidole* (Lillico-Ouachour & Abouheif, 2017), *Solenopsis invicta* (Goudie & Oldroyd, 2018) and *Monomorium pharaonis* (Pontieri et al., 2020). The same is true for *Cardiocondyla obscurior* (Heinze et al., 2006). The question that arises is how worker lost their reproductive power and which underlying mechanisms are responsible.

Worker sterility is linked to division of labor (DOL). Corona et al. (2013) describe two levels of DOL: a) reproductive division of labor (RDL), in which one or several queens monopolize reproduction, while sterile workers perform all tasks related to the maintenance of the colony; b) DOL among workers, in which they perform different tasks in an age-dependent order. This means that the majority of young

workers stay in the nest tending to the brood, while old workers primarily leave the nest to forage. In order to understand reproductive division of labor better, West-Eberhard described a theoretical framework called ovarian ground plan hypothesis (OGPH) (West-Eberhard, 1987). In it, physiological pathways regulate reproductive and behavioral cycles of solitary ancestors in the order of hymenopterans. These pathways have been co-opted and selected against to evolve into queen and worker castes of existing eusocial insects. The reproductive ground plan hypothesis (RGPH) extends the OGPH to explain the evolution of worker division of labor and was initially described in honey bees. The co-option of reproductive pathways to regulate behavior is a major director in the evolution of sociality in insects. Honey bees and ants are both hymenopterans and have evolved sociality independently but have retained similar conserved mechanisms to regulate division of labor. One of them being the yolk protein vitellogenin (Vg). Vg genes seem to be involved in caste specification, so for example in *Pogonomyrmex barbatus* (Corona et al., 2013).

As mentioned before, altruistic behavior requires reproductive division of labor. It is a key feature of eusociality in ants, especially when it comes to the worker caste. Workers show major differences in their reproductive organs compared to queens. The ovaries are either limited in their function due to the reduction of ovarioles, loss of their spermatheca or the complete absence of the reproductive organs altogether (Gotoh et al., 2016). If workers retain a functional spermatheca they can mate and produce offspring in the absence of a queen. In this case they are referred to as “gamergates” and are found in the subfamilies of Ambyloponinae, Ectatomminae and Ponerinae. The absence of ovaries requires separate developmental trajectories for the queen and worker caste in their early development. Khila and Abouheif (2010) refer to these modifications in ovarian and germ cell development during oogenesis and embryogenesis as “reproductive constraints” (RC) and classified five stages (Figure 3.1). These reproductive constraints can be considered as proximate mechanisms, for instance developmental processes or traits, to maintain social harmony in ants. Besides the developmental RC, there are behavioral reproductive constraints, namely policing or self-restraint. While workers refrain from reproducing (i.e., self-restraint), policing is a mechanism to prevent other workers to reproduce by either displaying aggressive behavior against them or eating their eggs (Dijkstra et al., 2005).

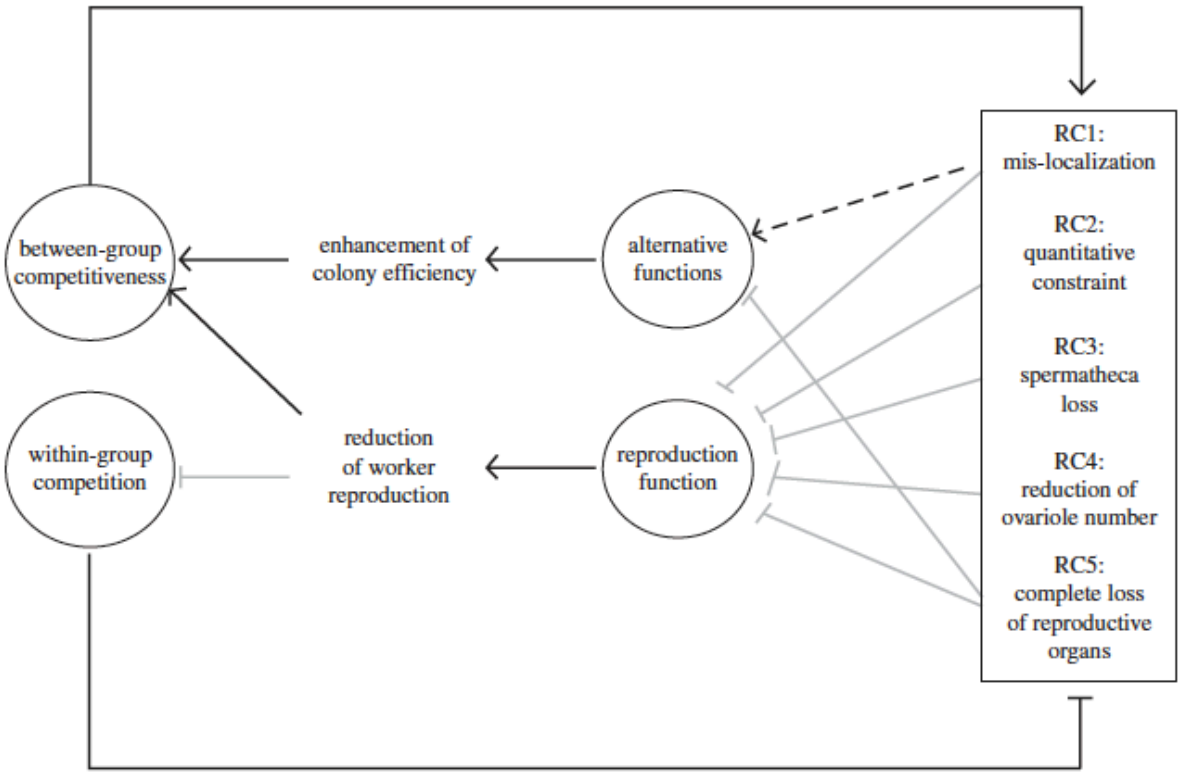

FIGURE 3.1: **Overview of reproductive constraint crosstalk.**
The dashed line led to alternative functions in RC1 (from Khila & Abouheif, 2010).

The mis-localization of maternal determinants as described in RC1 directs ovary function in workers to an alternative function. By doing so workers keep some of their reproductive power. Ant species showing RC1 produce either non-viable trophic eggs meant for consumption (Schultner et al., 2017; Schultner & Pulliainen, 2020) or viable unfertilized eggs. The latter results in males and helps worker to increase their direct fitness (Giehr, Senninger, et al., 2020; Giehr, Wallner, et al., 2020).

The queen and worker caste originate both from the same genetic background. Queen development follows a different trajectory than workers in species with worker sterility. While queens develop gonads the development of these are interrupted in workers, due to the reduction or complete loss of germ cells (Figure 3.1, RC5). This ultimately leads to the loss of reproductive power in workers altogether. It is one of the most crucial aspects when speaking of reproductive division of labor. Only few ant genera show this dramatic and irreversible turning point in worker development (Table 3.1).

The underlying molecular mechanisms involved in this developmental bifurcation and the exact time point remain elusive. It does suggest that caste determination occurs during embryogenesis and recent studies underline this assumption (Pontieri et al., 2020; Rafiqi et al., 2020).

TABLE 3.1 Ant species and their respective subfamilies experiencing worker sterility.

Subfamily	Species
Dorylinae	*Eciton*
Ponerinae	*Anochetus* *Leptogenys*
Myrmicinae	*Solenopsis* *Monomorium* *Tetramorium* *Pheidole* *Pheidologeton* *Cardiocondyla*

3.2 THE MODEL ORGANISM *CARDIOCONDYLA OBSCURIOR*

The myrmicine ant *Cardiocondyla obscurior* has its roots in the Southeast of Asia with its subtropical climate (Heinze, 2017). From there it has spread throughout commercially used trading routes, making it a tramp species. Populations can now also be found in countries of the "New World" like in Brazil or in the United States. *Cardiocondyla* also dispersed in the "Old World" in habitats of the Mediterranean Sea and was also found in a botanical garden in Freising, Germany. Even though the population found in Freising is rather a rare case it illustrates the adaptability and invasiveness of this species to other climate zones.

Cardiocondyla obscurior is a rather small ant with its size roughly around two millimeters. Its nests are usually found in tree branches, rolled up leaves or in rock crevices. The small nests consists of several dozens to hundreds workers and one to multiple queens, making it a polygynous ant species (Heinze, 2017). The small size of the colonies as of the ant itself makes it ideal to rear under laboratory conditions. They are easy to keep in plaster-bottom nests with inlets simulating natural living conditions (Figure 3.2). In climate chambers with a humid climate at 23 °C to 26 °C they experience optimal living conditions.

FIGURE 3.2: Nests of *Cardiocondyla obscurior*.
(A) Square bottom nest with inlets. Inlets are covered by plastic foil to prevent direct light exposure of the colony. (B) The inlets simulate natural living conditions by imitating tree branches. (C) Colony in a round bottom nest. (D) In rare cases winged disperser males can be observed (yellow arrow).

Cardiocondyla obscurior is a polyphenic ant with a female caste consisting of morphological distinct queens and workers. Queens are slightly bigger in size, have ocelli, wings, and ovaries. The workers of *C. obscurior* possess no ovaries and are therefore completely sterile (Heinze et al., 2006). Besides the female caste *C. obscurior* has two male phenotypes: the winged disperser males and wingless males, also referred to as ergatoid (worker-like) males (Figure 3.3). The ergatoid males display a much more aggressive behavior as their winged rival (Cremer et al., 2012).

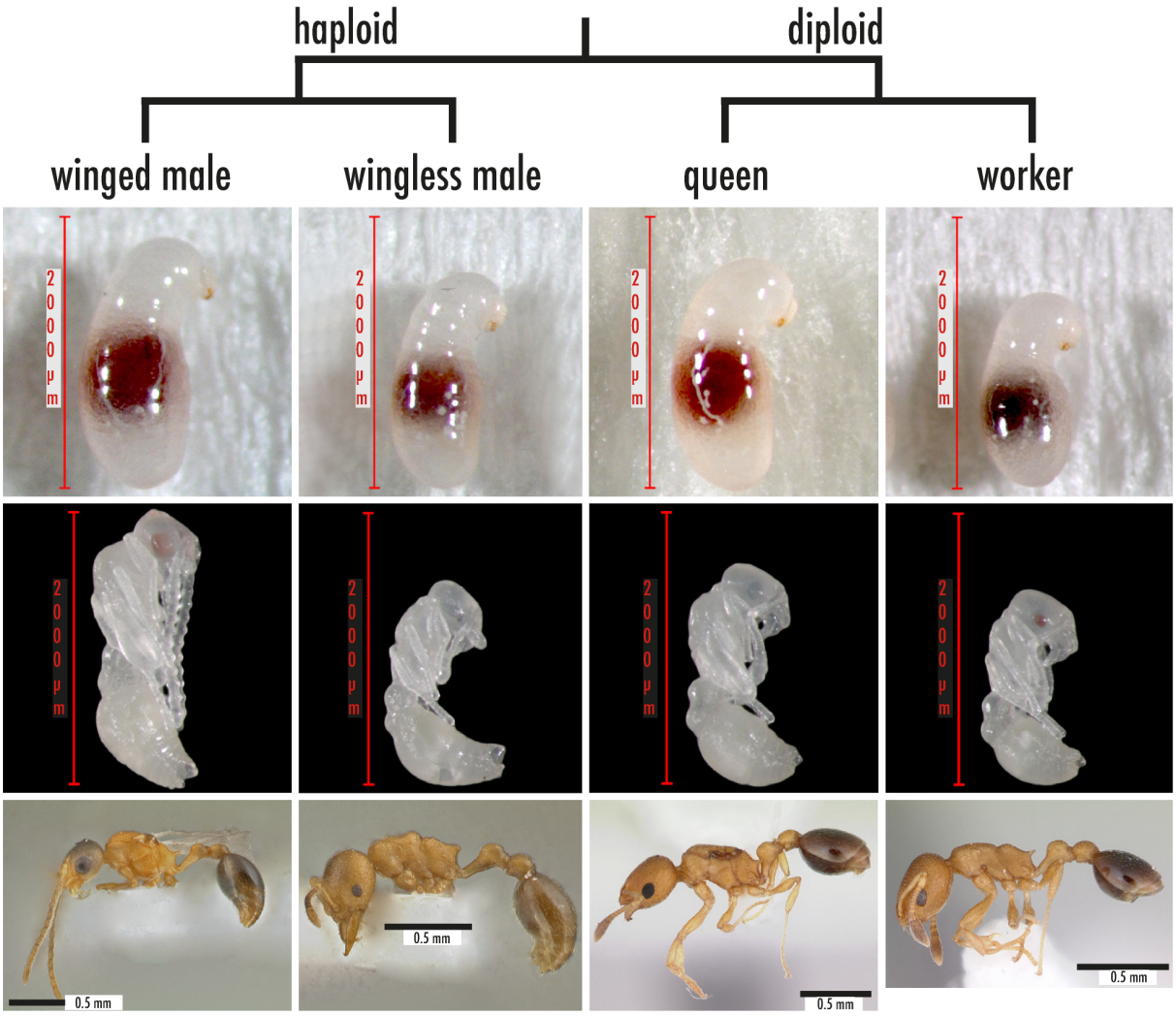

FIGURE 3.3: *Cardiocondyla obscurior* with its four morphs.
Larvae are shown on the top, pupae in the middle and the adult stages on the bottom. In *C. obscurior* there are two distinct male phenotypes present: winged and wingless (ergatoid) males (Oettler et al., 2018).

We find three larval stages in *Cardiocondyla obscurior*, which can be distinguished by their head capsule width and size and coloration of the mandibles (Schrempf & Heinze, 2006). The three distinct larval stages allow to follow developmental trajectories and study the regulation of developmental plasticity (Schrader et al., 2015). The two female castes also allow to study senescence and caste allocation in *C. obscurior* (Jaimes Nino et al., 2021).

In the last several years the ant *Cardiocondyla obscurior* has emerged as a promising model organism to study many different aspects of evolutionary biology, neuroanatomy (Bressan et al., 2015), host-endosymbiont interaction (Klein et al., 2015), the sex differentiation cascade (Klein et al., 2016), cytoplasmic incompatibility (Ün et al., 2021) and developmental plasticity (Oettler et al., 2018; Schrader et al., 2015).

3.3 AIMS OF THIS THESIS

In the last few years research has shifted its focus on gene expression (RNA-seq) obtaining large amounts of data in the process. One main factor driving this development is certainly the increasing efficiency and cost-reduction of RNA-seq over the last years, which allows even small work groups with less financial resources to generate data. These studies for example address fundamental questions like division of labor (Walsh et al., 2018), caste differentiation (De Souza et al., 2018) or species-specific differences (Gstöttl et al., 2020) in ants. These studies have undoubtedly their entitlement, but a major criticism is the vast amount of generated bioinformatic data that needs to be sorted, analyzed, and interpreted. Without specific questions and careful illustration, these data might add to confusion rather than clarification. The run for transcriptomic studies has left basic fundamental research to fall behind. In particular developmental studies have been left out for the past decades. Yet, a basic understanding of developmental processes and a precise description thereof is essential to interpret for example the generated transcriptomic data.

The field of eco-evo-devo (ecological evolutionary developmental biology) tries to understand how evolution works by disentangling the interactions of environment, genes, and development in an organism, leading for example to phenotypic variation (Abouheif et al., 2014). And even though that is said, the devo part misses an integral part to understand these interactions. This integral part is the prime event the development of any species is based on: its embryogenesis. To our surprise we found very little studies portraying it. One must almost admit that it has been neglected since Ganin presented the first recorded study on the embryogenesis of *Formica fusca* in 1869 (Ganin, 1869). Almost 140 years later embryogenesis was moved into focus again. The first study to present a complete ontological series of its embryogenesis was done in the ant *Monomorium pharaonis* (Pontieri et al., 2020). Related studies gave only a glimpse of the complete embryogenesis, presenting only snapshots with moments-of-interest (Khila & Abouheif, 2010; Rafiqi et al., 2020). While other species serving as model organisms have a detailed embryogenesis (Campos-Ortega & Hartenstein, 2013; Strobl et al., 2015), this is missing in ants with its high variety in species.

Cardiocondyla obscurior is a prime model to address these open questions. For one, queen and worker caste can be visibly distinguished in their embryonic and larval stages (Chapter 4), which makes *C. obscurior* an excellent, and to our knowledge, only model to study caste determination. Further, the description of its embryogenesis (Chapter 5) provides further insight into its caste determination (Chapter 6) and sets a groundwork for broader, more precise studies on the relationship of environment, genes, and development in an evolutionary perspective.

4 THE DEVELOPMENT OF *CARDIOCONDYLA OBSCURIOR*: URATE DEPOSITIONS AND OVARY DEVELOPMENT

4.1 INTRODUCTION

Alternative developmental trajectories leading to the division of labor between reproductive queens and non-reproductive workers form the basis of superorganismality, thereby permitting one of the major transitions in evolution (Boomsma & Gawne, 2018). Caste development has mainly been studied in the honeybee, where caste fate is under strict nutritional control, and the ease with which queen and worker brood cells can be identified facilitates developmental studies. Research on caste development in ants also has a long tradition (e.g. (Brian, 1973; Gösswald & Bier, 1953)), and conceptual discussions are ongoing (e.g. (Oxley & Chandra, 2018; Trible & Kronauer, 2017)). However, how the processes of caste determination and differentiation are regulated at a proximate level is not well understood.

Compared to honeybees, the factors underlying caste fate in ants are more diverse, ranging from genetic to socio-environmental (Corona et al., 2016). With this comes variation in the timing of developmental divergence (e.g. (Brian, 1973; Khila & Abouheif, 2010)), so that ants exhibit different degrees of "reproductive constraints" (Khila & Abouheif, 2010). In some species of Ponerine ants, workers retain full reproductive potential, including the ability to mate and store sperm. In a majority of ant species workers have lost the spermatheca but retain more or less functional ovaries capable of producing haploid, male-destined eggs. Finally, workers from 11 genera completely lack ovaries. These obligately sterile workers are an example of an extended phenotype without any direct fitness, representing a highly derived form of superorganismality. The biology of some myrmicine species with fully sterile workers has been studied extensively (*Cardiocondyla obscurior, Monomorium pharaonis*, *Pheidole* spec., *Solenopsis invict*a), but comparably little is known about their development. Even less is known about development in the remaining six genera with workers lacking reproductive organs (to the best of our knowledge; Myrmicinae: *Wasmannia*, *Tetramorium*, *Pheidologetum*; Dorylinae: *Eciton*; Ponerinae: *Leptogenys*, *Hypoponera*, *Anochetus*).

Across the range of reproductive constraints, a diverse set of signals spanning nature and nurture is likely to be involved in caste-specific development. Together with the facts that ant larval mobility is variable, ant brood is reared in piles, brood is often relocated and can serve functional roles in the colony (Schultner et al., 2017), this has impeded research on ant development compared to "true" laboratory model species such as *Drosophila*. In particular, it has been difficult to study caste-specific developmental trajectories because it is not possible to distinguish worker-destined larvae from queen-destined and male-destined larvae (e.g. (Pontieri et al., 2020)). Here, we close this gap for the

ant *Cardiocondyla obscurior* by showing that queen- and worker-destined embryos and larvae can be visually distinguished by white spots surrounding the developing ovaries of queen-destined larvae. This discovery will greatly facilitate the study of caste determination and differentiation at the extreme end of the superorganismality spectrum, thus bringing us closer to a general understanding of the mechanisms underlying caste polyphenism in social insects.

4.2 METHODS

4.2.1 ANTS

C. obscurior is a cosmotropical tramp ant (Heinze et al., 2006). Adult queens and workers differ in size and morphology and workers lack ovaries (Heinze et al., 2006). Females develop via three larval instars which can be distinguished by the shape of the body and the degree of sclerotization of the mandibles (Schrader et al., 2015; Schrempf & Heinze, 2006). The colonies used in this study were collected in Okinawa, Japan (Schrader et al., 2014), Tenerife, Spain, Bahia, Brazil. Stock colonies were kept in a climate chamber under a 12h/12h and 22°C/26°C night/day cycle at 70% humidity. Experimental colonies were kept in round plaster-bottom nests with nest indentations covered by dark foil under the same conditions. Stock colonies and experimental colonies were provided with water *ad libitum* and fed three times a week with honey and pieces of insects (cockroaches and fruit flies).

4.2.2 WHITE ABDOMINAL SPOTS

All larvae of *C. obscurior* exhibit white spots. After producing semi-thin sections (see below), we used a polarization filter that revealed a crystalline reflection. These crystalline structures are common in insect larvae and have been described as urate crystals (see discussion). Hence, because it is a parsimonious explanation we use “urate depositions” in the following when we refer to the white spots, even though we are aware that this may not be correct and requires future verification.

4.2.3 URATE LOCALIZATION

We characterized urate depositions in eggs and first instar (L1), second instar (L2) and third instar (L3) larvae as unpaired (= worker-destined, Figure 4.1 A) or paired (= queen-destined, Figure 4.1 B) by visually inspecting brood from stock colonies under a stereomicroscope. For better detection of the patterns, eggs and L1 larvae were submerged in a dissection dish containing PBT (0.3 %), after which they were mounted on a microscope slide and sealed with nail polish. From each development stage, we selected and photographed one representative individual with a paired pattern and one individual with an unpaired pattern using a stereomicroscope connected to a camera (Keyence VHX 500FD, Neu-Isenburg, Germany).

We additionally characterized urate patterns of 3rd instar larvae of eight *Cardiocondyla* species available in the lab. We further examined brood of six species from four subfamilies: Myrmicinae, Dolichoderinae, Ponerinae and Formicinae. Lastly, we accessed Alex Wild’s photo library for a broader

overview of species (https://www.alexanderwild.com/Ants/Natural-History/Metamorphosis-Ant-Brood/).

4.2.4 CASTE FATE AND SURVIVAL ACCORDING TO URATE LOCALIZATION

We tracked development of all stages to confirm that urate localization patterns are associated with caste. Brood was randomly sampled from several stock colonies and separated by development stage and urate pattern as described above.

After being sorted by urate pattern, eggs and L1 larvae were transferred to filter paper to remove excessive buffer. Eggs were then transferred in groups of 15 to experimental colonies containing 10 workers (eggs: paired=192, unpaired=165). L1 larvae were transferred to experimental colonies containing 10 workers; two colonies were setup with 17 queen-destined larvae each, and two colonies with 19 and 4 for worker-destined larvae, respectively (L1: paired=34, unpaired=23). L2 and L3 larvae were transferred in groups of ten to experimental colonies containing 10-12 workers (L2: paired=50, unpaired=40, L3: paired=50, unpaired=40). Experimental colonies were monitored three times per week and, when necessary, workers added from the corresponding stock colonies to standardize worker number. All pupae were counted and classified according to female caste until no more brood remained. From these data, we calculated average survival until pupation and caste ratios. Survival of castes and accuracy of caste prediction were tested with Fisher exact tests in R version 4.0.3 (R Core Team, 2020).

We tracked development of L3 larvae from six additional *Cardiocondyla* species to validate that urate patterns accurately predict caste (Table S 3).

4.2.5 LARVAL HISTOLOGY

L3 larvae were collected from stock colonies and sorted according to their urate patterns. Sorted larvae were transferred into fixation solution consisting of 25% glutaraldehyde (GAH) in cacodylate buffer [(50 mM cacodylic acid, pH 7.3) containing 150 mM Sucrose] (GAH : cacodylate buffer = 1 : 12,5) and kept overnight at 11 °C. Samples were then rinsed in cacodylate buffer on ice, and fixated in 4% osmium tetroxide in cacodylate buffer. After fixation, larvae were washed in cacodylate buffer, dehydrated in a graded ethanol series and embedded in Epon. Transversal semithin sections of 1 µm were cut and stained with methylene blue and Azur II (Richardson's stain). Semi-thin sections were scanned with a Zeiss Primo Star microscope and imaged with a Moticam 580 digital microscope camera.

4.2.6 OVARIAN DEVELOPMENT

Queen L2 and L3 larvae were dissected in PBT 0.3% (PBS 1x + Triton 0.3%) by cutting below the meconium with a micro scissor. The posterior part of the larvae was then cleared of excessive fat tissue. The larval ovaries were placed in an ice-cooled well filled with PBT. We chose two different stages of queen pupae depending on their development. The first stage (=early-stage) was unsclerotized white queen pupae with unpigmented ommatidia and ocelli (Figure 4.5 A) The second stage (=mid-stage) was queen pupae with pigmented ommatidia and ocelli (Figure 4.5 B). Ovaries from queen pupae and adults were obtained by carefully pulling on the last tergite of the abdomen with a forcep, which removes the entire reproductive apparatus.

Larval, pupal, and adult ovaries were fixated in 4% paraformaldehyde diluted in PBS for 20 min at room temperature. The fixated ovaries were then washed three times with PBT for 15 min on a tumbler. After washing, the ovaries were processed for staining.

Vasa protein was stained with a rat anti-vasa antibody and actin filaments were visualized using a rabbit anti-actin antibody. Both antibodies were generated from *Drosophila* (Khila & Abouheif, 2010). Cell nuclei were stained using DAPI. The primary antibodies were diluted 1:200 in PBT 0.3% with 5% normal goat serum overnight at room temperature on a tumbler. To remove the primary antibody, the larval, pupal and adult ovaries were washed three times with PBT for 15 min. The secondary antibodies goat anti-rat and goat anti-rabbit were used to visualize the rat anti-vasa and rabbit anti-actin antibodies, both diluted 1:200 in PBT. After 2 h of incubation at room temperature, the ovaries were again washed three times with PBT for 15 min each. Finally, the larval, pupal and adult ovaries were washed with PBT containing DAPI (1:10000). Ovaries were then mounted in VECTASHIELD® on a microscope slide and sealed with nail polish (Chapter 10.1.1).

Images for the antibody staining were obtained using a Leica SP8 confocal microscope under 40x and 63x objective lenses. Images were then processed using the open source platform FIJI (Schindelin et al., 2012).

Complete confocal series of ovarioles of early- and mid-staged queen pupae were imported and processed using the FIJI plugin TrakEM2 (Cardona et al., 2012) for 3D rendering and analysis (Figure 4.5 C).

4.2.7 *NANOS* EXPRESSION

Nanos expression was measured in queens and workers from all larval stages. Whole L1 and L2 larvae were collected and transferred to individual Eppendorf tubes (L1: n=5 queen larvae, n=7 worker larvae; L2: n=5 queen larvae, n=5 worker larvae). L3 larvae were sliced beneath the meconium at the posterior end (containing the developing ovaries in queen larvae) and transferred to individual tubes (L3: n=5 queen larvae, n=4 worker larvae). All samples were immediately frozen in liquid nitrogen and stored at -75°C prior to RNA extraction. Total RNA was extracted using the ReliaPrep™ RNA Cell Miniprep Kit (Promega) and RNA concentrations measured using the Qubit™ RNA HS Assay Kit (Invitrogen). RNA concentrations were standardized to 2.5 ng and RNA reverse-transcribed to cDNA using the iScript™ gDNA Clear cDNA Synthesis Kit (Bio-Rad Laboratories). Expression of the gene *nanos* was quantified with qPCR with the primer pair nos_for/nos_rev and normalized with two housekeeping genes (Y45F10D_JO1_for/Y45F10D_JO1_rev and Actin_JO1_for/Actin_JO1_rev; Table 4.1 for primer sequences). All qPCR reactions were performed in triplicates and specificity of reactions confirmed by manual melt curve inspection. Relative target gene expression was calculated as $2^{-\Delta Cq}$ following Livak & Schmittgen (2001), using the geometric mean of the two housekeeping genes for normalization.

TABLE 4.1: Primer sequences used for real-time quantitative PCR (qPCR).
Primers are based on the *C. obscurior* genome version 1.4 (Schrader et al., 2014). HK = housekeeper.

Primer ID	Sequence (5‘ – 3‘)	Gene ID	Usage	Primer efficiencies
Y45F10D_JO1_for	CATCGGCGCGACGTCCAAGA	Cobs_04843 (iron-sulfur cluster assembly enzyme ISCU, mitochondrial)	qPCR (HK)	(Klein et al., 2016)
Y45F10D_JO1_rev	GCCCCCACCAGACCTGTTCC			
Actin_JO1_for	TGCCAACACCGTTCTGTCTG	Cobs_04257 (actin)	qPCR (HK)	100%
Actin_JO1_rev	GACGCGAGAATAGATCCGCC			
Nos_for	ACGAGGCCAATGCCGAACGTTGAG	Cobs_12201 (nanos)	qPCR	95.85%
Nos_rev	GCAGAACACGCATTCCGTGGG			

4.3 RESULTS

4.3.1 URATE LOCALIZATION IS ASSOCIATED WITH CASTE

We found distinct localization in queen and worker-destined eggs and larvae (Figure 4.1, Figure 4.2, Figure S 1) of what we think are urate crystals. In late embryos and first instar larvae, patterns associated with queen caste are already visible (Figure 4.1, Figure 4.2). Queen patterns appear either as a pearl of strings (Figure S 2, A, B) or are snail shell-like (Figure S 2, C, D). Patterns become more recognizable over the course of development (Figure 4.1, L2, L3), however we found that handling L1 larvae results in extreme mortality. L2 and L3 individuals can be attributed to the two castes with high precision (Table 4.2).

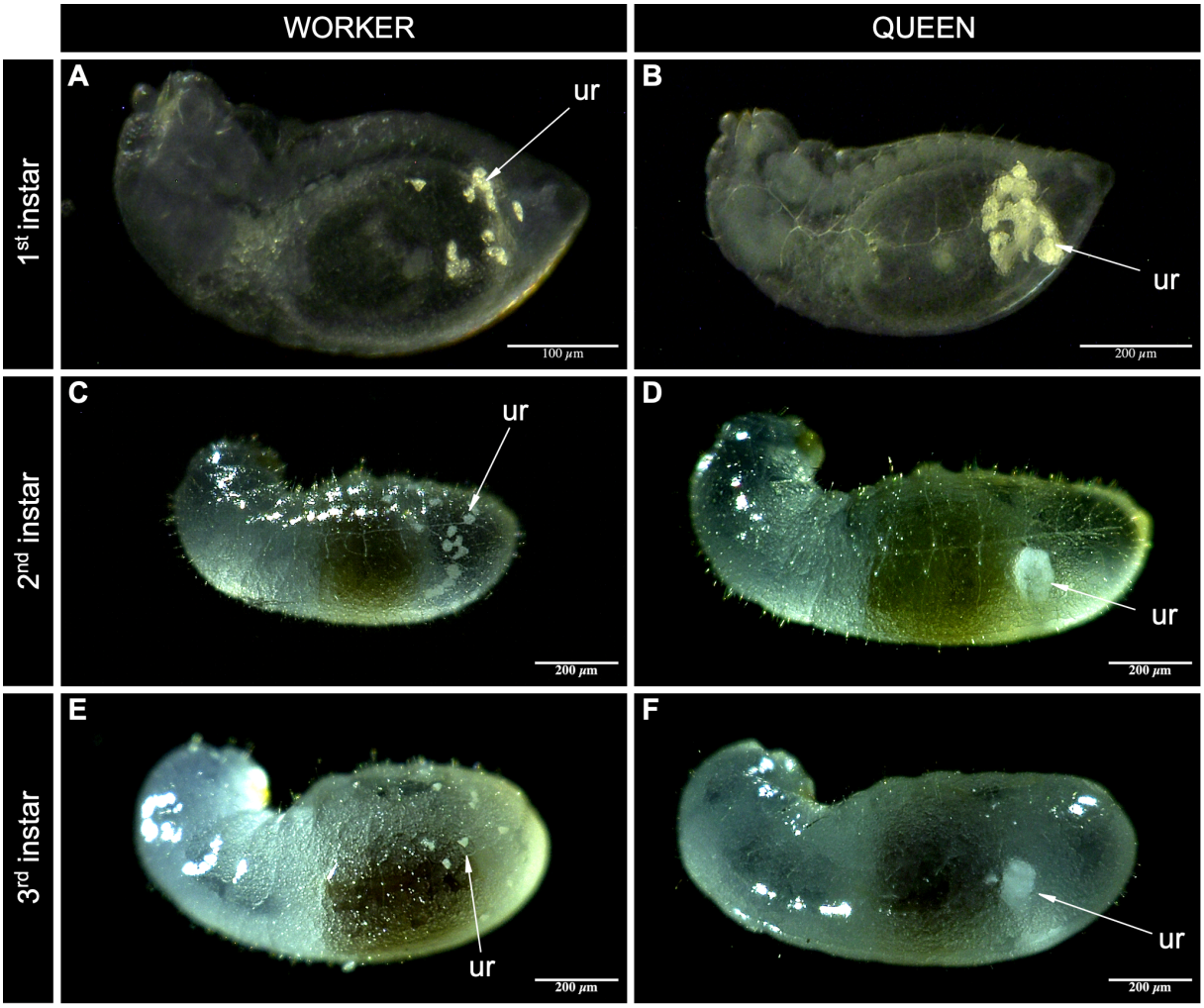

FIGURE 4.1: Urate localization patterns distinguish queen- and worker-destined larvae in the ant *C. obscurior*.
Light microscope images of worker-destined larval instars (A, C, E) and queen-destined larval instars (B, D, F). ur = urate.

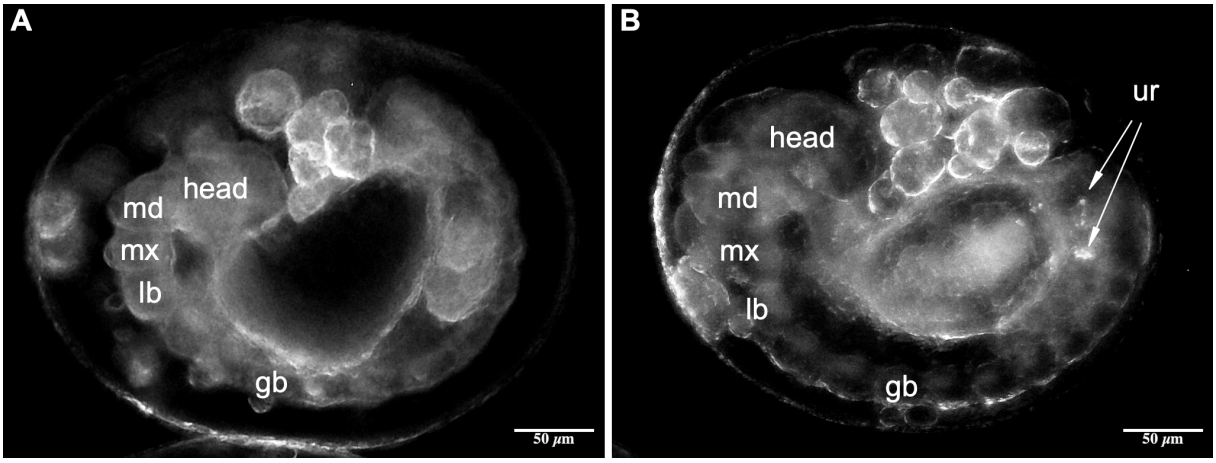

FIGURE 4.2: Urate localization in queen- and worker-destined embryos in the ant *C. obscurior*.
Worker-destined embryos show no urate (ur) (A), while queen-destined embryos have urate localized in the last segments of their germ band (gb) (B). The first segments of the embryo can be clearly separated between head and the three gnathal segments, mandibular (md), maxillary (mx) and labial (lb).

TABLE 4.2: Urate localization patterns predict caste in the ant *Cardiocondyla obscurior*.

Development Stage	Predicted caste	n	Survival			Produced caste		
			Proportion	Differences between castes		Proportion	Accuracy of caste prediction	
				Odds ratio	p		Odds ratio	p
egg	queen	165	24.9% (41/165)	1.276	0.342	78% (32/41)	5.398	**<0.001**
	worker	192	29.7% (57/192)			42.1% (24/57)		
1st instar larva	queen	34	5.9% (2/34)	1.512	1	0% (0/2)	-	-
	worker	23	8.7% (2/23)			100% (2/2)		
2nd instar larva	queen	50	62% (31/50)	0.334	0.019	90.3% (28/31)	97.129	**<0.001**
	worker	40	35% (14/40)			92.9% (13/14)		
3rd instar larva	queen	50	60% (30/50)	0.439	0.062	100% (30/30)	infinite	**<0.001**
	worker	40	42.5% (17/40)			100% (17/17)		

Transversal semithin sections of 3rd instar larvae showed that urate depots clustered around the developing ovaries in queen larvae in a paired and bilateral manner (Figure 4.3 B), while worker larvae lack ovaries and urate depositions are distributed randomly throughout the caudal end (Figure 4.1, left column; Figure 4.3 A).

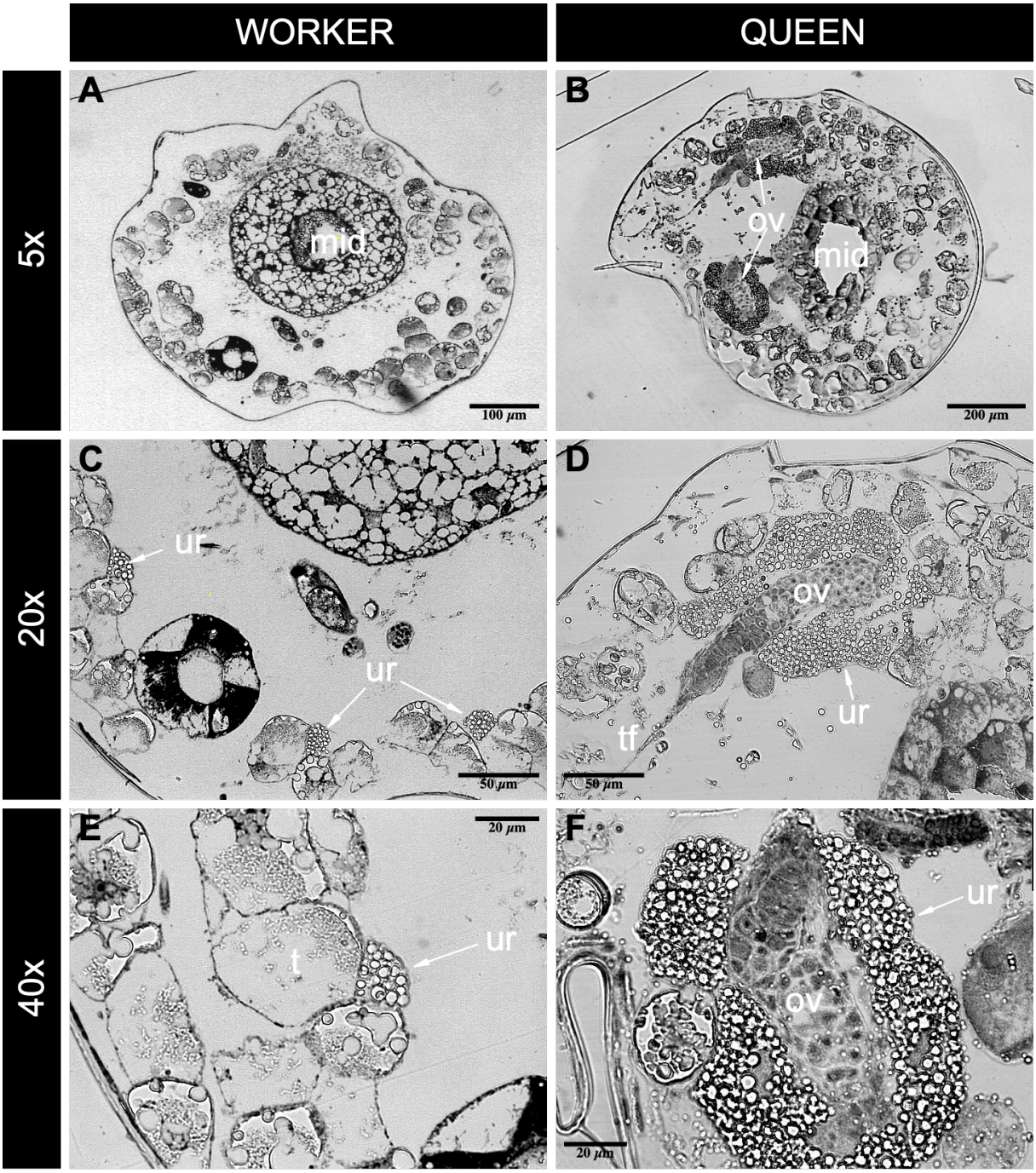

FIGURE 4.3: Histological sections of *C. obscurior* larvae.
(A) Transversal section of a worker-destined L3 larva. In workers ovaries are missing. (B) Queen--destined larvae show paired ovaries (ov) close to the midgut (mid). (C) In worker-destined larvae urate (ur) accumulates in small randomly distributed depots. (D) Ovaries in queen-destined larvae are surrounded by large urate depots. (E) Small urate depots aggregate close to trophocytes (t). (F) Urate encloses the developing ovary in queen larva. Tf = terminal filament.

In both castes urate comes in the shape of translucent birefringent spherocrystals. These cluster in small aggregates (diameter from 10 to 20 µm) close to trophocytes in workers (Figure 4.3 C, E). In queens, urate crystals form large aggregations surrounding the developing gonads (Figure 4.3 D, F), which are in close proximity to the midgut (Figure 4.3 B). The developing ovaries are inside a “pocket”

of urate crystals, with outward extending ovarioles. The apical end reflects the terminal filament (Figure 4.3 D).

4.3.2 OVARIAN RECONSTRUCTION

Urate localization patterns allowed for specific selection of queen-destined L1-L3 larvae (Figure 4.1), making it possible to analyze the development of the gonads for each larval stage. The ovarian development of L1 larvae failed because their small size made dissection technically unfeasible. In L2 larvae the developing gonads are visible as a bilateral cluster of germ cells located at the posterior end of the last abdominal segments (Figure 4.4 A-D). The gonads are in close proximity to the caudal end of the central nervous system (Figure 4.4 D, CNS). From a mere cluster of cells in L2 larvae, the developing gonads in L3 larvae differentiated into three ovarioles per ovary (2+3). The ovarioles face “inwards”, with their tip extending in an anterior-apical orientation (Figure 4.4 H). In the larval ovarioles, disc-shaped cells can be found which stack in a medial-lateral orientation (Figure 4.4 H, asterisk). These cells are likely cap cells (CC) (Sahut-Barnola et al., 1995), which segregate the germarium from the terminal filament (Ting, 2013). In pupae, the ovaries are completely differentiated, with fully extended terminal filaments (Figure 4.4 L). The germ cells in the germarium have differentiated into cystocytes, which will later give rise to the oocyte with its nurse cells (Figure 4.4 L) (Okada et al., 2010). After reaching the adult stage, the fully matured ovarioles developed egg chambers, containing oocytes with their corresponding nurse cells. The oocytes are surrounded by follicle cells, and these egg chambers are in different stages of maturation (Figure 4.4 P).

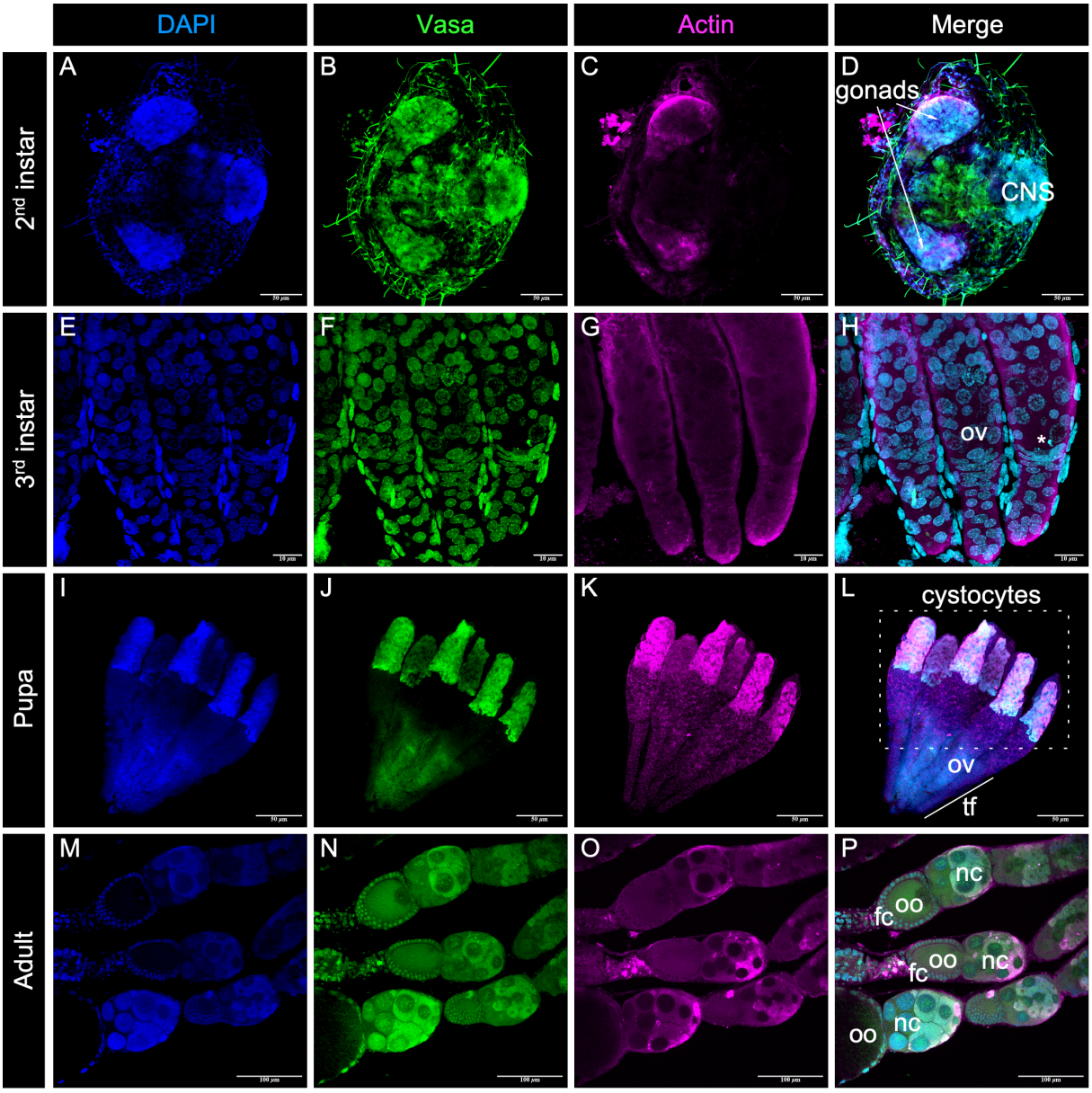

FIGURE 4.4: Ovarian reconstruction in queens of *C. obscurior*.

(A-D) Early gonadal formation in second instar larva. DAPI is used to show the cell nuclei. Vasa stains against germ cells and actin visualizes the cytoskeleton. (A) DAPI, (B) Vasa, (C) Actin, and (D) Merge with a visible central nervous system (CNS). (E-H) Ovarioles (ov) of a third instar queen larva. (E) DAPI, (F), Vasa, (G) Actin and (H) Merge. The asterisk (*) shows cap cells. (I-L) Ovary of a queen pupa with its six ovarioles. (I) DAPI, (J), Vasa, (K) Actin and (L) Merge. The germ cells have differentiated into cystocytes in this stage, inhabiting the caudal end of the ovariole. Tf = terminal filament. (M-P) Mature ovarioles in adult queens. (M) DAPI, (N) Vasa, (O) Actin and (P) Merge showing the oocyte (oo) with its nurse cells (nc). The oocyte is encircled by follicle cells (fc).

The reconstruction of the cystocytes inside the ovarioles of early- and mid-staged queen pupae (Figure 4.5 A, B, C) showed that the developing cells increase in size during pupation. Cystocytes in early-staged pupae are smaller than in mid-staged (early-staged pupae: >800 µm^2, >100 µm^3; mid-staged pupae: >1200 µm^2, ≥100 µm^3; Linear regression, R^2=0.9036, p<0.001) (Figure 4.5 D), illustrating that the growth and specification of the cells continues during pupal development. Some cells in pupal ovarioles are immensely larger in size than others (early-staged pupae: >400 µm^2, >400 µm^3; mid-staged pupae: >800 µm^2, >600 µm^3) (Figure 4.5 D).

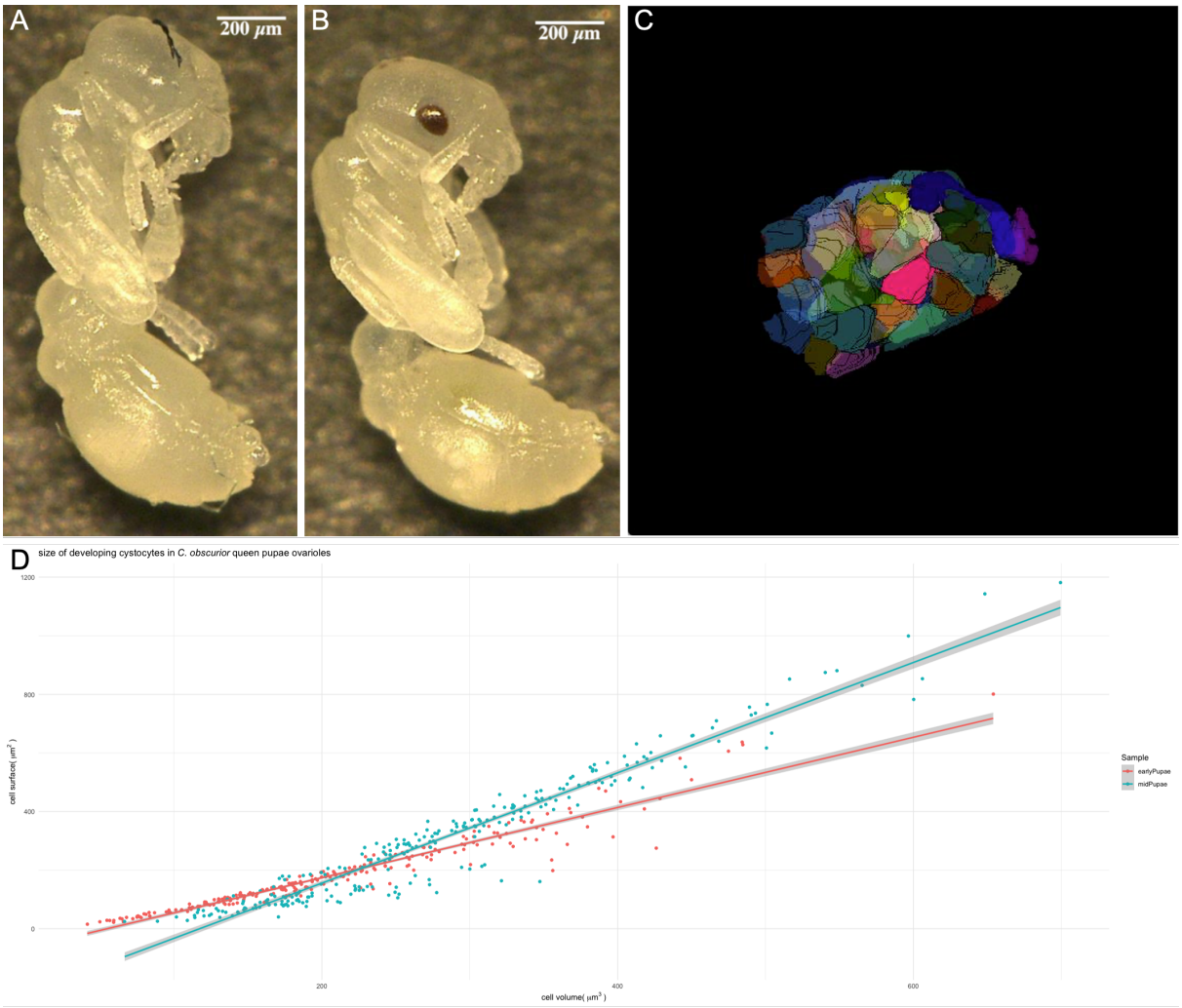

FIGURE 4.5: Images of queen pupae.
(A) Early-stage queen pupae with unpigmented ommatidia and ocelli. (B) Mid stage queen pupae with pigmented ommatidia and ocelli. (C) Example of a 3D rendered ovariole with TrakEM2. Data generated form the reconstruction was used for data analysis. Colors represent individual cells. (D) Cell volume to cell surface in *C. obscurior* queen pupae. The plot illustrates the different sizes of cells in developing cystocytes in queen ovarioles of the two pupal stages.

4.3.3 *NANOS* EXPRESSION IS LINKED TO THE GERMLINE

The expression of the germline marker *nanos* was higher in L2 and L3 queen larvae compared to worker larvae (Wilcoxon test with Benjamini-Hochberg (BH) correction: p=0.01587; Wilcoxon test with Benjamini-Hochberg (BH) correction: p=0.01587, Figure 4.6). A similar non-significant trend was found in L1 larvae (Wilcoxon test with Benjamini-Hochberg (BH) correction: p=0.2677, Figure 4.6). The expression of *nanos* in workers in all three larval stages did not change over time. While the expression of *nanos* between queen and workers does not differ significantly in L1 larvae, the expression pattern changes significantly, starting in L2 and becomes more distinct over time as seen in L3.

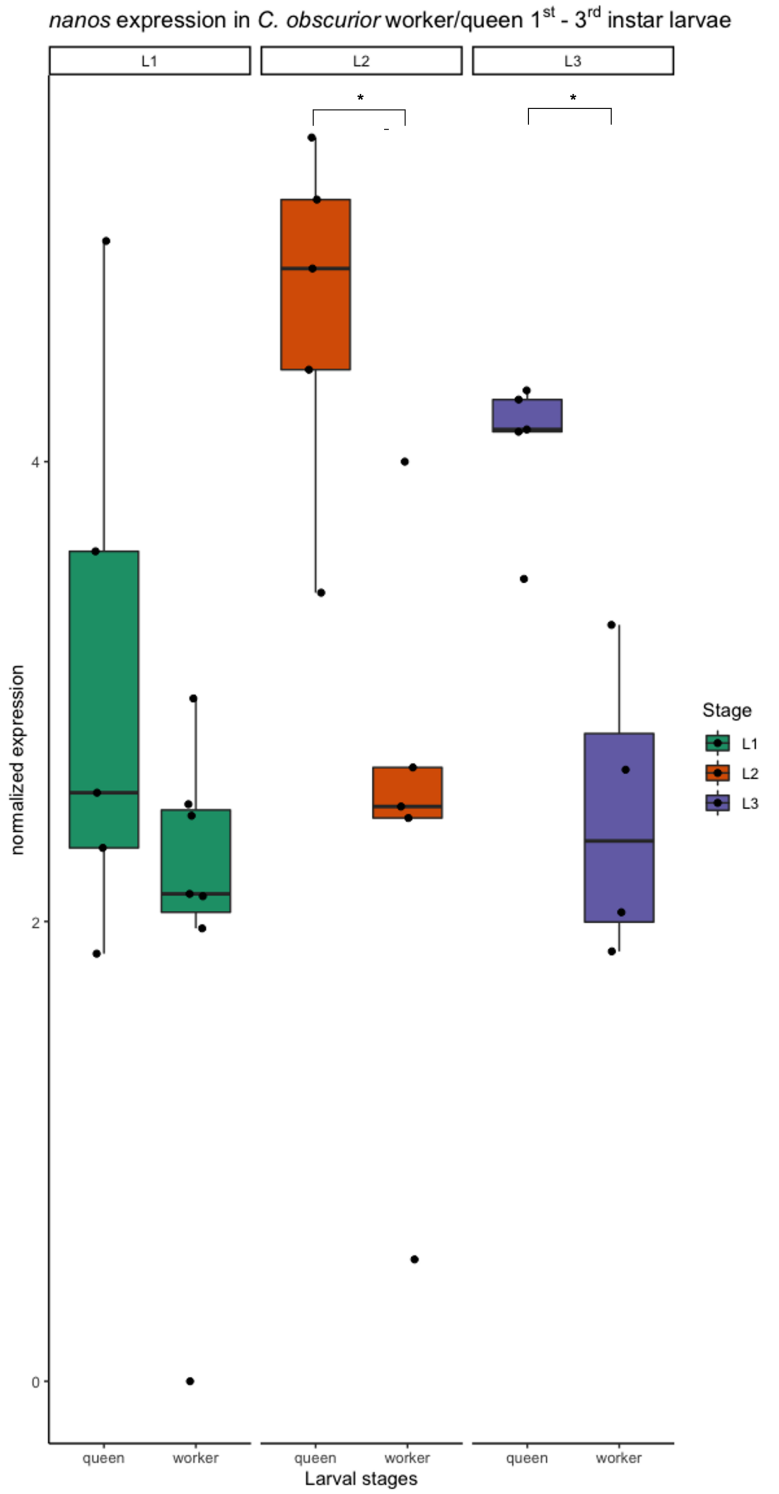

FIGURE 4.6: Caste specific expression of the germline gene *nanos* in the ant *C. obscurior*.
Normalized gene expression of the germline marker in queens and workers in all three larval stages. Expression of *nanos* is significantly higher expressed in L2 and L3 queen larvae compared to workers. * $P < 0.05$, Wilcoxon test.

4.3.4 URATE IN DIFFERENT SPECIES

In addition to *C. obscurior* we found queen-like urate patterns in larvae of three more *Cardiocondyla* species (*C. venustula*, *C. wroughtonii* and *C. nuda*) (Figure S 3; Table S 1). In the remaining four species (*C. thoracica*, *C. elegans*, *C. argyrotricha* and *C. minutior*) we did not find obvious caste-specific patterns (Figure S 4).

All 49 species representing seven ant subfamilies had larvae with obvious urate depositions (Table S 3; Figure S 5). We could not find paired urate depositions resembling the paired pattern observed in *Cardiocondyla* queens.

4.4 DISCUSSION

"Auch ein blindes Huhn findet irgendwann mal ein Korn" (German saying)

Cardiocondyla obscurior is unique among the Formicidae due to the occurrence of wingless fighter males (Heinze & Holldobler, 1993) and the repeated loss of the winged male morph across the genus (Oettler et al., 2010). Because colonies of this ant can be easily reared and manipulated, the species has been used to address all kinds of questions in diverse biological contexts (Heinze, 2017; Oettler & Schrempf, 2016), ranging from genome evolution (Errbii et al., 2021; Schrader et al., 2014), to social behavior (De Menten et al., 2005), symbiosis (Klein et al., 2015; Ün et al., 2021), and phenotypic plasticity (Klein et al., 2016; Schrader et al., 2015, 2017). In this respect, *C. obscurior* has been considered a "gold mine" (E. Abouheif pers. com.). Now, as is the case in mining, sheer luck led to the discovery that queen and worker embryos and larvae in some *Cardiocondyla* species can be distinguished using the localization of urate deposits. We could not find a similar pattern in other ant genera, but 49 species of 30 genera is not representative of the vast diversity of ant species. We hope that our discovery inspires others to take a closer look at the brood of their favorite species.

In insects, urate is typically deposited in specialized cells – so-called urocytes (Costa-Leonardo et al., 2013) – which together with trophocytes (Costa-Leonardo et al., 2013) and oenocytes (Furtado et al., 2013) represent the three major cell types in the fat body. Urocytes store urates either in vacuoles (Locke, 1984) or as circular, birefringent spherocrystals (Costa-Leonardo et al., 2013), and can occupy a large fraction of the fat body, for instance in the termite *Mastotermes darwiniensis* (Costa-Leonardo et al., 2013). In the termite *Reticulitermes flavipes*, uric acid is recycled by gut bacteria as a nitrogen source (Potrikus & Breznak, 1981), and urate deposits have been linked to oocyte development (Elliott & Stay, 2007). In *Pachycondyla* ants, urocytes specialize in the storage of nutrients and excretion products (Zara & Caetano, 2004) and a composition assay in *Melipona quadrifasciata* bees identified Na, Ca, Mg, P as main elements in urocytes, as well as traces of Zn, Mn, and K (Furtado et al., 2013). In *C. obscurior* we found circular, birefringent spherocrystals but no cell nuclei, indicating that urate is deposited directly. Worker larvae exhibited small, randomly distributed urate clusters which were found closely associated with what appeared to be trophocytes rather than urocytes. These smaller clusters may originate as a by-product of metabolic processes in trophocytes. Queen larvae showed dense aggregations of urate surrounding the developing ovaries. These large urate deposits may constitute an energy reservoir for ovary growth, a process that is energy-demanding since cells proliferate at rapid rates.

Caste-specific urate patterns only occurred in some *Cardiocondyla* species and in none of the species representing other ant genera. At the moment we can only speculate as to why this is the case. It is unlikely that the presence of the bacterial symbiont *Cand.* Westeberhardia cardiocondylae is directly

linked because the same urate patterns occur in a *C. obscurior* lineage that is naturally free of Ca. Westeberhardia (Klein et al., 2015), as well as in larvae which have been experimentally cleared of their bacterial symbionts with antibiotic treatment (Ün et al., 2021). There is also no obvious phylogenetic signal. *C. obscurior* and its sister species *C. wroughtonii* both exhibit caste-specific patterns but cluster together in clade A with *C. thoracica* and *C. argyrotricha*, both of which do not. In clade B, *C. nuda* and *C. venustula,* which exhibit the caste-specific patterns, cluster together with *C. minutior* (Oettler et al., 2010). All species with the queen pattern have two alternative male morphs and can be kept in the lab with minimum effort, making the genus perfect for comparative studies of female and male diphenic development.

Urate deposit patterns allowed us to reconstruct ovarian development in *C. obscurior*. The female reproductive apparatus is conserved in insects, and consists of two paired ovaries, the oviduct, the uterus, accessory glands and the spermatheca (Snodgrass, 1935). Large variation can be found in the number of ovarioles making up each ovary, ranging from 15-20 in the fruit fly *Drosophila melanogaster* (Sahut-Barnola et al., 1995) to 200 in the honey bee (Cridge et al., 2017). In ants ovariole number ranges from six in *Cardiocondyla nuda* queens (Heinze et al., 1993) to ~ 70 in *Leptogenys sp.* (Gotoh et al., 2016; Ito & Ohkawara, 1994) and reaches over 200 in *Solenopsis invicta* queens (Tschinkel, 1987). To date, ovarian development has been mainly studied in the fruit fly (e.g., (Park et al., 2018; Slaidina et al., 2020)) and some aspects of ovary formation during embryonic development have been studied in ants (Khila & Abouheif, 2010; Pontieri et al., 2020). However, development of functional ovaries has not yet been described.

In *C. obscurior*, the physiological processes involved in ovariole formation appear to differ from those described for fruit flies and honeybees. In *Drosophila* ovarioles form in second instar larvae. Somatic cells referred to as terminal filament cells (TFCs) begin to stack in the subapical region of the medial side of the ovary, creating a wave that spans across the larval ovary. This wave creates about 20 stacks, which corresponds to the maximum number of ovarioles in *Drosophila* (Sahut-Barnola et al., 1995). The exact processes involved in ovariole formation are still unclear (Sarikaya et al., 2012). In *A. mellifera* autophagic and apoptotic cell death events appear responsible for the formation of ovarioles in queen and worker larvae (Dallacqua & Bitondi, 2014). In contrast, ovarioles in *C. obscurior* are not formed by stacks of TFCs or programmed cell death, but rather by elongation (Figure 4.7). Directed proliferation suggests the involvement of growth factors and active migration of cells into the apical tip of the ovariole, similar to the migration of germ cells. Germline stem cells (GSCs) are typically located in the germarium at the tip of the ovarioles, close to the TFCs (Khila & Abouheif, 2010; Ting, 2013). These GSCs continuously renew themselves and produce new germ cells. Since the ovarioles in *C. obscurior* outgrow from the initial gonadal cell cluster, the GSCs together with the follicle stem cells (Slaidina et al., 2020) must migrate actively to their respective destination. The GSCs then proliferate

and produce differentiated cystoblasts, which divide synchronously to form cystocytes (Okada et al., 2010). These cystocytes are found in the germarium of pupal ovarioles in *C. obscurior,* with some cells larger than others. Cystocystes go on to differentiate into oocytes with their corresponding nurse cells. We suspect that the largest cells are pre-determined oocytes in the pupal germarium, which allow the queen to initiate oocyte maturation soon after hatching. *Cardiocondyla* queens mate inside their natal nest within days of reaching adulthood (Cremer et al., 2012; Oettler et al., 2010) and can almost immediately begin with the production of sexual offspring (Suefuji et al., 2008). This accelerates the development of the next generation and presumably helps this tramp species to establish in novel environments.

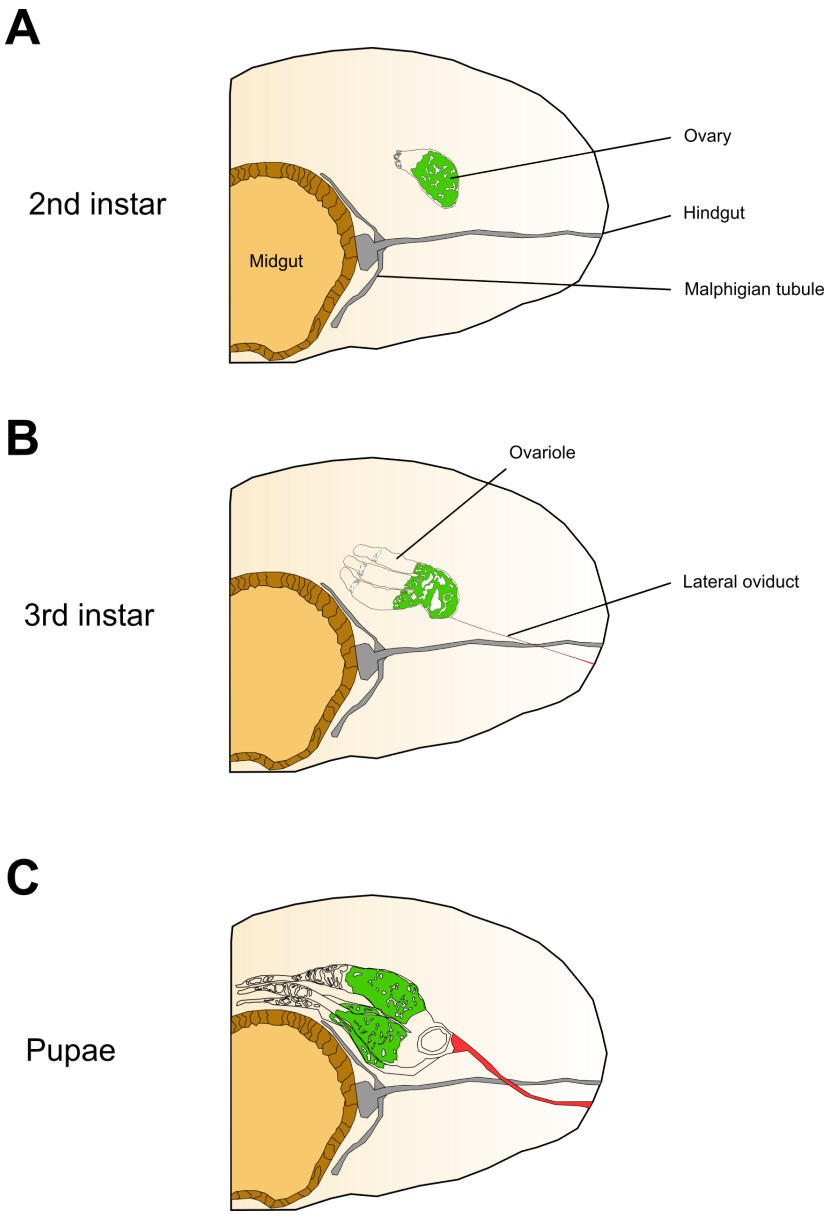

FIGURE 4.7: Schematic illustration of postembryonic ovarian development in the ant *C. obscurior*.
The sketched images represent the 2nd instar (A), 3rd instar (B) and pupal (C) stage of queens. In the 3rd instar the lateral oviduct (red) is already distinct. The green coloration represents the germ cells as seen in Figure 4.4.

Our discovery has important implications for understanding both the specific biology of *C. obscurior* and the general mechanisms underlying caste development in ants. At the life history level, it is now possible to study questions revolving around the phenotypes of developing queens and workers. For example, do the larval phenotypes differ in morphology, behavior or cuticular chemistry? We can also test whether workers discriminate between queen- and worker-destined brood, and if larvae are treated differently depending on caste. In the future, it should even be possible to track individual larvae without the need for tagging by using their unique patterns for individual recognition, similar to the way whale fins are used for studying population structure. Only creativity limits possibilities now, not vice versa. Because caste-specific urate patterns are already visible in late embryos, we are also finally able to study caste development beyond obvious features such as wing discs in late larvae (Oettler et al., 2018). *C. obscurior* queens produce increasingly queen-biased caste ratios with age (Jaimes Nino et al., 2021), allowing for efficient sampling of queen-destined embryos, and opening numerous avenues for the study of the mechanisms involved in ant caste determination and differentiation, and in social insect polyphenism in general. It has already been shown that ant and honeybee development shares some features, with an overlapping set of genes involved in growth (e.g. TOR, Insulin-like) (Mutti et al., 2011)) and juvenile hormone (JH) synthesis and degradation (Kayukawa et al., 2012) playing a role in developmental regulation (Corona et al., 2016; Schrader et al., 2015). Upstream, the importance of transcription factors involved with the sex differentiation cascade also finds support in ants (Jia et al., 2018; Klein et al., 2016), and honeybees (Johnson & Jasper, 2016; Pan et al., 2021). Recently, we postulated that a major evolutionary transition, the evolution of sex, has facilitated another major transition, the evolution of eusociality, via co-option of the same developmental switch mechanism (Klein et al. 2016). Now we can test this hypothesis, bringing us one step closer to a conceptual understanding of how social insect polyphenism evolved.

The *nanos* gene is a highly conserved germline marker and found in different insect species like *Drosophila* (Becalska & Gavis, 2009; Renault, 2012), *Nasonia* (Lynch & Desplan, 2010), *Bombyx* (Nakao et al., 2008) and *Apis* (Tanaka & Hartfelder, 2009). In the recent past *nanos* has been successfully established in different ant species (Khila & Abouheif, 2010; Pontieri et al., 2020; Rafiqi et al., 2020), supporting the high conservation across social Hymenoptera.

In our study we found differences in gene expression between queen and worker larvae in *C. obscurior*. *Nanos* is expressed in queens and workers alike, pointing to a putative role for *nanos* in the development of gonads in reproductive females and unknown functions in the sterile worker caste. This is supported by the constant expression of *nanos* in worker larvae throughout all three larval stages. In queens *nanos* is higher expressed, probably because of the presence of gonads and therefore an existing germline.

The gene *nanos* serves as an excellent germline marker to identify germ cells in queen larvae.

In conclusion, this discovery has many implications for our research, both for understanding the biology of the species as well as for describing phenotypic plasticity. At the life history level, it is now possible to study specific questions at the intersection of developmental stages. Can workers discriminate between queens and workers? And, if so, do workers treat larval castes differently? Do the larval phenotypes differ in morphology, behavior or cuticular chemistry? Larvae produce an anal fluid that they pass on to workers when solicited. Is this caste specific? In the future it should even be possible to track individual larvae, using their unique patterns for individual recognition, similar to the role of whale fins in studying population structure.

Additionally, caste differentiation is already visible at the late embryonic stage and we are now able to study caste specific development efficiently, beyond obvious features such as wing discs in late larvae (Oettler et al., 2018). For example it will be possible to study how neuronal tissue and sensory organs project and develop and form the final structure (Bressan et al., 2015). In *Monomorium*, the worker caste is already determined at the stage when the posterior germ band differentiates (Khila & Abouheif, 2010). We will see if the same interruption point exists in *C. obscurior*. Queens produce increasingly queen biased caste ratios with age (Jaimes Nino et al., 2021), which allows for more efficient sampling of queen destined embryos (eggs) to study early development and the ultimate point of determination, which remains elusive.

5 EMBRYOGENESIS IN THE ANT *CARDIOCONDYLA OBSCURIOR*

5.1 INTRODUCTION

Insect embryogenesis has been extensively studied in the past, specifically the fruit fly *Drosophila melanogaster* and the red flour beetle *Tribolium castaneum*. *D. melanogaster* possesses a well described embryogenesis with 17 distinct stages (Campos-Ortega & Hartenstein, 2013).

Insect taxa differ significantly in their embryonic development. One of the most prominent differences is the formation of the germ band. In higher ranked holometabolous insects like *Drosophila* (Diptera), honey bee (Hymenotpera), *Bombyx mori* (Lepidoptera) and *Chrysopa* (Neuroptera) the germ anlage is comprised of nearly the entire surface of the blastoderm, a single layer of cells covering the whole egg surface (Figure 5.1, Figure 5.2).

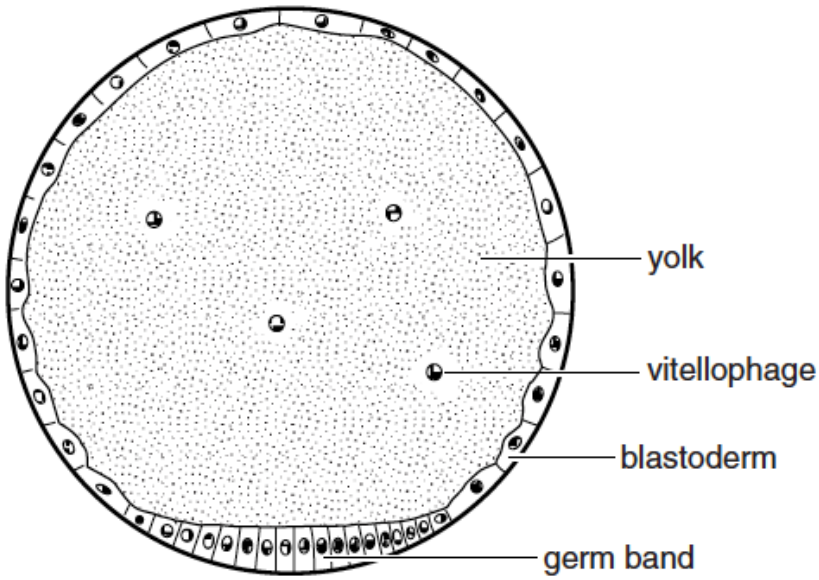

FIGURE 5.1: Cross-section of an egg.
The germ band is visualized as a ventral thickening of the blastoderm (Chapman et al., 2013).

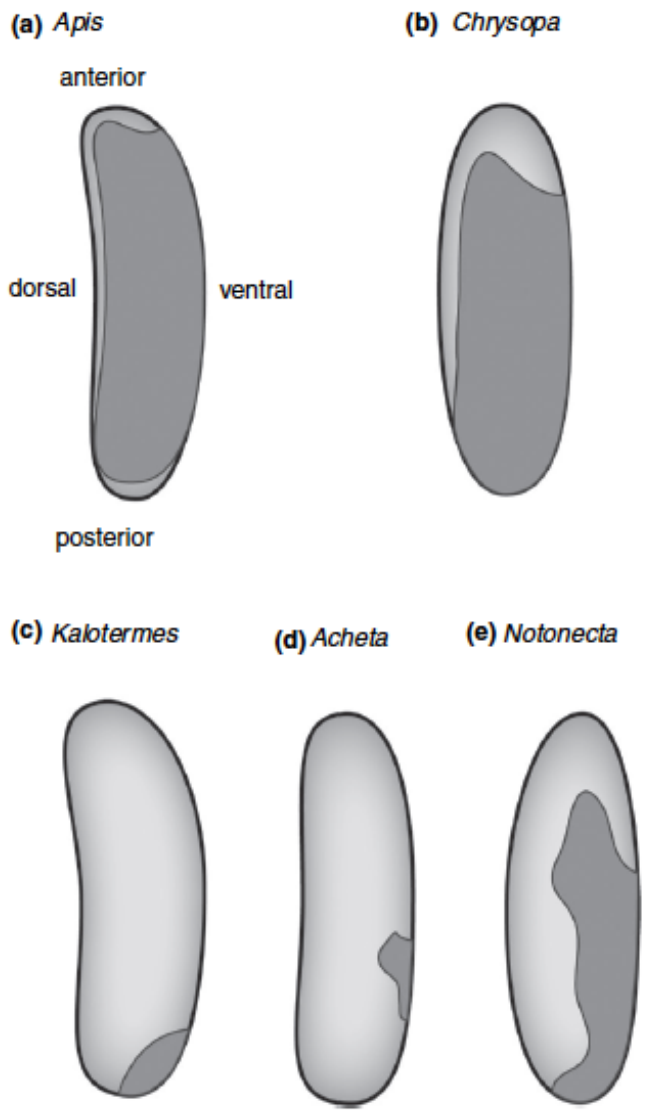

FIGURE 5.2: Examples for different germ-band-type embryos.
Apis and *Chrysopa* are examples for long-germ-type embryos (a, b). *Kalotermes* and *Acheta* for short-germ-type (c, d) and *Notonecta* for intermediate-germ-type embryos (e). The germ anlage is illustrated in light grey (Chapman et al., 2013).

Embryos developing from this type of germ anlage are classified as long-germ-type. In contrast to long-germ-type or long-germ band embryos, short-germ band embryos are found among the lower or primitive hemimetabolous order of insects but also in the order of Coleoptera. There, the germ band is restricted to a smaller part of the blastoderm located posterior in the embryo. Examples for short-germ-type embryos are *Acheta* (Orthoptera), *Kalotermes* (Isoptera) and *Tribolium* (Coleoptera) (Figure 5.2 c, d). Besides the long- and short-germ-type a third type, the intermediate-germ-type, can be found in the backswimmer *Notonecta* (Hemiptera) (Figure 5.2 e). In long-germ band embryos all body segments are formed by the germ anlage almost simultaneously. In contrast, short-germ band embryos undergo a second growth process (Chapman et al., 2013; Tautz et al., 1994). After the head lobes and the most anterior segments of the thorax have differentiated, the remaining abdominal segments are added gradually during gastrulation (Schröder et al., 2008).

Although the embryogenesis is well described in some insect taxa, this is not the case in ants. The number of studies focusing on the development of embryos is very limited. The earliest description of embryogenesis was done by Ganin in 1869 for *Formica fusca* (Ganin, 1869). Since then, only few studies presented data on other ant species. Khila & Abouheif (Khila & Abouheif, 2010) focused on germ cell development in the myrmicine ants *Aphaenogaster*, *Messor* and *Monomorium*, but studied only selected time points of their embryonic development. In *Drosophila* or *Tribolium* complete series staging the embryonic development already exist (Campos-Ortega & Hartenstein, 2013; Strobl et al., 2015), and recently an extensive embryogenesis for the myrmicine ant *Monomorium pharaonis* has been published (Pontieri et al., 2020).

This study is the first description of the embryogenesis of the myrmicine ant *Cardiocondyla obscurior*. *C. obscurior* is a model for caste differentiation (Klein et al., 2016; Oettler et al., 2018; Schrader et al., 2014, 2015) and additional work identified that the point of caste determination occurs prior to the 1st larval stage (Chapter 6). Here we characterize embryonic development to facilitate further in-depth studies.

5.2 Materials and Methods

5.2.1 Ants

The colonies used in this study were collected in Okinawa, Japan 2011 (Schrader et al., 2014). Stock colonies were kept in square plaster-bottom nests (100 mm x 100 mm x 20 mm, Sarstedt, Germany) with plastic inserts containing three chambers covered in dark foil in a climate chamber under a 12h/12h and 22°C/26°C night/day cycle at 70% humidity. All experimental colonies described below were kept in round plaster-bottom nests with nest indentations covered by dark foil under the same conditions as stock colonies. Stock colonies and experimental colonies were provided with water *ad libitum* and fed three times a week with honey and pieces of insects (cockroaches and fruit flies).

5.2.2 Embryo collection

We followed egg development by transferring single mated queens into experimental colonies containing 10 workers. Colonies were kept at 26 °C. Queens were left to lay eggs for 24 hours and then removed thereafter. Eggs were tended to by workers while being aged. Eggs were collected every 24 hours to determine the current developmental stage of the embryo. The selected eggs were submerged in a dissection dish containing PBT (0.3 %) and then transferred on a microscope slide. The slides were sealed with nail polish and imaged using a stereomicroscope connected to a camera (Keyence VHX 500FD, Neu-Isenburg, Germany).

5.2.3 Image analysis

The obtained images were processed using the open source platform Fiji (Schindelin et al., 2012) and the software ScientiFig (Aigouy & Mirouse, 2013).

5.3 RESULTS

In *Cardiocondyla obscurior* embryonic development lasts for approximately nine days after egg laying (AEL). After that first instar larvae hatch. We oriented ourselves on the embryonic development of the red flour beetle *Tribolium castaneum*. Strobl (Strobl et al., 2015) describe five embryonic stages, which serve as a good basis for the first description of the embryogenesis in our model organism.

Stage 1 (One to two days AEL).

Stage one is characterized by the location of the amniotic fold at the posterior end of the embryo (Figure 5.3 A-C). This is followed by the formation of the syncytial blastoderm. At the posterior end of the syncytial blastoderm a region of the blastoderm thickens and forms the germ anlage, which later gives rise to the germ band (Figure 5.3 D) (Chapman et al., 2013).

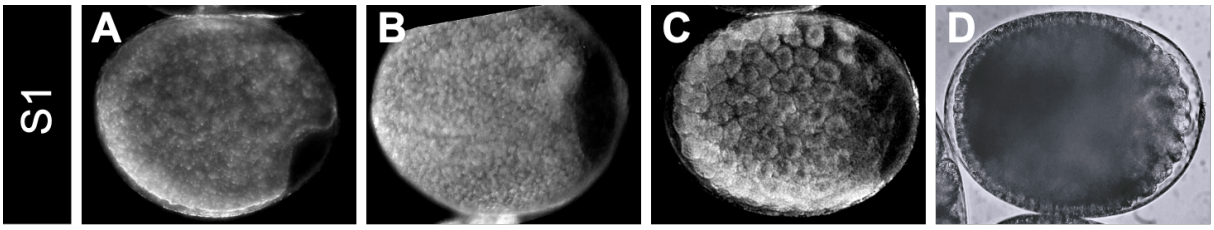

FIGURE 5.3: Stage 1 of the embryonic development in *C. obscurior*.
(A-C) The amniotic fold is located at the posterior end of the embryo. (D) By the end of stage one the syncytial blastoderm has formed (View: anterior left, posterior right).

Stage 2 (Three to four days AEL).

This stage is defined by the gastrulation of the germ anlage. Cells along the midline invaginate and proliferate (Figure 5.4 A, B). The single-layered germ anlage becomes two-layered. This process forms the germ band. Later, the anterior and posterior amniotic fold merge, giving rise to the serosa window. The serosa and amnion will be separated after the window closes ventrally. This step ends gastrulation (Chapman et al., 2013; Strobl et al., 2015).

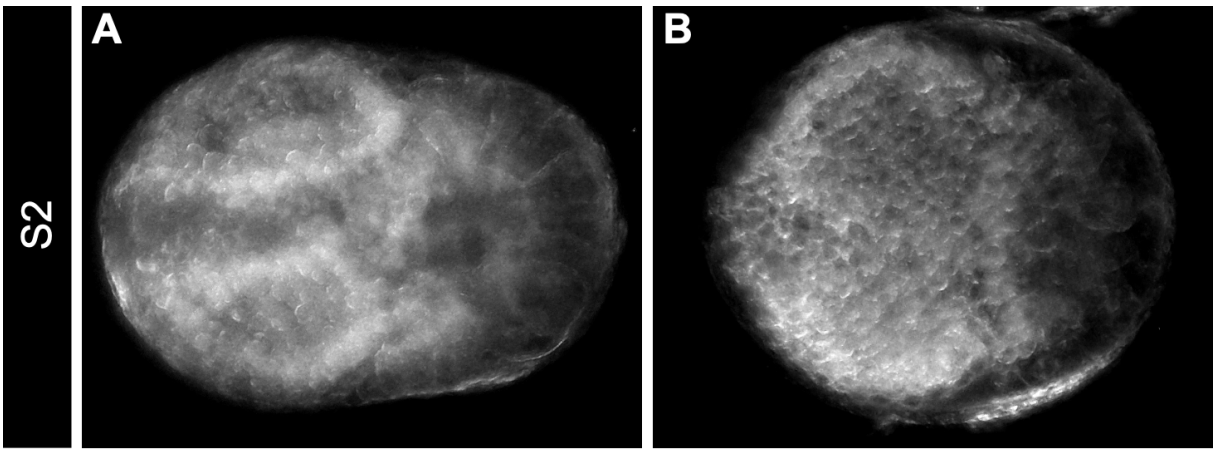

FIGURE 5.4: Stage 2 of the embryonic development in *C. obscurior*.
(A, B) Ventral view at early gastrulation. The horseshoe-shaped amniotic fold is visible (View: anterior left, posterior right).

Stage 3 (Five to six days AEL).

In stage three the germ band is fully elongated and starts to retract dorsally. Separation of head and thorax is visible (Figure 5.5).

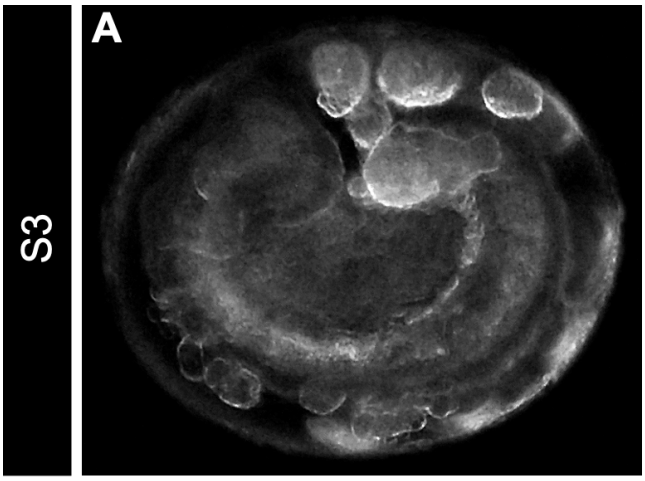

FIGURE 5.5: Stage 3 of the embryonic development in *C. obscurior*.
(A) Lateral view of an embryo with fully elongated germ band. Large yolk cells nourish the developing embryo (View: anterior left, posterior right).

Stage 4 (Seven days AEL).

Stage four is characterized by the simultaneously segmentation of the germ band and dorsal closure. The head, thorax and abdominal segments are well defined, making the gnathal segments (mandibular: md; maxilla: mx and labium: lb) distinguishable. Urate deposits are starting to be visible (Figure 5.6 B).

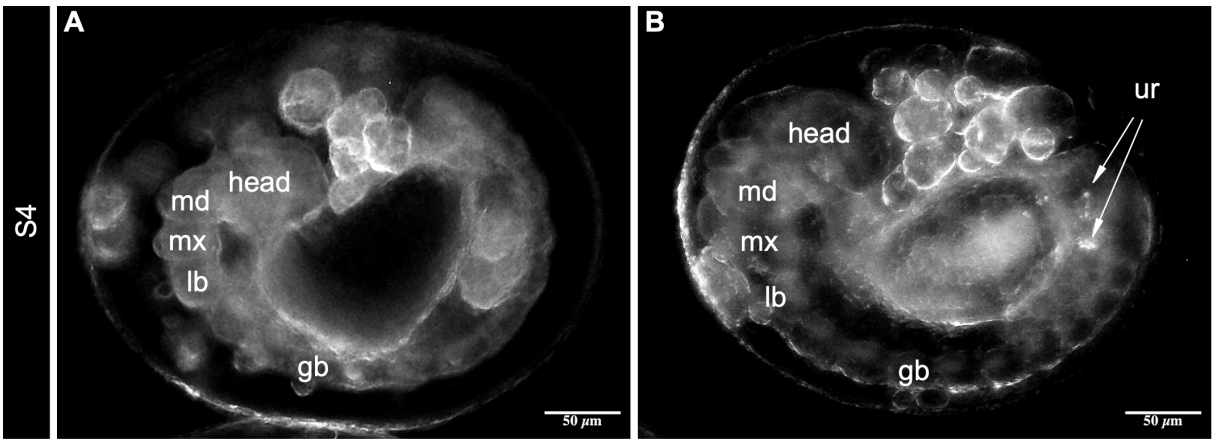

FIGURE 5.6: Stage 4 of the embryonic development in *C. obscurior*.
(A) Lateral view of an embryo with segmented germ band (gb). (B) Lateral view of an embryo with visible urate (ur) deposits. md: mandibular segment; mx: maxillary segment; lb: labial segment (View: anterior left, posterior right).

Stage 5 (Eight to nine days AEL).

This is the final stage before the embryo hatches. During this stage the head changes its orientation from a ventral to anterior-ventral position. The embryo starts with muscular movement. This step results in the hatching of the embryo. The localization of urate is very distinct, making it possible to separate queen- from worker-destined embryos (Figure 5.7 B).

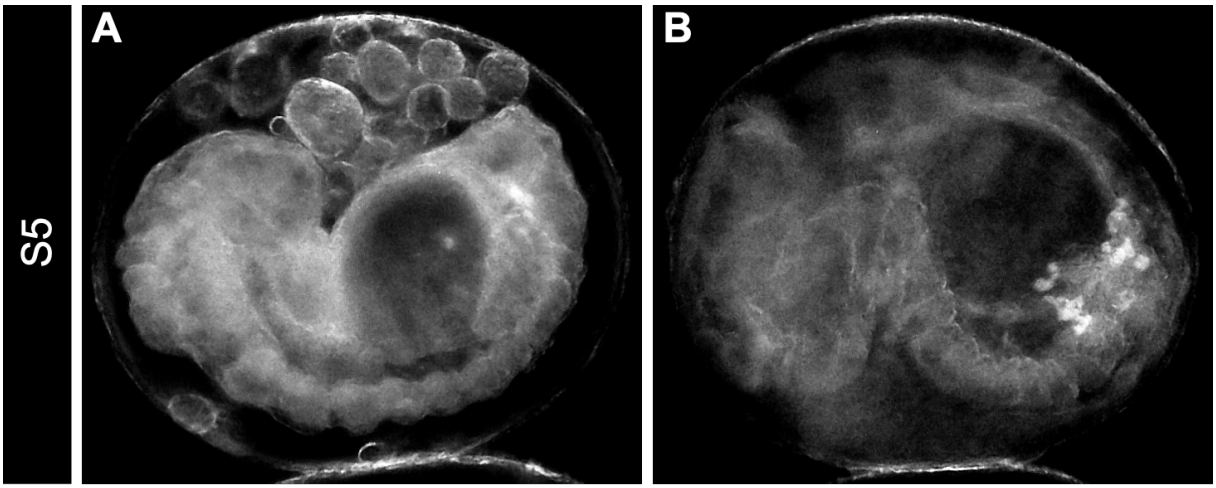

FIGURE 5.7: Stage 5 of the embryonic development in *C. obscurior*.
(A) Lateral view of a fully developed embryo. Segmentation of the germ band is completed. The head is in a ventral position. (B) Lateral view of an embryo with completed head turn to an anterior-ventral orientation. The urate deposits are clearly visible as white dots (View: anterior left, posterior right).

	Stage	Time (AEL)	Developmental event
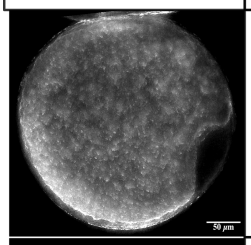	1	Day 1-2	Syncytial blastoderm formation
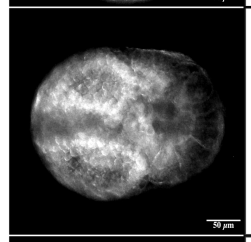	2	Day 3-4	Gastrulation of germ anlage
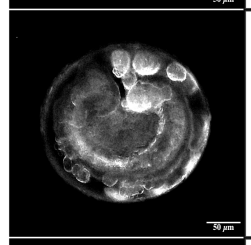	3	Day 5-6	Germ band retraction
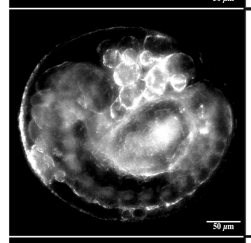	4	Day 7	Germ band segmentation and dorsal closure
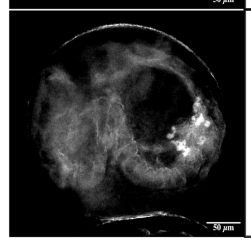	5	Day 8-9	Muscular movement

FIGURE 5.8: Timetable for *C. obscurior* embryogenesis.

5.4 DISCUSSION

This is the first description of the embryogenesis in the myrmicine ant *Cardiocondyla obscurior*. We defined five embryonic stages by using light microscopy and created a general timetable including the main developmental events (Figure 5.8). In *C. obscurior* embryonic development lasts approximately 9 days. In the following a comparison of this rough developmental scheme with the more detailed description for the myrmicine ant *M. pharaonis* is presented:

The first stage of *C. obscurior* embryogenesis (syncytial blastoderm formation, formation of germ anlage, pole cell formation) is analogous to stage four and five in *M. pharaonis* (Pontieri et al., 2020). Unlike in *D. melanogaster*, we could not observe the formation of morphological distinct pole cells (Liang et al., 1994). This is in accordance with *M. pharaonis* and suggests a conserved mechanism between *Cardiocondyla* and *Monomorium*. Stage two in *C. obscurior* is characterized by the process of gastrulation and is identical to stage six and seven in *Monomorium*. After the germ band has elongated to its maximum, the head lobes start to grow, making it possible to separate head from thorax. This we observe in both species during stage three in *C. obscurior* and stage nine in *M. pharaonis*. This is followed by the segmentation of the germ band, defining head, thorax and abdominal segments in stage four (*C. obscurior*) and stage 11 (*M. pharaonis*). In *Monomorium* the primordial germ cells are located in the last abdominal segment, similar to *C. obscurior* (Chapter 6, this thesis). Then, the germ band starts to retract at the posterior and dorsal closure begins. The head changes its position to the ventral side of the embryo and the embryo starts to move. Embryos of both *C. obscurior* and *M. pharaonis* exhibit these events during stage five and stages 15-17, respectively. Embryogenesis in both species is followed by hatching of 1st instar larvae.

While we could observe many analogous stages between *C. obscurior* and *M. pharaonis* one difference is the developmental time of the embryos. The embryogenesis in *Cardiocondyla* lasts between eight and nine days, in *Monomorium* it takes eleven days. This could be due to the rearing conditions, with temperature being an important factor. We observed that the embryogenesis of *C. obscurior* is accelerated at higher temperatures. When reared under 33 °C larvae hatch already after six days.

The urate patterns start to be visible in the fourth stage in *C. obscurior* and become more distinct with time. Pontieri et al. (2020) also found white dots in embryos of stage 15 in *M. pharaonis* and describe these as oenocytes. Whether these are actually urate crystals, as suggested for *C. obscurior* remains to be investigated. If this is the case than urate might serve a conserved role in both species and could be related to ovarian development (Chapter 4), with queen-destined embryos experiencing larger amounts of urate deposits than sterile worker-destined embryos.

Both *C. obscurior* and *M. pharaonis* belong to the same subfamily (Myrmicinae). This suggests an evolutionary conserved embryogenesis between both species. In support, we find fundamental similarities (gastrulation, germ band elongation and retraction, dorsal closure) between the embryonic development of *Cardiocondyla obscurior* and *Monomorium pharaonis*.

The embryonic development of *Cardiocondyla obscurior* is consistent with other holometabolous insects. We observed similarities between *Drosophila melanogaster* (Campos-Ortega & Hartenstein, 2013), *Tribolium castaneum* (Strobl et al., 2015), *Apis cerana* (Hu et al., 2019) and *Monomorium pharaonis* (Pontieri et al., 2020) (e.g., blastoderm formation, gastrulation, germ band elongation, dorsal closure). While *Tribolium* is a representative for short-germ-type embryos, the major embryonic stages are analogous. *C. obscurior* possesses a long-germ-type, since all body segments are formed concurrently during stage four.

Nevertheless, even when the embryonic development is highly conserved among holometabolous insects the high variation between ant species might point to unknown developmental divergences. Already differences in germline development between species exist (Khila & Abouheif, 2010; Pontieri et al., 2020; Rafiqi et al., 2020). In *Camponotus floridanus* obligate endosymbiosis between bacteria and its host lead to an altered embryogenesis (Rafiqi et al., 2020). Ant species with worker sterility also modified their germline to prevent the development of gonads, which caused another aberration of the embryonic development (Khila & Abouheif, 2010) (Chapter 6). However, these events are prior to the elongation of the germ band and unknown mechanisms are responsible for them.

This study serves to gain insight into the embryogenesis of one myrmicine ant and is a good baseline for a more detailed description. Together with nuclear staining methods and timed aging experiments a first developmental table for the embryonic development of *C. obscurior* is established. This allows to synchronize major events and identify key moments with *M. pharaonis*, ranging from early cleavage division, the cellularization of the blastoderm, to the beginning of gastrulation.

Caste determination in ants is still not understood. To disentangle the divergent developmental trajectory between reproductive (queens) and sterile non-reproductive (workers) females, a detailed description of its embryogenesis is inevitable to understand the underlying mechanisms involved. This could help to pinpoint the exact moment when the development of both castes bifurcates, and study factors involved in caste determination. One major goal would be the genetic manipulation of the embryo via RNA-interference or CRISPR to manipulate putative caste determining and differentiating major genes and pathways, such as genes involved in sex differentiation in ants (Klein et al., 2016). To successful establish these methods accurate timing of the duration of distinct embryonic stages is of the essence (Glastad et al., 2020; Rafiqi et al., 2020; Rajakumar et al., 2018). This study lays the foundation for future eco-evo-devo studies on ant phenotypic plasticity using the model *C. obscurior*.

6 CASTE DETERMINATION IN *CARDIOCONDYLA OBSCURIOR*

6.1 INTRODUCTION

Reproductive division of labor is one of the key features of eusociality (Wheeler, 1911). In ants, this has led to the development of morphological distinct castes: reproductive (queens) and non-reproductive (workers) (Sumner et al., 2018). While non-reproductives have either lost their ovaries completely, and therefore their reproductive power, or retained certain functions of their reproductive apparatus (i.e., functioning spermatheca, reduced number of ovarioles), reproductives have fully functional reproductive organs (i.e., ovaries) (Gotoh et al., 2016; Khila & Abouheif, 2010).

Even though both castes develop from the same genetic background, the development of the worker caste is plastic and allows for its adaptation depending on task and function. This phenotypic plasticity is found for example in *Eciton* with its minor and major workers (Jaffé et al., 2007) or in *Pheidole* with its supersoldier caste (Rajakumar et al., 2018). This so called caste differentiation gives rise to discrete alternative phenotypes in response to extrinsic factors like nutrition, rudimentary organs (forewing discs), temperature, pheromones or maternal genes (Jaffé et al., 2007; Miyazaki et al., 2010; Nijhout, 2003; Rajakumar et al., 2018). Contrary to caste differentiation, caste determination describes the irreversible development of a caste once it is set.

Complete worker sterility has evolved only in very few social Hymenoptera (Ronai et al., 2016). For example, in the stingless bee *Frieseomelitta varia* (Boleli et al., 1999) and in ants it is found only in eleven out of 283 genera (Heinze et al., 2006; Khila & Abouheif, 2010). The queen and worker dimorphism is based on diverging developmental trajectories, but the underlying mechanisms are not understood to this day.

Gonadal development requires the presence of primordial germ cells (PGCs). In *Drosophila* these are formed by a specialized cytoplasm at the posterior pole of the oocyte during oogenesis, the germ plasm. The germ plasm contains specific RNAs important for germ cell specification like *nanos* (*nos*), *germ cell-less* (*gcl*), *oskar* (*osk*), *polar granule component* (*pgc*) and the RNA binding proteins Vasa, Tudor, Oskar and Aubergine, which are essential for germ plasm assembly (Figure 6.1) (Becalska & Gavis, 2009; Lehmann, 2016; Mukherjee & Mukherjee, 2021; Richardson & Lehmann, 2010; Santos & Lehmann, 2004). The gene *nos* acts as a translational repressor and affects abdominal development in the embryo. This is accomplished by a localized translation of *nos*, which generates a posterior-to-anterior gradient of Nos protein that directs abdominal segmentation by repressing translation of maternal *hunchback* (*hb*) mRNA (Gavis et al., 2009). Additionally, it is important for germline development since *nos* mRNA is integrated in germ cells during their formation at the posterior of the embryo (Becalska & Gavis, 2009; Lehmann, 2016). *Nos* mRNA associated with the germ plasm is

protected from degradation (Gavis et al., 2009). This stresses the importance of *nos* to establish a functional germline in the next generation.

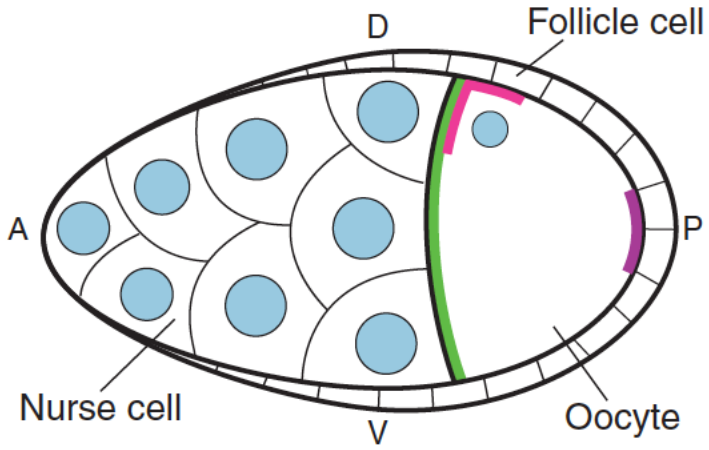

FIGURE 6.1: Germ plasm components in *Drosophila* egg chamber.
The germ plasm consists of specific mRNAs and RNA binding proteins located at the posterior pole (P) of the oocyte (purple), *bcd* (green) and *grk* (pink). Shown here during mid-oogenesis (stage 9) (Becalska & Gavis, 2009).

Besides the presence of PGCs embryonic gonads in *Drosophila* contain somatic gonadal precursor cells (SGPs). These are 20 to 25 cells of mesodermal origin and their precursors arise from a primordium encompassing parasegments 10 to 12 (Boyle & DiNardo, 1995). Parasegments (PS) are reiterated developmental units dividing the embryo into defined domains along the anterior-posterior axis. They emerge when maternal and zygotic segmentation genes (*engrailed*, *wingless*) act in a temporal cascade (Mullen & DiNardo, 1995). The abdominal region of the embryo is patterned by the homeotic genes *Ultrabithorax* (*Ubx*), *abdominal-A* (*abd-A*) and *Abdominal-B* (*Abd-B*). While *Ubx* and *abd-A* are expressed in the mesoderm during all stages of embryonic gonad formation, including parasegments 10 to 12, *Abd-B* expression is more dynamic. The strongest mesodermal expression of *Abd-B* is found in PS11 to 14. For proper SGPs specification, and to coalesce the gonads, *abd-A* is required. It restricts SGP formation to PS10 to 12 by blocking the action of *serpent* (*srp*). This gene promotes fat body development in other parasegments of the embryo (DeFalco et al., 2004). In anterior located parasegments *abd-A* is required to define gonadal cells to an anterior fate. Together with *Abd-B*, *abd-A* defines gonadal cells to a posterior fate (Figure 6.2 A). Gonadal precursors migrate actively to PS10 and are specified within the mesoderm in bilateral clusters of PS10 to 12, where they associate with germ cells. The migration of the SGPs is arrested at PS10, enabling additional SGPs to join the bilateral clusters. In the end both SGPs and PGCs coalesce into bilateral round compact gonads, composed of approximately 12 PGCs and 20 to 25 SGPs (Figure 6.2) (Boyle & DiNardo, 1995; Dansereau & Lasko, 2008). In male *Drosophila Abd-B* is necessary for specification of male-specific SGPs (msSGPs) in PS13 and restricts development of msSGPs to PS13 (DeFalco et al., 2004).

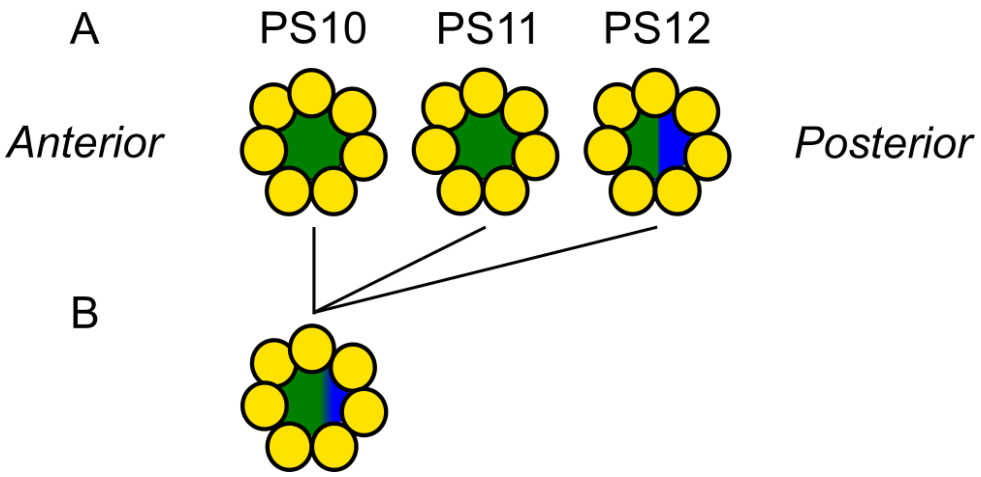

FIGURE 6.2: Schematic illustration of SGPs specification.
(A) SGPs expressing *abd-A* (green) and *Abd-B* (blue) associated themselves with germ cells (yellow) in the parasegments 10-12 at stage 11 and 12. (B) Coalesced embryonic gonad at stage 15 (adapted from DeFalco et al., 2004).

In females msSGPs are lost through programmed cell death, which is regulated by the sex determination genes *transformer* (*tra*) and *doublesex* (*dsx*). Interaction of *doublesex* and *Abd-B* has been observed in the genital disc of *Drosophila*, where they guide development in a sex-specific manner to form the proper adult reproductive system (Foronda et al., 2006; Keisman et al., 2001). This suggests that *dsx* and *Abd-B* are a conserved mechanism to promote sexual dimorphism in gonadal development in *Drosophila* as well (DeFalco et al., 2004).

Although much is known about the formation of gonads in *Drosophila* embryos there is little knowledge about how this occurs in social Hymenoptera and particularly in ants. Germ cell development has been studied in a few ant species and revealed conserved mechanism like germ plasm assembly and localization of germline genes like *nanos* and *oskar* mRNA and vasa protein at the posterior of the embryos (Khila & Abouheif, 2008; Pontieri et al., 2020; Rafiqi et al., 2020). Further downstream development has not been studied in ants. In *Drosophila* PGCs migrate actively to reach the somatic part of the gonad during gastrulation. While the germ band extends dorsally the PGCs are carried into the lumen of the invaginating posterior midgut (PMG). The PGCs loosely associate and migrate through the PMG epithelium, where they split into two groups moving laterally away from the midline, to then assemble with three bilateral clusters of SGPs in parasegment 10 to 12. During germ band retraction the resulting groups of somatic and germline cells migrate anteriorly until they coalesce into the embryonic gonad (Dansereau & Lasko, 2008). This migration process of germ and somatic cells has not yet been observed in ants but is essential because the default pathway leads to the formation of gonads in reproductives (i.e., queens and males). In *Monomorium* workers this default or ancestral pathway is interrupted through the complete loss of both germline and somatic components (Khila & Abouheif, 2010). The underlying physiological or molecular mechanisms responsible for this developmental deficiency remain elusive. Further, it is unknown whether this is the default pathway in species with complete worker sterility.

Our study reveals that embryonic gonad formation occurs during the third embryonic stage (S3, Chapter 5), 5-6 days after egg-laying, and observed embryos missing gonadal anlagen (worker-destined). We propose that during this stage the female caste in *Cardiocondyla* is determined into reproductive (queen) or non-reproductive (worker). We further found compelling evidence of the involvement of the gene *doublesex* to cause sexual dimorphism among the female castes.

6.2 Materials and Methods

6.2.1 Ants

The colonies used in this study were collected in Okinawa, Japan (Schrader et al., 2014) and Bahia, Brazil. Stock colonies were kept in square plaster-bottom nests (100 mm x 100 mm x 20 mm, Sarstedt, Germany) with plastic inserts containing three chambers covered in dark foil in a climate chamber under a 12h/12h and 22°C/26°C night/day cycle at 70% humidity. Stock colonies were provided with water *ad libitum* and fed three times a week with honey and pieces of insects (cockroaches and fruit flies).

6.2.2 Embryo collection

Embryos were collected from random stock colonies and submerged in a dissection dish containing PBT (0.3 %). The embryos were visually classified into their respective stage, according to the previously described embryogenesis (Chapter 5). The sorted embryos were then used for in situ hybridization.

6.2.3 Whole mount In situ hybridization

Fluorescent in situ probes were designed against the germline gene *nanos*, the female-specific splice form of *doublesex* (*dsxF*) and *Abdominal B* (*Abd-B*) using the custom available Stellaris® RNA FISH Probe Designer (Biosearch Technologies, Inc., Petaluma, CA) available online at www.biosearchtech.com/stellarisdesigner. *DsxF* mRNA was labeled with Quasar® 570, *nanos* mRNA with Quasar® 670 and *Abdominal B* with CAL Fluor® Red 610 dye (Table S 2). The Stellaris® protocol for *Drosophila* embryos was adapted to our ant species *Cardiocondyla obscurior* (Chapter 10.2.2). The original protocol is available online at www.biosearchtech.com/stellarisprotocols.

6.2.4 Immunofluorescence and Image Analysis

Images for in situ hybridization were visualized using a Zeiss LSM 880 and LSM 980 with Airyscan 2 laser scanning microscope under 40x objective lenses. Images were then processed using the open source platform Fiji (Schindelin et al., 2012) and the software ScientiFig (Aigouy & Mirouse, 2013).

6.3 RESULTS

We wanted to investigate at what exact time point queen and worker embryos diverge in their embryonic development. Adult workers in *C. obscurior* are sterile and therefore miss reproductive organs. In embryos the presence of germ cells is essential for the formation of gonads. During their embryonic development worker-destined embryos deviate from the ancestral state by losing the germline through unknown developmental processes (Chapter 4).

Abdominal-B (*Abd-B*) is a homeotic gene that specifies the posterior identity of somatic gonadal precursor cells (SGPs) and is therefore important for the formation of the somatic gonads in *Drosophila melanogaster* (Boyle & DiNardo, 1995; DeFalco et al., 2004). The high conservation of this gene among insect taxa raises the question if the pathway is conserved in our ant species.

We performed whole-mount fluorescent in situ hybridization (wmFISH) on embryos to address this question.

6.3.1 EXPRESSION OF GERM CELLS IN EARLY S3 EMBRYOS

In the first embryonic stage (S1) the amniotic fold and the germ plasm (gp) are localized at the posterior pole of the embryo (Figure 6.3 A). The second stage (S2) is defined by the gastrulation of the germ anlage. The progenitors of the germ cells, the pole cells (pc), are found at the posterior pole of the embryo (Figure 6.3 B) (Lerit & Gavis, 2011). To study the embryonic gonadal development, the first two stages are timed to early, since the germ band has not elongated yet. Hence, we focused on the following embryonic stages starting with S3.

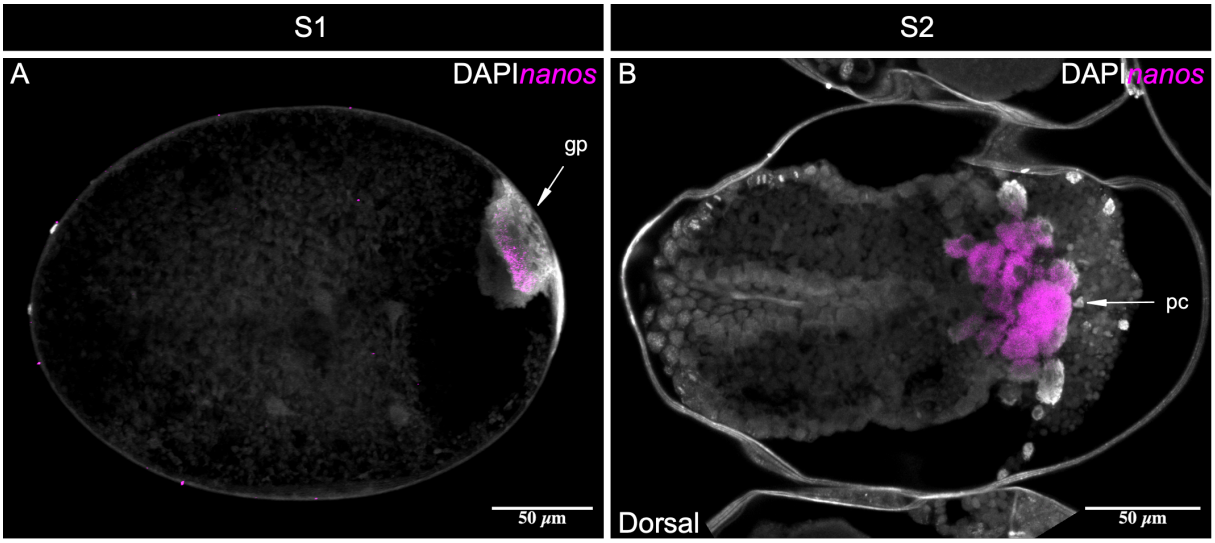

FIGURE 6.3: Early-stage embryos expressing maternal determinants.
(A) Stage 1 embryo with the germ plasm (gp) located at the posterior pole. (B) Stage 2 embryo with pole cells (pc) (dorsal view). Both embryos express *nanos*. Cell nuclei are stained with DAPI.

To follow germ cell development in embryos, we used specific fluorescent probes targeting *nanos* mRNA. *Nanos* is expressed in large cells at the posterior pole of S3 embryos (Figure 6.4 C, D). This is in agreement with earlier findings in other ant species (Khila & Abouheif, 2010; Pontieri et al., 2020; Rafiqi et al., 2020), but provides for the first time a detailed high-resolution image of the germ cell population harboring the posterior abdomen. We observed a population of *Abd-B* expressing cells located in the midgut of the embryo (Figure 6.4 B, D), located outside of the germ band.

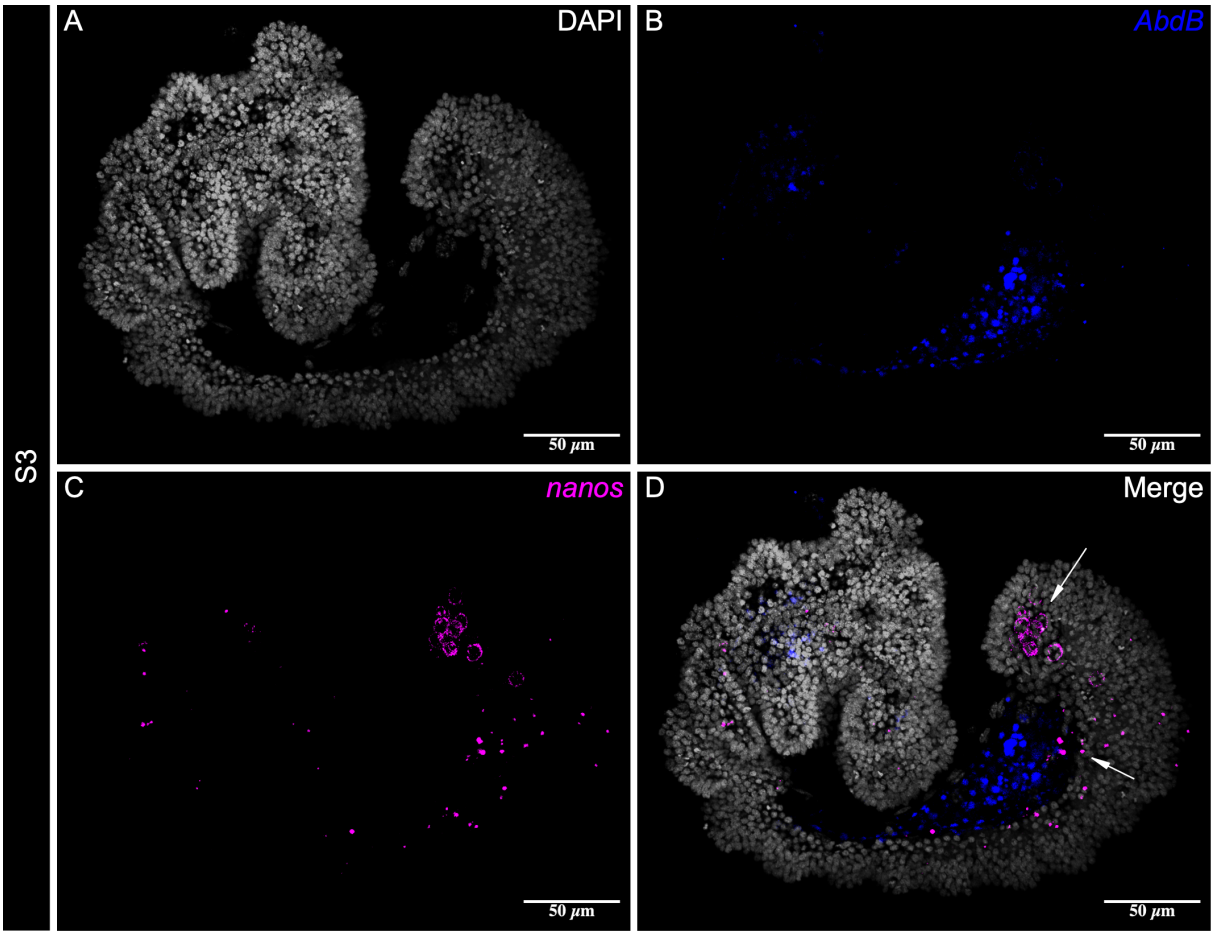

FIGURE 6.4: *Nanos* and *AbdB* are expressed in early-staged S3 *C. obscurior* embryos.
(A) Stage 3 embryo counterstained with DAPI against cell nuclei. (B) *Abd-B* mRNA expression is located outside the germ band. (C) *Nanos* mRNA is expressed at the posterior pole of the embryo. (D) Single germ cells migrate through the embryo (arrows).

6.3.2 *Abd-B* specifies populations of SGP cells

In late-staged S3 embryos the former distributed cells expressing *Abd-B* located in the midgut have now formed three separate cell clusters located posteriorly in the embryo. In *Drosophila* similar cell clusters can be found and are called parasegments (PS) and are located in the abdominal segments 10 through 13 (PS10-13) (Boyle & DiNardo, 1995; Chapman et al., 2013) (Figure 6.5 A, white arrows). Analogously to *Drosophila*, the expression of *Abd-B* in these cells indicate their somatic origin in *C. obscurior* embryos. Together with germ cells (Figure 6.5 B, white arrows) these SGPs coalesce into the precursors of the embryonic gonad (Boyle & DiNardo, 1995; Chapman et al., 2013).

In the third embryonic stage a minority of somatic and germ cells have not migrated to their respective destination and are located anteriorly of the midgut (Figure 6.5, red arrows).

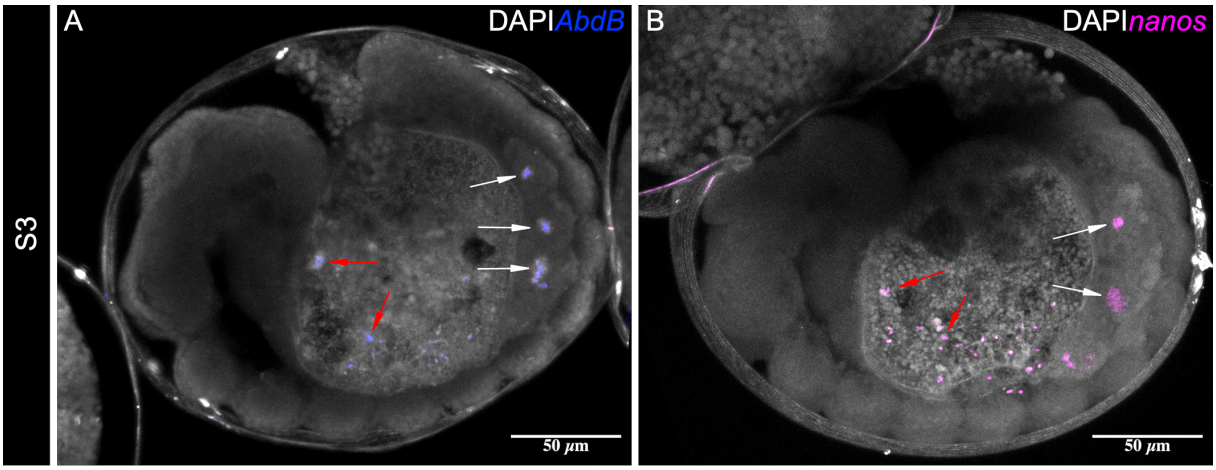

FIGURE 6.5: *Abd-B* is required for specification of SGPs.
(A) *Abd-B* is expressed in cluster of cells resembling parasegments (white arrows), indicating SGPs. (B) Germ cells expressing *nanos* are found in the same parasegments, coalescing with the SGPs (white arrows). The red arrows indicate cells that appear to migrate posteriorly towards the parasegments.

6.3.3 Expression of germ cells in S4 embryos

In stage four the embryos undergo dorsal closure and the segments become more distinct. The former embryonic gonadal precursors observed in late-stage S3 embryos co-expressing *Abd-B* and *nanos* (Figure 6.5) have merged into one larger cluster enclosing the last abdominal segments (Figure 6.6 B, C, D). These resemble a cloud-like structure surrounding the area where the clusters have merged.

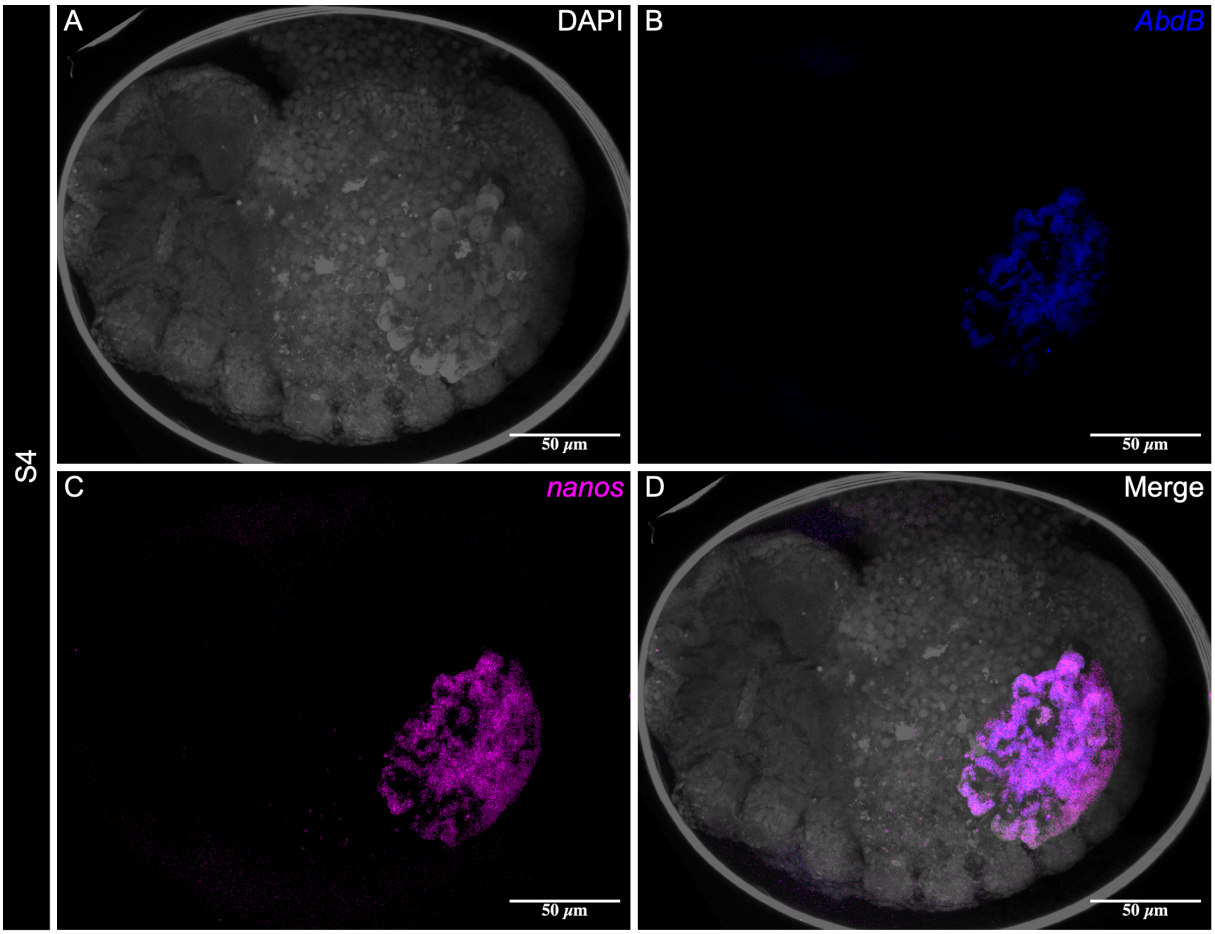

FIGURE 6.6: Co-expression of *Abd-B* and *nanos* in S4 staged embryos.
(A) Stage 4 embryo counterstained with DAPI against cell nuclei. (B) Cluster of cells expressing *Abd-B*. (C) Germ cells expressing *nanos*. (D) The merged parasegments co-express *Abd-B* and *nanos*.

6.3.4 Expression of germ cells in S5 embryos

The larger cluster co-expressing *Abd-B* and *nanos* has now been shaped into two distinct bilateral cell aggregations located posteriorly in the embryo (Figure 6.7 D, arrows). Later, they will give rise to the larval gonads in the hatched larvae (Figure 4.4, Chapter 4). The expression of both *Abd-B* and *nanos* mRNA in this stage is significantly weaker compared to stage four embryos (Figure 6.6). Apparently, mRNA is being degraded after the embryonic gonads localize at their correct destination.

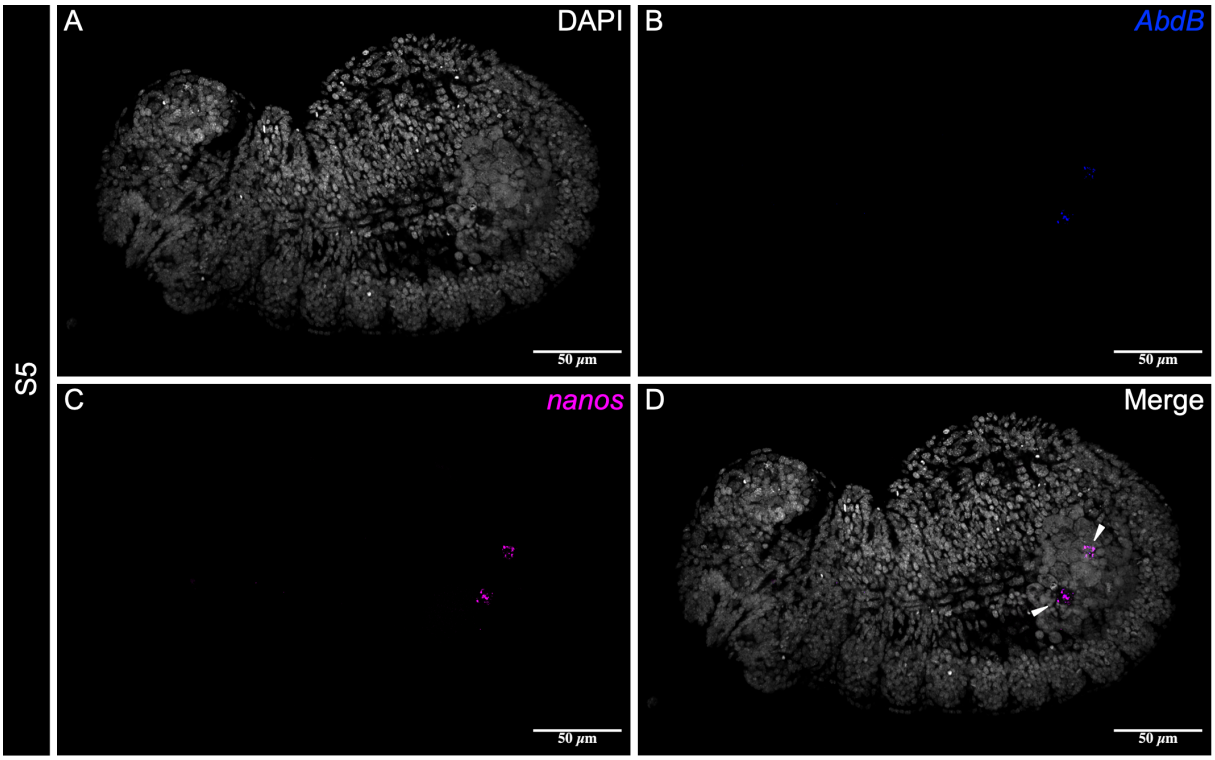

FIGURE 6.7: Embryonic gonad formation in S5 embryos.
(A) Stage 5 embryo counterstained with DAPI against cell nuclei. (B) Expression of *Abd-B* marking SGPs. (C) Germ cells expressing *nanos*. (D) The embryonic gonads coalesced into two distinct cell clusters co-expressing *Abd-B* and *nanos* (arrows).

6.3.5 INTERRUPTION OF EMBRYONIC GERMLINE DEVELOPMENT IN *C. OBSCURIOR* WORKERS

In *C. obscurio*r we observed two types of embryos. Queen-destined embryos with developing embryonic gonads (Figure 6.8 A, C, E) and worker-destined embryos lacking germ cells and SGPs. In the latter we detected no gonadal development (Figure 6.8 B, D, F). We were not able to observe the absence of germ and somatic gonadal precursor cells in first and second stage embryos (Figure 6.1).

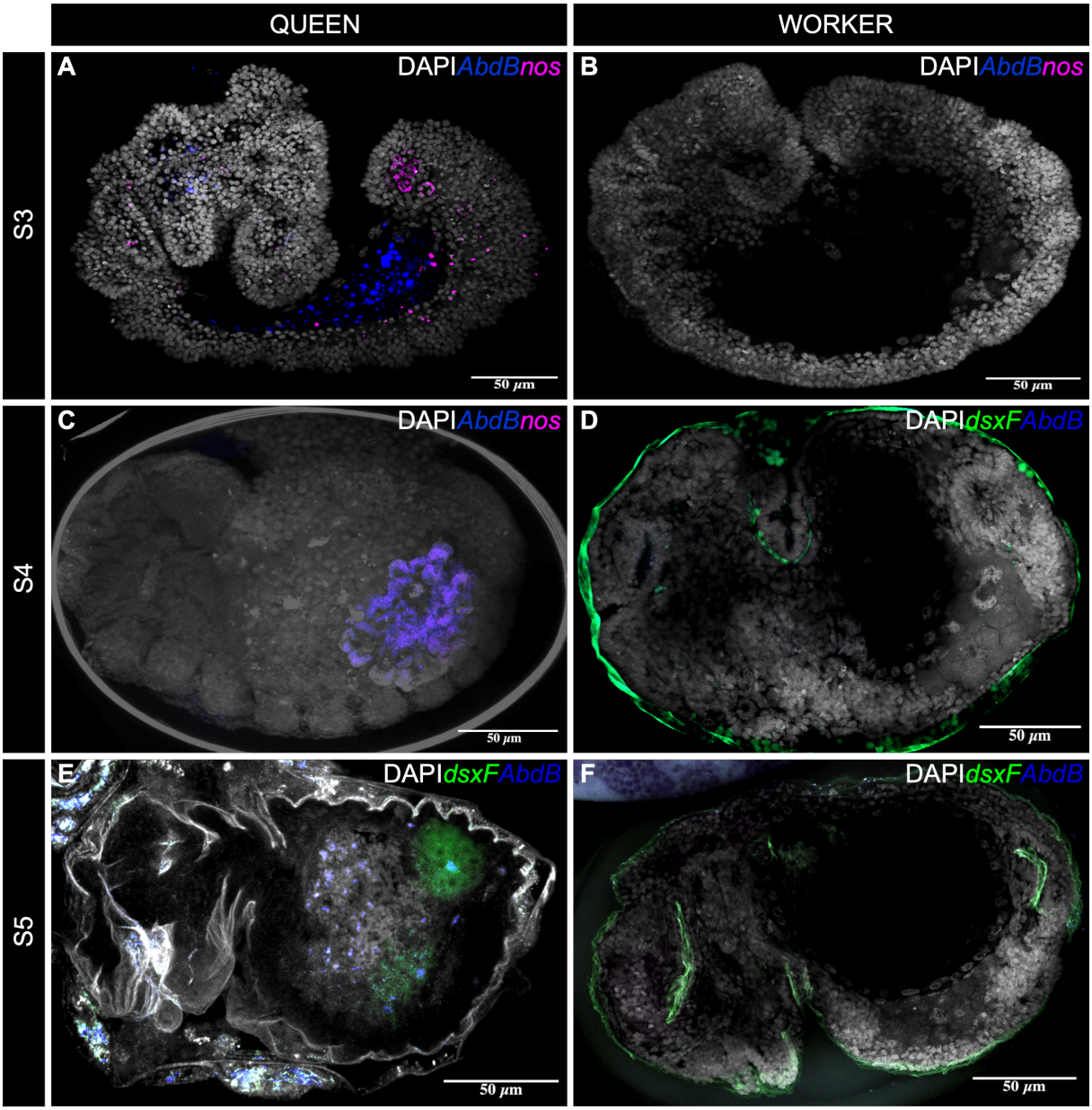

FIGURE 6.8: Embryonic gonadal development in queen- and worker-destined embryos.
Embryos of different stages stained against *nanos* mRNA to visualize germ cells, *Abd-B* to visualize SGPs and *dsxF* to picture female-specific sex determination. (A) S3 queen-destined embryo expressing *nanos* and *Abd-B*. (B) S3 worker-destined embryo with absence of *nanos* and *Abd-B* staining. (C) S4 queen-destined embryo with coalescing germ cells and SGPs. (D) In S4 worker-destined embryos neither *Abd-B* nor *dsxF* is expressed. (E) S5 queen-destined embryo with *Abd-B* expressing SGPs with female-specific identity, shown through expression of *dsxF*. (F) S5 worker-destined embryo with absence of SGPs.

6.3.6 *DOUBLESEX* REGULATES SGP IDENTITY

To investigate when sexual dimorphism is first observed in the embryonic gonadal development, we analyzed expression of sex-specific *doublesex* isoforms. We noticed that the embryonic gonads display sex-specific expression of *dsx* in somatic cells: In particular the female-specific isoform *dsxF*. In stage four embryos, cells positive for *dsxF* co-localize with somatic gonadal precursor cells expressing *Abd-B* (Figure 6.9 A, white arrows). This becomes more distinct in S5 embryos, where the embryonic gonads have arranged in a bilateral manner. There, the cells marking the somatic gonadal precursors by *Abd-B* expression are found located in the center of the embryonic gonads (Figure 6.9 B, yellow arrows).

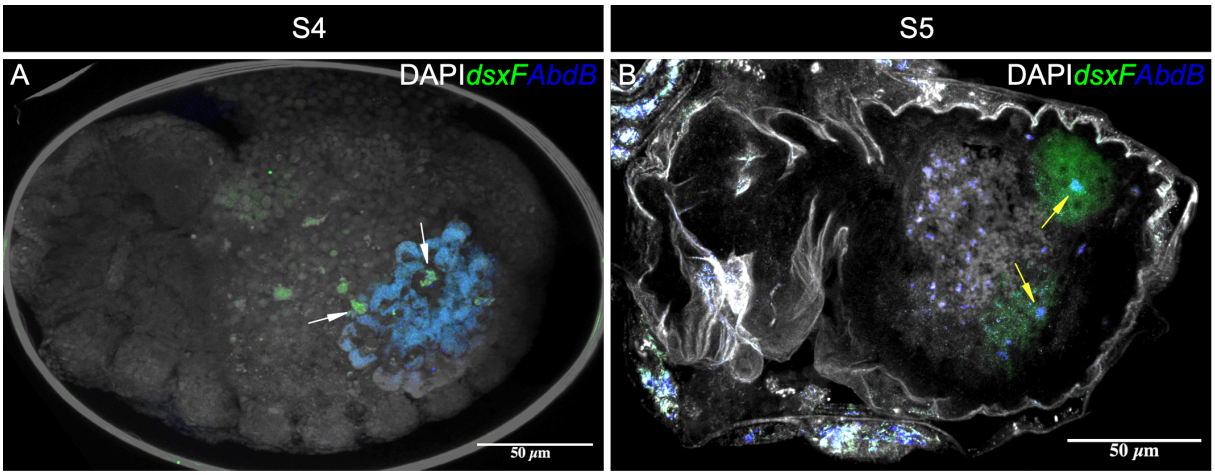

FIGURE 6.9: Sex-specific regulation of SGPs in embryos.
(A) Stage 4 embryo expressing the female-specific isoform of *doublesex* (*dsxF*) in SGPs (white arrows). (B) Stage 5 embryos co-expressing *dsxF* and *Abd-B* in the embryonic gonads (yellow arrows).

In addition, to study female-specificity of somatic cells, we stained against the male-specific isoform of *doublesex* (*dsxM*). We observed a co-localization of *dsxF* and *dsxM* transcripts in SGPs in S3 embryos (Figure 6.10 A, arrows). The expression of both isoforms is restricted to the abdominal regions containing the precursors of the embryonic gonad. This suggest that the sexual identity of the somatic cells is already set in stage 3 embryos. We further detected the transcripts of both isoforms in S4 embryos, where they co-localize with the estimated coalesced embryonic gonad (Figure 6.11 D, arrow).

The co-expression of both sex-specific isoforms of *doublesex* in the SGPs suggest that the embryonic gonads are sex mosaics. Additionally, we find cells co-expressing *dsxF* and *AbdB* (Figure 6.9 A) and *dsxF*/*dsxM* respectively (Figure 6.11). These cells are located around the midgut and are possibly PGCs that failed to migrate to the posterior segments of the abdomen.

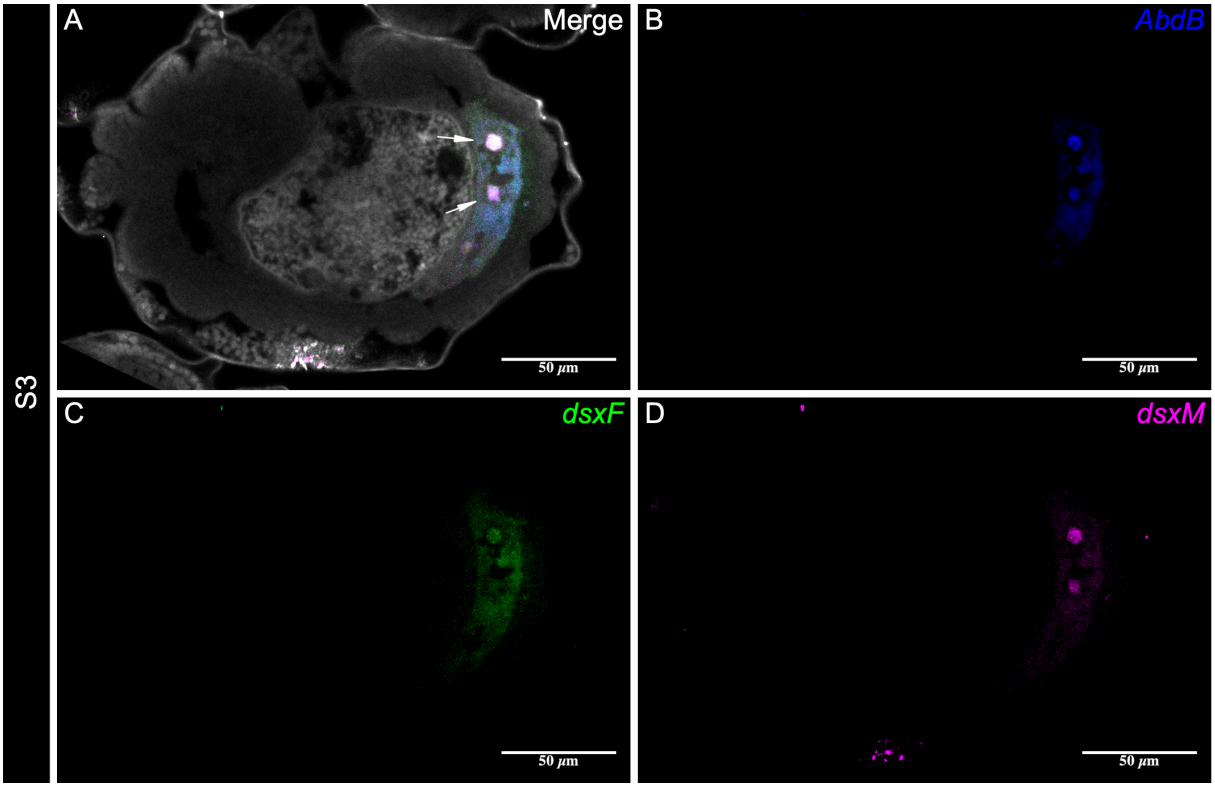

FIGURE 6.10: Co-expression of *dsxF* and *dsxM* isoforms in SGPs in S3 staged embryos.
(A) Stage 3 embryo co-expressing both sex-specific isoforms *dsxF* and *dsxM* in SGPs (arrows). (B) *Abd-B* expression marking SGPs. (C) Expression of the female-specific isoform of *doublesex* (*dsxF*). (D) Expression of the male-specific isoform of *doublesex* (*dsxM*). Grey = DAPI.

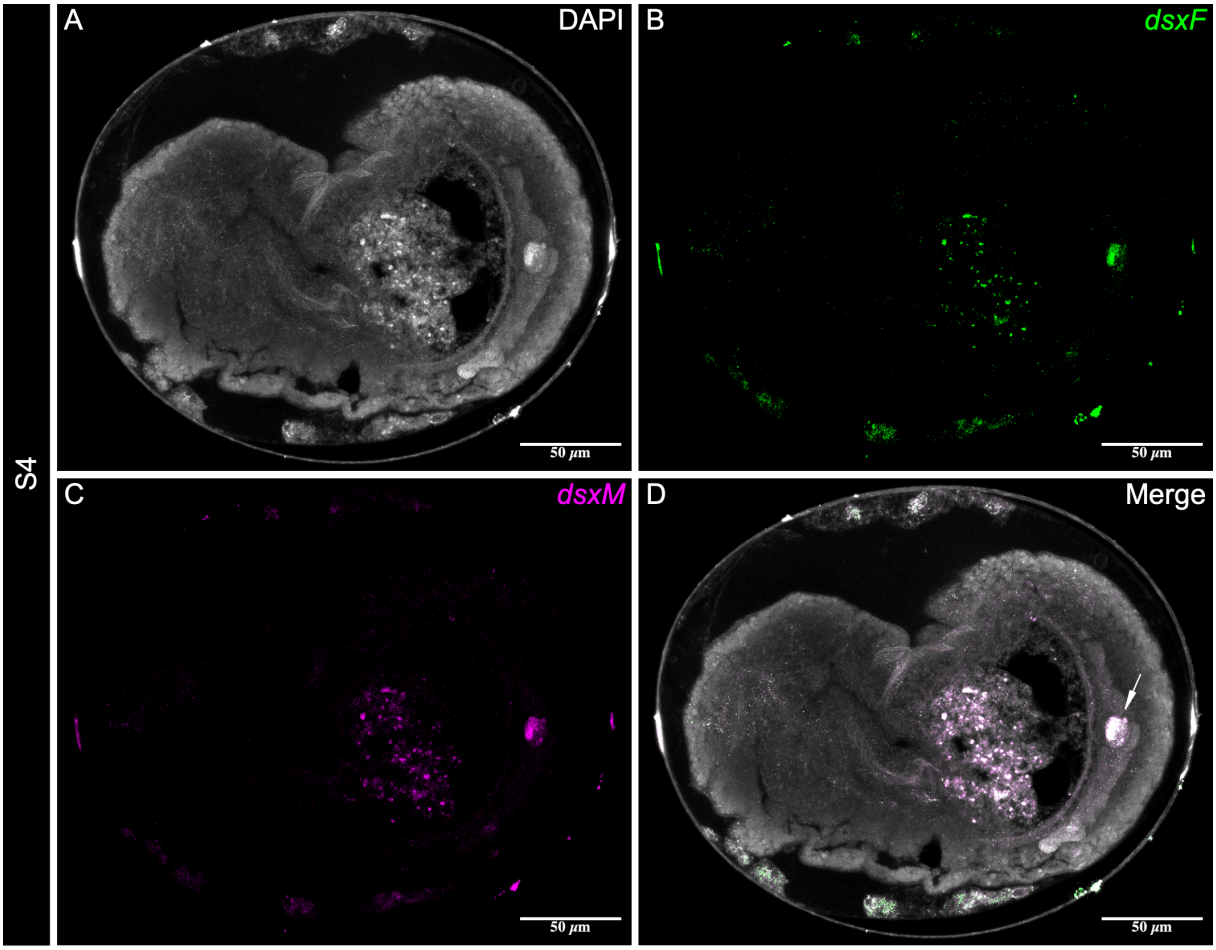

FIGURE 6.11: Co-expression of *dsxF* and *dsxM* isoforms in SGPs in S4 staged embryos.
(A) Embryo stained against cell nuclei. (B) *dsxF* expression in the posterior abdomen, marking SGP. (C) Expression of *dsxM*. (D) Stage 4 embryo co-expressing both sex-specific isoforms *dsxF* and *dsxM* in the coalesced embryonic gonad (arrow).

6.4 Discussion

We identified five distinct embryonic stages in *Cardiocondyla obscurior*. These contain prime developmental events and give a general overview over its embryogenesis (Figure 5.8). Even though the recently described embryogenesis in *Monomorium pharaonis* is more detailed (with 17 embryonic stages) (Pontieri et al., 2020), our description serves as a good basis to select live embryos and sort them according to their respective stage with standard available microscopes.

Our results indicate that the embryonic gonads develop during their third embryonic stage. We observed three clusters of somatic gonadal precursor cells (SGPs) resembling parasegments (PS) 10 to 13 as seen in *Drosophila* (Boyle & DiNardo, 1995). The homeotic gene *Abd-B* localizes these clusters to the PS10 to 12 in *Drosophila* females and in males specifies an additional cluster of male-specific SGPs (msSGPs) to PS13. Our findings suggest a similar mechanism for the spatial orientation of the SGPs clusters in the posterior abdominal segments, in which *Abd-B* acts as an organizer to localize the SGPs to this region.

We used in situ probes against *nanos* (*nos*) to localize the primordial germ cells (PGCs) in early S3 embryos at the germ band posterior. This resembles germ cell specification in *Drosophila* during stage 10 in which the PGCs migrate from the midgut to the mesoderm (Dansereau & Lasko, 2008; Santos & Lehmann, 2004). In *C. obscurior* somatic and germ cells are located in the midgut in late S3 embryos.

In *Drosophila* germ cells migrate actively. Responsible are repellents like the phospholipid phosphatases Wunen and Wunen2 which express repulsive cues for the PGCs. Contrarily, Hedgehog (Hh) and 3-hydroxy-3-methylglutaryl coenzyme A (HMG-CoA) reductase (Hmgcr) are attractants. Both Hh and Hmgcr are expressed by SGPs and guide the PGCs towards them (Dansereau & Lasko, 2008). Missing either one of these repellent or attractant signals could lead to a mis-localization of PGCs and SGPs resulting in an imperfect gonad formation.

As described in *Drosophila* the three clusters of SGPs coalesce with the PGCs to shape into a round compact gonad in later stages (Dansereau & Lasko, 2008). We observe the same process during our embryonic development, indicating that this is a conserved mechanism and found throughout insect taxa. During the fourth stage we noticed high expression of mRNA for both *nos* and *Abd-B* in the coalesced gonad. These findings point to the question if the process of gonad formation either requires high gene activity or is the result of large amounts of transcript through the fusing process of three separate clusters containing PGCs and SGPs. The spatial regulation of both *abd-A* and *Abd-B* is necessary to position the embryonic gonad to a specific abdominal segment (DeFalco et al., 2004). The high levels of *Abd-B* could serve as an explanation for this observation.

As embryogenesis continues so does the development of the gonads. In S5 embryos the gonads have formed bilateral groups of cells, which is in accordance to *Drosophila* embryos in stage 14 (Santos & Lehmann, 2004). After the embryo hatches the gonadal development continues in larvae, resulting in three ovarioles per ovary.

The sex differentiation pathway is regulated by the gene *doublesex* (*dsx*) to control morph-specific development (Klein et al., 2016). It produces sex-specific transcription factors through alternative splicing of its transcripts. The resulting sex-specific isoforms are important for tissue-specific identity in males and females. This is the case for the genital disc in *Drosophila*. Depending on the expressed isoform either male or female reproductive organs are developing (Chatterjee et al., 2011). The hypothesis is that caste development adopted the pre-existing machinery that produces two sexes to direct morph-specific development in eusocial insects (Klein et al., 2016). To gain insight into the *doublesex* pathway we used in situ probes targeting the female- (*dsxF*) and male-specific (*dsxM*) isoforms of *dsx* to reveal sex-specific tissue in the embryo. We found a physical interaction with the SGPs during the third embryonic stage. To our surprise the SGPs express both isoforms, making the embryonic gonad a sex mosaic. This has been observed in *Drosophila*, where specific tissues experience the expression of both isoforms, giving them the ability to sexually differentiate (Robinett et al., 2010). Why *dsxM* is expressed in the embryonic female gonad is unclear.

One possibility could be a putative feedback-loop, with *dsx* acting downstream of Abd-B. In *Drosophila* it has been observed that *Abd-B* and *dsx* are capable of physically interacting with each other through their highly conserved homeodomain (HD) and *doublesex-mab3* (DM) domain (Ghosh et al., 2019). This suggest that Abd-B and *dsx* are possibly acting as co-regulators and regulate themselves. In this feedback-loop dsxF acts as a repressor for Abd-B and dsxM up-regulates Abd-B, resulting in a dimorphic expression of both *dsx* and Abd-B (Figure 6.12).

The interaction and regulation of sex-specific *dsx* transcripts seems to be conserved throughout the insect taxa. Isoform-specific function of *dsx* has been linked to tissue-specific expression in wings of the butterfly *Papilio*, resulting in wing polymorphism (Deshmukh et al., 2020). In the dung beetle *Onthophagus sagittarius dsx* functions to regulate sex-specific development of horns. It is promoted by *dsxM* in large males, while *dsxF* inhibits horn formation in females (Kijimoto et al., 2012).

In the developing central nervous system (CNS) of *Drosophila* the interaction of Abd-B and *dsxF* causes sex-specific transcriptional activation of the RHG family of apoptotic genes *grim* and *reaper* to generate sexual dimorphism. Furthermore, *dsx* has been linked to the hox gene *Abd-B* to regulate sex-specific abdomen morphology. During pupal development the Hox protein Abd-B regulates the transcription of *dsx*. In the posterior abdomen dsx and Abd-B are responsible for dimorphic changes like segment

number, abdominal cuticle pigmentation and sex combs morphology. The expression of *dsx* in the abdomen is sexually dimorphic, with expression higher in males than in females (Wang & Yoder, 2012).

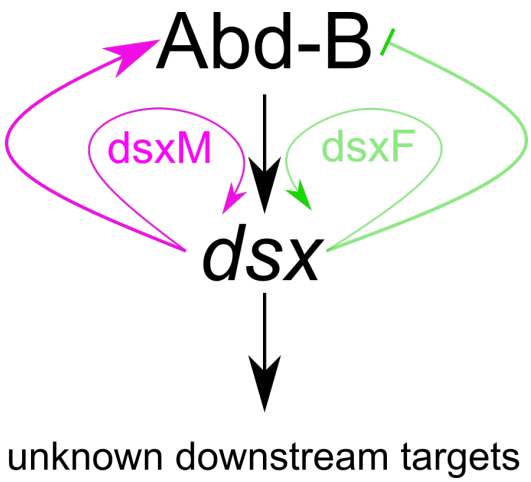

FIGURE 6.12: Putative feedback-loop regulating Abd-B expression.
DsxM activates Abd-B, while dsxF represses it. Higher levels of dsxM promote *dsx* expression, which acts on unknown downstream targets (adapted from Yan, 2015).

Using this putative feedback-loop the expression of both *dsx* isoforms in the embryonic female gonad could serve as a hypothetical explanation for the divergent developmental trajectory of reproductives (queens) and non-reproductives (workers) in our ant species. Klein et al. (2016) demonstrated sex- and morph-specific expression of *dsx* in *Cardiocondyla obscurior*. Workers express less *dsxM* than queens and in contrast, queens express less *dsxF* than workers during their pupal stage. If more *dsxF* transcript is expressed in workers, the feedback-loop could lead to a repression of Abd-B. The missing spatial signal in the posterior segments would manifest in a defective localization of SGPs and prevent the somatic cells from settling in the accurate parasegments. This would ultimately prevent the gonads from coalescing during the third embryonic stage. The embryos resulting from this mis-localization of SGPs would be workers without the presence of reproductive organs (i.e., sterile) (Figure 6.13).

One of the major challenges to establish a working in situ protocol is the removal of the chorion and vitelline membrane protecting the embryo against physical trauma and desiccation. Fluorescent in situ hybridization probes target RNA transcripts using antisense RNA labelled with a fluorescent dye (Lécuyer et al., 2008). They are used to study target genes to understand their function and spatial distribution in fixed tissue. The chorion prevents the penetration of these probes and therefore needs to be removed to be able to detect strong enough fluorescent signals. In *Drosophila* the chorion and vitelline membrane can be easily removed by using for example chlorine-based chemicals or mechanically through sonication (Manning & Doe, 2017). In our ant species the chorion and vitelline membrane proved to be rather thick and stable and made it nearly impossible to be removed by chemicals or sonication. This might be due to the arboreal lifestyle of *C. obscurior*, inhabiting tree

branches and living in tropical areas with high humidity, causing the evolution of its thick chorion and vitelline membrane. Previous studies on larger ants established a working protocol by removing the chorion manually using fine forceps (Abderrahman Khila & Abouheif, 2009; Rafiqi et al., 2011). The eggs of *C. obscurior* are rather small with an average length of 250 and width of 185 µm (Eva Schultner, personal communication). Removing the chorion and vitelline membrane mechanically will prove to be a major challenge in the future but is inevitable to achieve adequate signal strength for in situ probes.

In addition, this approach will be necessary to stain the embryos better against cell nuclei using DAPI. The idea is to build on chapter five of this thesis to stage the embryos in more detail as seen in *Monomorium pharaonis* to create an accurate developmental table (Pontieri et al., 2020).

This work provides the first description of gonad formation in embryos in the myrmicine ant *Cardiocondyla obscurior*. The developmental divergence between queen and worker caste occurs prior to the third embryonic stage. The co-regulation and interaction of the sex-specific isoforms of *doublesex* with the hox gene *Abd-B* is a conserved mechanism to create sexual dimorphism and determines caste fate in this species. Future research is needed to disentangle this developmental process and answer the question of whether caste is determined in much earlier stages of embryogenesis. Here we present evidence of an interaction of *Abd-B* and the sex-specific transcripts of *doublesex* to regulate embryonic female gonad formation in queen and worker S3 embryos.

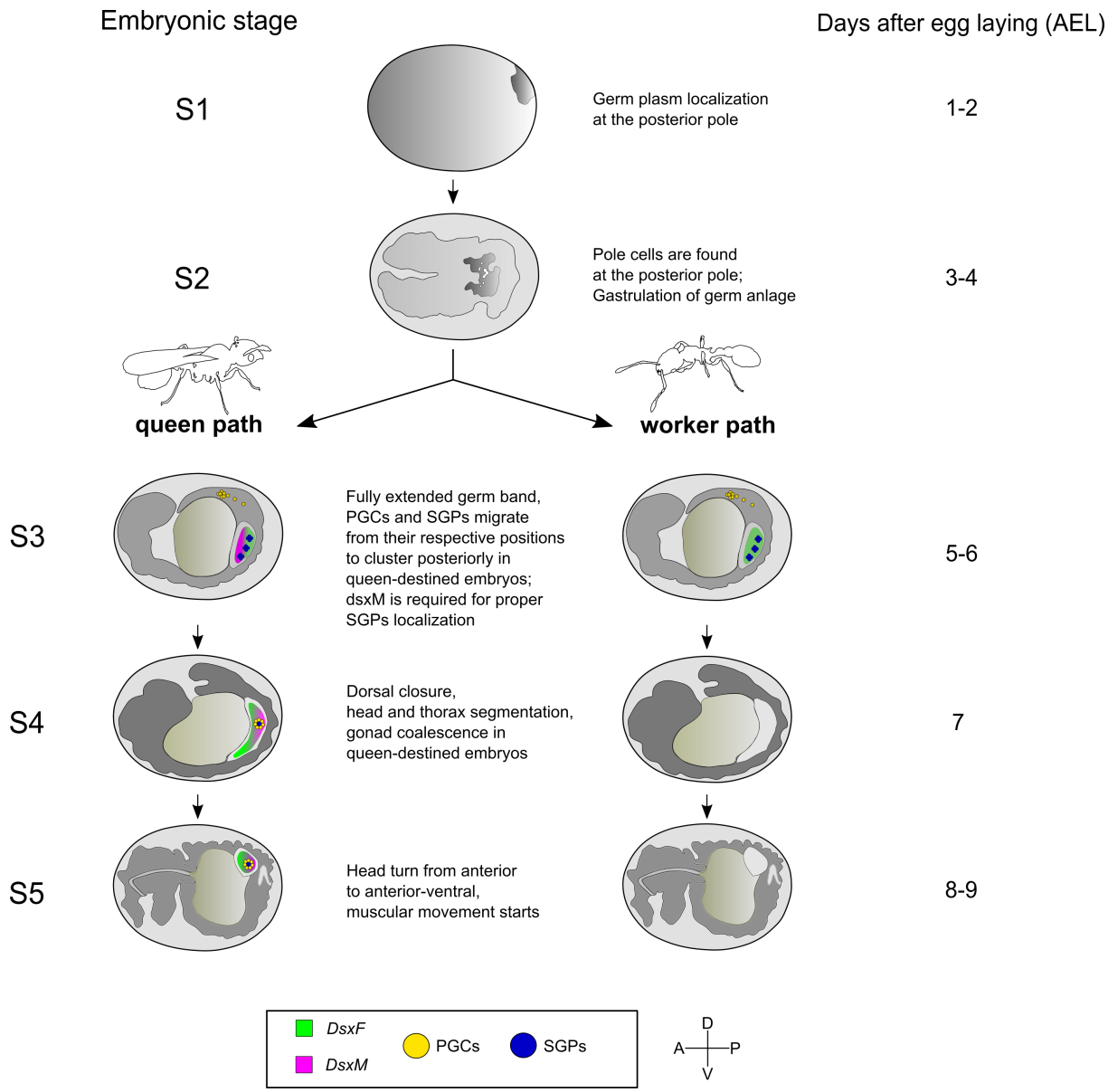

FIGURE 6.13: Putative model pathway of queen- and worker-destined development in embryos.
After S2 the development between queen and worker diverges. In the queen path gonads form through the presence of SGPs, PGCs and dsxM. In the worker path the absence of the latter leads to a mis-localization of SGPs and gonad formation. This results in sterile workers.

7 SUMMARY AND FUTURE DIRECTIONS

One of the key features of eusocial Hymenopterans is based on reproductive division of labor. Wheeler understood queens as “germline” and workers as “soma” (Wheeler, 1911) pointing out their major differences but also their co-dependency. Without this clear separation superoganismality would have never evolved.

Social Hymenoptera have been studied for decades, yet caste differentiation and caste determination remain largely black boxes. Worker development in ants is plastic, reaching a high degree of specialization and therefore resulting in different phenotypes (e.g., soldiers and minor workers in *Pheidole* (Rajakumar et al., 2018)). In contrast, queen development is fixed. Understanding the developmental bifurcation of queen and worker caste is crucial to gain insight into the different behavior of castes, as well as different reproductive tactics and colony organization (Corona et al., 2016; Kuhn et al., 2018; Wilson, 1980).

In chapter four a visible morphological difference between the queen and worker caste in the larval stage of *Cardiocondyla obscurior* is described. Large clusters of white deposits in a bilateral ventral manner right below the meconium were observed in some larvae. These were missing in others and instead were spread randomly in the posterior abdomen. In larvae with paired clusters, we discovered developing ovaries. The white deposits are likely urate crystals, serving a yet unknown purpose, maybe related to ovarian development.

The same pattern observed in *C. obscurior* was found in its sister species *C. wroughtonii*, as well as the more distantly related C. *venustula* and *C. nuda*, suggesting a conserved mechanism. In *C. elegans*, *C. minutior, C. thoracica* and *C. argyrotricha* we failed to observe paired cluster of urates. If this is due to a seasonal effect since some species produces sexuals only during a brief time window during the year, remains to be investigated. To confirm this hypothesis larvae need to be monitored prior to the estimated eclosion of adult sexuals.

The presence of urate is not restricted to the species *Cardiocondyla* alone. We found urate patterns in species in most subfamilies, ranging from the major groups Formicidae, Dolichoderinae, Ponerinae and Myrmicinae to the more exotic Amblyoponinae, Ectatomminae and Pseudomyrmecinae (Chapter 4). Surprisingly, even though urate seems to be omnipresent in all these species, their exact function remains elusive, even though their presence points to a highly conserved function across the family of Formicidea. Whether urate is linked to nutrition, symbiotic bacteria, cuticular hydrocarbon profiles (i.e., important for nestmate recognition) or is involved in yet unknown functions, remains to be investigated.

Previous work described a general time frame for the development of queens and workers in *C. obscurior* (Schrempf & Heinze, 2006). The now possible distinction of caste as early as the 1st larval instar allowed for creating a detailed survey of developmental time for each caste. To this end, we set up single egg colonies and monitored their development until eclosion (unpublished data).

To understand caste differentiation better the selective caste-dependent manipulation of larvae is one possibility. In particular the genetic manipulation of target genes through the RNAi mediated gene silencing complex. RNAi has been successfully established in the fruit fly *Drosophila*, the flour beetle *Tribolium castaneum* (Lee et al., 2004; Tomoyasu & Denell, 2004) and as the representatives of social Hymenoptera the honey bee and the carpenter ant *Camponotus floridanus* (Glastad et al., 2020; Maori et al., 2019). Previous studies successfully established protocols for administering RNAi to *C. obscurior* larvae by using either a micromanipulator for injection or by feeding (Ermer, 2020; Hacker, 2019; Haller, 2020). The manipulation of embryos requires the establishment of an injection protocol, which is pending. The ability to manipulate embryos and larvae on the genetic level will help to gain deeper insight in regulatory pathways involved in development and create phenotypes to study caste-polyphenism in our ant species.

The detailed developmental survey as well as the genetic manipulation can help to gain more insight into the diverging developmental trajectory of the female caste in *C. obscurior*.

A further question addressed is whether urate patterns distinguishing queen from worker larvae are already visible in embryos. Indeed, the same patterns located in larvae can be observed in embryos (Chapter 4 and 5). The inability to stage the embryos correctly due to a missing documented embryogenesis, led us to an initial description thereof and is addressed in chapter five of this thesis. We classified embryogenesis in five stages, covering the main developmental events. In the fourth embryonic stage urate patterns start to be visible and become more distinct until the fifth stage, mirroring the larval patterns. This suggests that caste determination already occurs during embryogenesis. The ability to distinguish queen- from worker-destined embryos allow for their selective collection and use them for further studies. One intriguing possibility is to study microRNAs (miRNAs) in early embryos, which are involved in post-transcriptional regulation of gene expression. Sequencing miRNAs (miRNA-seq) will permit to examine tissue-specific expression patterns and study their involvement in the regulation of many developmental and biological processes. This approach would help to answer if miRNAs are maternally provisioned and therefore determine caste in *C. obscurior* in early embryos (unpublished data).

In chapter six we performed whole-mount in situ hybridization on embryos targeting germline genes and genes necessary for the development of the somatic structures of the gonads. We found an interaction between the gene marking somatic gonadal precursor cells (SGPs) *Abd-B* and the sex differentiation gene *doublesex* (*dsx*). The interplay of *Abd-B* with the sex-specific isoforms of *doublesex* (*dsxF* and *dsxM*) are important for spatial orientation of the SGPs to the posterior segments in the abdomen and allow for correct coalescence of the germ cells with the SGPs to form the embryonic female gonads. This process occurs in the third embryonic stage.

Localization of the primordial germ cells (PGCs) at the posterior of the embryo has also been observed in other species like in the silkmoth *Bombyx mori*, the pea aphid *Acyrthosiphon pisum* and in the ant species *Monomorium pharaonis* (Chang et al., 2006; Nakao et al., 2008; Pontieri et al., 2020). During the same embryonic stage germ cells can be found at the same position in the abdomen in both *Monomorium* and *Cardiocondyla* (Pontieri et al., 2020). Surprisingly this is not the case when compared to other ant species. In *Lasius niger* and *Camponotus floridanus* germ cells are located outside of the embryo but are still in close proximity to the posterior end of the abdomen. Both *Lasius* and *Camponotus* belong to the subfamily of Formicinae, while *Cardiocondyla* and *Monomorium* are part of the subfamily of Myrmicinae. These two subfamilies have diverged millions of years ago and apparently so did their localization of germline cells. Additionally, *Camponotus floridanus* experiences an alteration in the development of its germline during embryogenesis due to its obligate endosymbiosis with the bacteria *Blochmannia*. This is not the case in *Lasius*, where this bacterium is missing (Rafiqi et al., 2020). The similarities between *Cardiocondyla* and *Monomorium* in their germ cell localization could be explained by their close evolutionary relatedness and reproductive division of labor (DOL) since both species are polygynous (multiple queens) and experience worker sterility. In contrast to *Camponotus* and *Lasius* which are monogynous (single queens) and workers have reproductive power by retaining functional ovaries.

A failure in the positioning signal of Abd-B results in an interruption of gonad coalescence and missing embryonic gonads, causing the development of sterile workers. The use of the previously established RNAi methods could shed some light on the mechanisms regulating gonadal development in embryos. In addition, a gene expression study quantifying levels of *Abd-B* and the *doublesex* isoforms could help unravel a possible interaction between both genes in queens and workers.

Based on the putative feedback-loop regulating Abd-B described in chapter six, a RNAi mediated knockdown of the male-specific isoform of *doublesex dsxM* could result in the production of only worker-destined embryos. In contrast, knockdown of the female-specific isoform *dsxF* would result in pure queen-destined embryos. Data from the miRNA-seq could shed some light on possible interaction partners acting downstream of *Abd-B* and *dsx* and help create a regulatory network.

The ability to distinguish queen from worker larvae made it possible to select queen larvae from the second and third instar and observe their gonadal development. This allowed us to create the first reconstruction of ovarian development in an ant species using confocal imaging. To our surprise, ovary formation in *C. obscurior* was different from previous described species like *Drosophila* (Sahut-Barnola et al., 1995) and *Apis mellifera* (Dallacqua & Bitondi, 2014). In contrast to these species ovarioles in *C. obscurior* form through active elongation from the gonadal cell cluster. This suggests an unknown physiological mechanism involving growth factors. It also raises the question if this same mechanism is found in other species and is conserved throughout ants.

Our study revealed a pre-determination of oocytes in pupal cystocystes according to their respective size. To further investigate this, pre-determined oocytes can be labelled with the antibody Bicaudal-C (Bic-C) to confirm our hypothesis (Khila & Abouheif, 2010). Quantifying pre-determined oocytes for each ovariole will allow to draw conclusions about queen fertility and fitness in our ant species.

We successfully established the germline marker *nanos* to distinguish queen- from worker-destined larvae throughout all three instars by quantifying its gene expression. The gene *nanos* belongs to the germ plasm and is found in oocytes during oogenesis. Besides *nanos* many more RNAs and RNA binding proteins can be found in the oocyte and are involved in germ line formation. For future studies it could prove useful to establish more markers and disentangle their interaction with each other to create a regulatory network.

This work provides elementary insight into the development of *C. obscurior* and lays the basis for future endeavors in regard of caste differentiation and determination.

8 LIST OF FIGURES

9 LIST OF TABLES

10 SUPPLEMENTS

10.1 SUPPLEMENTARY TABLES

TABLE S 1: Urate localization patterns predict caste in *Cardiocondyla* species.

Species	Clade	detected urocyte patterns	larvae with paired pattern			larvae with unpaired pattern		
			survival until pupation	queens	workers	survival until pupation	queens	workers
C. wroughtonii	A	paired + unpaired	10% (3/30)	100% (3/3)	0% (0/3)	23% (7/30)	0% (0/7)	100% (7/7)
C. nuda	B	paired + unpaired	75% (12/16)	100% (12/12)	0% (0/12)	50% (10/20)	10% (1/10)	90% (9/10)
C. venustula	B	paired + unpaired	20% (4/20)	100% (4/4)	0% (0/4)	76% (16/21)	0% (0/16)	100% (16/16)
C. thoracica	A	unpaired	-	-	-	80% (8/10)	50% (4/8)	50% (4/8)
C. minutior	B	unpaired	-	-	-	60% (12/20)	8% (1/12)	92% (11/12)
C. agyrotricha	A	unpaired	-	-	-	0% (0/20)	-	-

TABLE S 2: Sequences for Stellaris® RNA FISH probes.

Dmel ortholog	**Probe**	**Sequence**	***Gene ID***	**Fluorophore**
Abdominal-B	AbdB_e1	ATGGGGACAGCAACCGGAGCGGGGAATTCCACCGGGGTGACCTGGTGGGCCATGATGAACGGTTCCCTCTACGAGGACAGCCC GCCGCCAGTTCCACCGACAGCCTCGACCCTCGTATCGATTCAGCAAACGACCTCGACGCCGGGCTCCCATCAGCAGGCAACGAC GCCGACTTCACCTGGTGCACCTGCTTCATCGGCAACGACAGCTCCTCCGGCACCCACCGCGAGCGCCAGCTCGACTTCGCCGAGC GCTTCTTCGGTGGCGAGCAACAGCGCGGCCGGGCCACTTCACATACCCGCCAAGAGATTAACCGCGACACCGGGAGGCGCCGG TACCACTTACGGCGAGGTAGGCTGCGTCGAATCATCGGGCGCGCCAGGCGGTGCGGGCGCAGCGGGCGTGATACGACACTCAC ACTCGGCCGGATCCCAGGGCGGCTGGAGCTACAGTCCGCACCATCCGCAGGACTCTCATTACTCGTCCACGGCGACCGAATCGTT GAACCATCATCAGACTTACGGGGGTAACAATCCCCCGACGTACTACAACCTGGCGGCTGATCCCACCTCGACCTCCGGCTCCTCC AGGGACAACCGGAAGACCGGGCTGTTCTGGTCGCCAGCGGCCGCCACCGCTGGATCGGCCAGCGCCGGCGGCTCTACCTCGGA CTACAAATCTTACAACTCGGCCGGCGTGGTGACCACGACGTCGACCACGGGAGGATCTACCACCGGCGCTACCGGCGCCACCGA CCCGGCCGTGTCCTGCCACCAGAACTTCTCCCAGAGCTGGTGTAGTAATTACGCGCCGTACACCACGGCGAGGCATCACCACCCG ATTGACACGGCCGGACACCATCATCCTCACTCGCAGGCGGGGGTACCACCGTATTTGGCGCCATCCGCGGCCGACGACCGTGGT AGGGTCGCTGCTGCAATGGTCGCCGCGGAAGGTGCCTTTCCCCACGATGGATACAGCGGCCTGAGGACCTACGCGCCAGAACCT GTTACTTCGAGTCCCTACCCACCTCCAG	Cobs_01831	CAL FLUOR® Red 610
Dsx^{F}	dsxF_e5	CTACAATATCTCGTCATTTGAAAAATATTCGCCGAAATATTCAAAATATAATTTTATTATTAATAAGTATATATTTAATATGCTTATT ATTTTTATTTAAATTTAATTTATTTCCACCTTGAATAATACATAATTAAAGTTATAAATTTTTGGAACTTAACATTGCTCTTCCTAACT GTTGCTGAATTTTACAACAGCTTGATTGCTTCTTGACAAGTCATTTTTGACTCAATTATTCATGGTGTAACAAAAGATAATTGATAA ATGATAATTGATAATTGATAAATTGATTGAACCAGCTCTTATTTCCATTTTAAACTATTTTTGCGTACACTTGATTATATTATAATAC GAATTGATGCCTTGTTGATTGCTATAAAATGATCGATTAAAAAATTATTTAACGTCTTCGTCGCAATACGAAGATACGTCGCATAC GAAGATAATCTGGAAGAAGCTTTGAAACAAAGCTGTGAGATATTTTAATTTTCTCATCTTGGAAGAAATACTTTCGATCCCGTCAT AGAAGATGTTACTTCGATATGAAGATCACGCAAATACGTGAGAACTCGTTTGGCATTGCGTTAAAATAAATCGTAAATGTTACGT ACATAATTTTCTCGCCGAGCGAGAAGCTCCGCGAGATAATTTTTCGGTGATAATTAATAAACGGCCTGATAATGCTTTTATAATTA ATAATCATCTACATCTGAAGATCTTCCACCAAAAATCACGCCTGCAACCATAACGTTCCTCGAAAATACTTGACGGATTATGTAAC GAACGTTAACAGAGCTAATGAAAATTATATGGAAATAAATGATAAACCA	Cobs_01393	QUASAR® 570

Dsx^{M}	dsxM_e6/7	TCATTCATGAAGAAGATATACACTTATTTATGATGACGTACTATTATAATTCATCATCGATGGTTGTGAGAACTTCAGAAGAGCGA CAATCTATCGGAGTACCATCATCGCCATTCCAAAATTTATCTGTTCCCCTTAATACCTTAGCAACGTTTCCAATACCCGATTTACTTA AACCTGGTGCTGATCGTCCTACCGAACCTTTTCAGTTACCTGACTTAGTTAAACCTCCTACTAAATCTTCTAGTGAACCGTCTGCTG GACCTTTCATCGATCCTGGTGCTAATTTTTCTCCCGAACCTTTTATTGATCCCGGTACTGATTCTTCTGCTGAACCTTTTATCGATCC CGGCATTGACTCTTCTACTGAACCTTCTACTAATCATTCTACCGAATCTTCTGCCGAATCTTCATACTACTGATCGTTTGCCGATAAT CAGTGAAGTTAATCGACGAAAGAAACATGTCGAATCCAAAGAAAATCGCGACACCTCCGAAGTGATAAAACGGTTGTCGGGAG CATTGGACCTGACCATCGATCATCACCAACTTATTTCAGGCATCGCTTCGCAAAGTATGCGGTCAACGCTGCTATATACCCAGTGG ACTAAGTAAATTATAACCAGTAAAAAAATTAGGGGATTTCCGTGCAAGAAAGTTGTGAGAAATCCCTCCGTGCCGATCCCGCGG GCTAAATGTTCCTACGTTTCTCGTCCCTTTTATTTCCCAATTCTCGACGAGACGAAAAGTTTTCAATCAAATTGTTGCTTCTCCGCG AAATATCACGGCGATCGATTCCTTCGCGACTTTCTGCCCGCAAGAACGCAGCTTCCATTTTCAAGCGAATCGCCCACGGTTTTCTT GGAGATGGACGCCGAAGTGTACGCACGGGAATTTTTGTTTCGAATGGAAATAAAACGGCTGGAACCAGAAAATCGCGTACGGC GGAGCAACTTTCGCGAGCTGACACGATCGTGCGAGATCTTAAGAAACGGAGAATCGTTGCGCCGTGTCGCTTTTGATTTTTCTCG ACTTTTTATGAATTCTGCGTCCTTCTCACATGTCCGTCCATTTTCAATTCGGTTCAAGAACGCGATGGCAAAGATGCAAAGCGGCG GCGAACTGCCGTTAGGGAACGACGACCGTAAACGCGACAAGCGTCAAGTTAAGGATCGCTGAGGAATCTGTTCAATCGTGAGC AATGCCTTTATCCGCTGGTTCCAACGACCTGTGTGGCCAATTTCACATGTAAAAAAATCAAACACGGGACGGCGGCGATGACCAC TCCCGTAAGCGAGGCGTTGGCCGAATTAATCGACGAAATATAATGATTTGACGCTTTCTGCTTTATTCACATGCATATTAACTATT GCAAACGCTATTTTCTCCATTAATATATGTTTATTGTCGCCGAAAGGTGCGAATCATGCAGCGCATGATCGAGCATAATGTAGTAA GGCATACAGATATTAATTACTCATCGTTTACGCAATTCTTGAAATTGTTTAATGAATTTTTTTAAATGTCTGCGCAAAGTTTTATTA AGTTGCGGAGTAAGGAAATACCTTCCTGAACTATATCTGTGGAAATCGTATTTGTCCAATGCTCAATGAACAGAATTACATAACA TCCTTTACGTGTAATATTGTAAATCAAATATCACTATTGCAGCAATTAACAAAAATGAAATCTTTAATCATGACGATGAGAATGTT GAGAATCATCAATCTTGGAGCATCGTAAATTAATTTGGTTGATATTAAAAGAAAAAGAAAAAAAAGGAAAAAAAAAATAATAAT TAAGAAAAAAAAGAAATTTTTTTTTTATTCACAAATTATCAGCTGCTATTCCTCGATAATTAAACTTTTCGTGCAAAGGCGAGCGCAT CTGCTCGCATAATCGCAAAATCGGCGGATGTGTCAGTCGTGCGATGCGGTACAATAAAATAGCCGCTCAAAAACTGGTCGCTCC AGCTCGCGGCAAATTAATTTACAAATAAGAGCACCAAAAAACACTGTCCCTTCGATATGCAGTCTCATTCTCTTCATCTTGCTTTTT TTTCTCGATCGCCTTCTTCCATACCTCTAGCTTCGTGCGAAACACGTTTCGAGCTACAATTTCATGCATAGTTCGACCGAATATTAC CATACAACGCTTAATGACTTGTTTCAATAATAAGCGTGTGCACTGCGCCGCGTCCGATTCATCATCATTTCACTTAATTTGTAACTA AGAATTTAATTTGCATATTAATTGGGCTATCGCAGATTTAGGACCGTACTTGGCGGCTCGATATTTTTCGCCTGAATTGCACAATT AAGTTCCCGATTTGTACGCTGTATATGCTTCCGTTTTTTTTATTTAGGTTGCCCAGTAGATTAGAAAATTTCACTAGAATTAATTCA GCAATTACGCAAACGGGCACGCCGTATAACACAGGATACCGCGATTATTTTATTCTCGCGTTGTGCACCGGTGCTAGATGTCCTT CCCATGTTTCAGCATACTTGCGTGTAGTATATTAAAAGGAGCGCTGCTTTTAAATAACTGTATCGCGAAGAAAAATTCTCACGGTC GTCAACATGGCGGCTCCGGACGATTTAATTTTAATTAACCATCGCACGACATTACACAAAATGCACGCACTTTCAATGCGATCCTT TTGTTACGTGTGAGACTCGCGTCAGATGTCCATCCGAAGACGACATATATGGCAACAGTATCGAGTGGCGGCCAATATCCTATAA TTTTCGGCATCCTGGTGTTTATTACCGTAACCCGCAATTTAACTTAAGGCAGCTCGCTTCGGCTTCGCTGTACGTAAAGAAACGCA GTTCCGGAGCGCAATCGCTTTATCATCTCGAAGCATTTAATGGAGAAAAAAAATTTGGGACGAGCAGTCGAATTTGTATAACGCG AAGCGATTTGCTTGCGCTTAGCGGGATTATCGTATTCTTTCGTGCAGATTTCACTATTGAAAAAGGTTACGTCAAACTCGTCGAAC GTGCGCTTACGTGAAATTTAGGATCGCGTAACGTTAACGTATAATAGTCGTCGTAAACGACGTGCATTATACTCACATCCGTTTAC CTTTGCGTGTGAAATATGTATCTGTTGTCGGCCGCGCGCATACGTGTCACCGCAGCTAAGTGTGTGCGTGTTCGCACGCATATTTC GCTAAGTATTGCACACGAATTGAATTCTCTGAATCTTCCGGGAAACAGAAAAAGGGAAGAAGCAAAAAAAAGAAAAAAAAAATT GGAAGATTCACCTGTAATTTCTCAGTGGTCTCTGTTGTCGAAAACTTGTCTTTTCTTTTTTTCTTTTTCAATAATGTGAATTCTTTTTT TTTACAAGCAGTTACAATTAGCTCGTTGTGCCGCCAATTAAATTATAATGAATTTTATTTAATTAATTTTGTTGTTATTTGTTAAACA TTGAAAAAAATTTTAGATTAATTCAGCTTTAGCTTTTGTTAATGCGAAATTAATTTCTCACTGCTACATTTTGCGGCGATGTGACGC	Cobs_01393	QUASAR® 670

		ACGCCTTGTACTTGGAACGTAATATTCACGCGTCTGATTGATATGGTCCTTATATTCCTCCGGCCATTAATGCACTTTTTTAAGGTA CACGATTTTAGAGATTCGACGATTTCGACGTGAGATGCTGCGCCAAGGACGCACGTGGCAGATTCGCTCGGCCTTGCGAACTAT ACATATTGTCGTCATATTTTTTTAAGCAATAACTTTTAATGTAATATCGTAATATAATCTATTTTGTAAGTGTATTTGGTACAGGCAC ATGTCCTTTCACTTTAGATAGAAACATCGCGCCGCATAAGTAAAGGCGCACACGTTCGAGCCTAAGCGACGAGGTAATCAGATTA TTGGTAGGAACGACGGCGATGAAATCGGTCTTCATATATCTCTCTTTAATTGTGATTTCTGTTTTTTTTTGTTTTTAATTTTAAGTAC TTATTGAGGGACTTATTCATGAATAATTTTCCGTGAACCAGCTCTCTAAAACGAAGTAGTTATTGATTGCTGTTCTTTCTTTCTCCT AAGAGTCGCTCGTTTCGCACAGAGACGGTTGATGAGAAATAGTGTGTTCGATATTTGACGTGTATATTCTATAGAGTATTTTCTA GCACGAGAAGGGTCGTAAATTCTCTCGGTTGTGAGCTCGTTCGTGGAAATGAAGTTCTGCATAATGCGGAAGCTCTCATTCCTCG ACGCCCCGAAGACTCTTCTAAGCGTTACTTTACATAAGTGTTACTTTACATTGATAAGATTTTCTTTTATTGATATAAAATTGTAAT AGACACCGTTTTCTAGTAATCGATAACTACGTATTATATTGAGATACTTTATTGAATCGTTTATCCAAAATAAATTGTGTATGCGCA ACTGCAAAGTTATTCTTCAACTTCGAAGTAGAATATGATGGTTAAGAATTACTATAACTTCTCGACCTACATAAAAAAAAGAACTA AATATATATATATATATATAATAAATATATATATATATATATATATTTATATACTTTATATCTTCACATGAAATATCGGTTAATGCGT GAGACCGCTAATATCACGAGCTCGGTTGCAATCGATCGATCATTTTATTAGCGCGTCTTGATTTTCGCGACTCATAACGAGTCAAG CCGGACATTGCTAGAATACGAAAAATGTAAAGAAGGAAAAAGAAAAAGGAAA		
Nanos	Nanos_e1-4	ATGCTGCCCACGCTGGAGGAGAACTCTCTGTTTCCCTTCAACCCGAGTCTGGACGACGAGATCAAGCGACTGTTCGATCTTACCC TGAACACGAGGCCAATGCCGAACGTTGAGGAGATAATGGAAGAATTTCGGCACAACGGCCGTGACTTCGAATATTGCCCAGATG TAAACGCAGACGTGTCAAGACAGATCACATCACGGCGAAAGAAAAATAAAAAGCCACTGCCCACGGAATGCGTGTTCTGCAAAA ATAACGGTGAGGAGGAGACGTACTACCGGAAGCATTTGCTCAAAGACATCGAGGGACGTGTCCGATGTCCTGTTCTTAGGGCTT ATACATGTCCGATATGCGGCGCGTGCGGTGACGACGCACATACGGTTAAACACTGTCCTAAGGGTCCATATAATCCCAATAGCAT TAGCACAGCGAATGCCTTTAAACTTTTAAGGAACGCAACGGGCAAACGTCAAAGCAAAGGTTCCACAACGCGTTCTAAGTAA	Cobs_12201	QUASAR®670

Vasa	Vas_e2	TTTGACGAAGGACGTGCACCTTGTCGTGGGAAAGGACGTGGTGCAGCAGTGGTCTATAACAACAATCAGTCAGATCACAAAGTA GGATACAATAATAATTCCTATAGCGGCAAGAAAGATGATTACGAAAAAAGCTATAATGATGATCACAATGAAGAGCGTGAAAAT AAATATAATGGTGATAATAGATTTGGAAGAGACAACAGGCAACAAGGCGAAAGACGTTTCGGAAACAGAGGTGATGGTGATCG AAGGCAGGGTAACAGGGACTGGAATACAAACAGTAGACGAAACAGAGATGATAACAACGACGGTGAAGATAATGGCTATGAC GGAAATAATCAAAATGATAGAAGAGATAGACCTAGAAGAGATAGAGATGATAATAGAGGAAGAAGCGGTGGATTCGGTAGAA ATAGAGATGGCGATGATGAAGGTGGCGACGATTTTGAAAATAGACGTGGAAGAAGAAACGGAGAATCTAGAGATGGCAATGA TGGTGAAGAACCTAAAAAGAGAGAGATTTACATTCCTCCGGAACAACCCGATGATGAAAATTCCTTATTTGGAAATGATGTGTCG GTAGGAATAAACTTTAATAAATATGACGATATTGAAGTAAAAGTATCTGGTGAGAACGCACCGCATCCGATTCAATCTTTCGATA AATCCGGCCTCAGGAATATTATTTTGGAGAACATCAAGAAATCAGGATATACAAAACCTACTCCTGTGCAAAAATATGCCATTCC GATTGTAATGAGCGGACGCGATTTGATGGCCTGTGCGCAAACAGGTTCTGGCAAAACTGCAGCGTTCGTAGTTCCGATTATACAT ACTTTGTTGGAAACTCCAAGAGAATTAGTTATAACTGCTACTTCATGCGAGCCACAAGCGATTATTATATCACCTACTCGCGAACT CACCTCTCAGATTCATCAACAAGTAAAAAAATTTTCTTTAAGTTCTATACTGCGCGTTGAGCTTGCTTATGGAGGAACATCGGTTA TGCACCAGTCAAATAAGGTACTCCACGGTTGCCATATTCTAGTTGCAACTCCAGGAAGATTATTAGACTTTATAGGACGAGGCAA AATTAAGCTTTCTTCTTTACGTTTTCTTGTGCTGGATGAAGCCGACAGAATGCTCGATATGGGTTTCCTACCGGATGTTGAAAAAA TTGTAGATCACGAAACAATGGCAGCTGCAGAAGAAAGACAGACTCTCATGTTCTCTGCCACTTTTCCAAATGAGATACAAGAACT TGCAAGTCGATTTTTGAAAAATTATCTATTTCTTGCAGTTGGAATCGTAGGTGGTGCTTGTTCTGACGTAGAACAAAACTTTTATC AAGCATCTGGTCAATGCGAAAAGCGAAAGCTGCTAAAAGACTTGATAGAAAAACAAAGTCAACTGGGAAGCATCGAAGGAACT TTAGTGTTCGTTGAACAGAAAAGACACACCGACTTCATCGCCGCTTTCTTGTCAGAAAATAATTTCCCGACAACTAGTATACATGG AGATAGATTGCAACGAGAACGAGAAGAAGCTTTAAACCACTTTAAACGAGGGAAAATGTTAATTTTAGTGGCAACGGCGGTTGC TGCGCGTGGATTAGATATTAAAAATGTTTCTCATGTAATTAATTTTGATATGCCAAAGACAATCGATGAATACGTTCATAGAATTG GACGAACTGGTCGGGTTGGAAACCGCGGCAAAGCGACTTCATTTTTCGATCTAACCAATGATGGACCTCTCACTGATGATTTGGT CAGAATTTTGAAGCAAGCTAAACAACCGATACCTGACTGGTTAGAATCTGGTGGCAGCGGCGGATCTAGAAGCTACATGCCAGG AAGAGGTTCGAGAAGATTTGGCGGAGAAGATATCAGAGGA	Cobs_06342	QUASAR® 570

TABLE S 3: Species experiencing urate patterns.

Species	Subfamily	detected urate patterns
Acromyrmex versicolor	Myrmicinae	unpaired
Adetomyrma goblin	Amblyoponinae	unpaired
Amoldius species	Dolichoderinae	unpaired
Aphaenogaster picae	Myrmicinae	unpaired
Aphaenogaster tennesseenis	Myrmicinae	unpaired
Azteca alfari	Dolichoderinae	unpaired
Calyptomyrmex piripilis	Myrmicinae	unpaired
Camponotus sansabeanus	Formicinae	unpaired
Cardiocondyla argyrotricha	Myrmicinae	unpaired
Cardiocondyla elegans	Myrmicinae	unpaired
Cardiocondyla emeryi	Myrmicinae	unpaired
Cardiocondyla minutior	Myrmicinae	unpaired
Cardiocondyla nuda	Myrmicinae	paired/unpaired
Cardiocondyla obscurior	Myrmicinae	paired/unpaired
Cardiocondyla thoracica	Myrmicinae	unpaired
Cardiocondyla venustula	Myrmicinae	paired/unpaired
Cardiocondyla wroughtonii	Myrmicinae	paired/unpaired
Doleromyrma darwiniana	Dolichoderinae	unpaired
Gnamptogenys mordax	Ectatomminae	unpaired
Gnamptogenys striatula	Ectatomminae	unpaired
Iridomyrmex victorianus	Dolichoderinae	unpaired
Linepethima humile	Dolichoderinae	unpaired
Monomorium floricola	Myrmicinae	unpaired
Myrmecia piliventris	Myrmicinae	unpaired
Myrmecia pilosula	Myrmicinae	unpaired
Nylanderia faisonensis	Formicinae	unpaired
Ochetellus species	Dolichoderinae	unpaired
Odontomachus clarus	Ponerinae	unpaired
Orectognathus versicolor	Myrmicinae	unpaired
Paraparatrechina	Formicinae	unpaired
Pheidole dentata	Myrmicinae	unpaired
Pheidole desertorum	Myrmicinae	unpaired
Pheidole floridana	Myrmicinae	unpaired
Platythyrea punctata	Ponerinae	whole body
Pseudomyrmex gracilis	Pseudomyrmecinae	unpaired
Pseudomyrmex simplex	Pseudomyrmecinae	whole body
Pseudoponera succedanae	Pseudomyrmecinae	whole body
Sericomyrmex amabilis	Myrmicinae	unpaired
Stigmatomma oregonensis	Amblyoponinae	unpaired

Strumigenys clypeata	Myrmicinae	unpaired
Strumigenys lujae	Myrmicinae	unpaired
Strumigenys rostrata	Myrmicinae	unpaired
Tapinoma sessile	Dolichoderinae	unpaired
Temnothorax sp.	Myrmicinae	unpaired
Temnothorax difficilis	Myrmicinae	unpaired
Temnothorax rugatulus	Myrmicinae	unpaired
Turneria bidentata	Dolichoderinae	unpaired
Wasmannia auropunctata	Myrmicinae	unpaired
Wasmannia rochai	Myrmicinae	unpaired

10.2 SUPPLEMENTARY PROTOCOLS

10.2.1 PROTOCOL FOR IMMUNOSTAINING L2 & L3 LARVAE

Dissection:

Take the queen/worker larvae (distinguishable through urate patterns) from the colony and put them in an Eppendorf tube (1,5 ml) with PBST 0.3 % (PBS 1X + Triton 0.3%). Collect as many as possible, at least 10.
Place larvae in a petri dish with PBST 0.3 %.
Cut worker larvae in the middle, queen larvae right above the urate deposits using micro scissors.
Remove excessive tissue as careful as possible, but don't remove the developing ovaries in queen larvae surrounded by the urate deposits.
Place the dissected larvae in a well filled with PBST 0.3 % on ice.

Fixation:
After 30 min of dissection fix the larvae.
Solution 4% PFA in PBS.
Incubation for 20 min @ RT.
Wash 3x in PBST for 15 min.
Place well in between washes on tumbler.

Staining:
Collect at least 8 larvae:
- AbI: dilution in 200µl (1:200) of PBST 0.3% (+ NGS 5%); Overnight @ RT on tumbler.
- Washes in PBST (minimum 3x 15 min).
- AbII: dilution in 200µl (1:200) of PBST 0.3%; Overnight 4°C or 2 - 4 h @ RT.
- Washes in PBST (minimum 3x 15 min).
- Wash with PBST 0.3 % + DAPI (1:10000) to counterstain for cell nuclei (minimum 15 min).

Mounting:
Transfer the larvae from the well to a glass cover slide, using a 200 µl pipette.
Remove extra tissue left after dissection and excessive liquid using cut up filter papers (make triangles).
Make a small drop of VECTASHIELD© on the cover slide.
Place each larva in a good orientation (anterior up).
Take a small cover glass (18 x 18 mm) and put some plasticine at each corner.
With forceps place the cover glass on the drop of VECTASHIELD© (avoid bubbles).
Use nail-polish to seal the cover slide.
Let dry for 24 h in the dark @ 4°C.
Slides can be kept for several weeks in the dark @ -20°C.
Proceed with imaging.

10.2.2 ADAPTED STELLARIS® RNA FISH PROBES PROTOCOL FOR *DROSOPHILA* EMBRYO

Stellaris® RNA FISH Probes

Protocol for Drosophila Embryo

General Protocol & Storage

Product Description

A set of Stellaris RNA FISH Probes is comprised of up to 48 singly labeled oligonucleotides designed to selectively bind to targeted transcripts. Stellaris RNA FISH Probes bound to target RNA produce fluorescent signals that permit detection of single RNA molecules as diffraction-limited spots by conventional fluorescence microscopy.

Storage Guidelines

Stellaris RNA FISH Probes

Stellaris RNA FISH Probes are shipped dry and can be stored at +2 to +8 °C in this state. Dissolved probe mix should be subjected to a minimum number of freeze-thaw cycles. For daily and short-term use of dissolved probe mix, storage at +2 to +8 °C in the dark for up to a month is recommended. For storage lasting longer than a month, we recommend aliquoting and freezing probes in the dark at -15 to -30 °C.

Stellaris RNA FISH Hybridization Buffer

Stellaris RNA FISH Hybridization Buffer should be stored at +2 to +8 °C for short-term and long-term use.

Stellaris RNA FISH Wash Buffer A and Wash Buffer B

Stellaris RNA FISH Wash Buffers A and B should be stored at room temperature for short-term and long-term use.

Embryo Fixation Solution

Embryo fixation solution should be stored at room temperature for short-term and long-term use.

Embryo Wash Buffer

Embryo Wash Buffer should be stored at room temperature for short-term and long-term use.

50% Bleach Solution

Bleach solution should be stored at room temperature protected from light for short-term and long-term use.

Reagents and Equipment

Reagents and Consumables:

TE buffer (10 mM Tris-HCl, 1 mM EDTA, pH 8.0)
Methanol for molecular biology
Sodium Hypochlorite
Sodium Chloride
TritonX-100
Tween-20
10% Formaldehyde methanol-free Ultra Pure (Polysciences Cat# 04018-1 or equivalent)
Heptane
Ethanol for molecular biology
10X Phosphate Buffered Saline (PBS), RNase-free
Nuclease-free water

Deionized Formamide
Stellaris RNA FISH Hybridization Buffer (LGC Biosearch Technologies Cat# SMF-HB1-10)
Stellaris RNA FISH Wash Buffer A (LGC Biosearch Technologies Cat# SMF-WA1-60)
Stellaris RNA FISH Wash Buffer B (LGC Biosearch Technologies Cat# SMF-WB1-20)
Prolong Diamond Antifade Mountant with DAPI (Life Technologies Cat# P36962 or equivalent)
RNase free consumables such as pipette tips
37 °C laboratory oven

Orbital platform shaker

Wheaton glass vials (Sigma Cat # Z115053 or equivalent)

Microscope:

Wide-field fluorescence microscope (*e.g.*, Nikon Eclipse Ti or equivalent). We provide limited support for confocal applications.

A high numerical aperture (>1.3) and 60-100x oil-immersion objective.

Strong light source, such as a mercury or metal-halide lamp (Xenon or LED are typically not bright enough).

Filter sets appropriate for the fluorophores.

Standard cooled CCD camera, ideally optimized for low-light level imaging rather than speed (13 µm pixel size or less is ideal).

Preparation of Reagents

NOTE: When performing Stellaris RNA FISH, it is imperative to limit RNA degradation. Please ensure that all consumables and reagents are RNase-free. Recipes below are for set volumes. Please adjust accordingly.

Reconstituting the dried probe stock:

ShipReady Probe Set (1 nmol): A ShipReady probe set can provide up to 80 hybridizations. Re-dissolve the dried oligonucleotide probe blend in 80 µL of TE buffer (10 mM Tris-HCl, 1 mM EDTA, pH 8.0) to create a probe stock of 12.5 µM. Mix well by pipetting up and down, and then vortex and centrifuge briefly.

DesignReady or Custom Probe Set (5 nmol): A DesignReady or custom probe set can provide up to 250 hybridizations. Re-dissolve the dried oligonucleotide probe blend in 400 µL of TE buffer (10 mM Tris-HCl, 1 mM EDTA, pH 8.0) to create a probe stock of 12.5 µM. Mix well by pipetting up and down, and then vortex and centrifuge briefly.

50% Bleach Solution:

Create a 1:1 mix of Nuclease-free water and Sodium Hypochlorite

Embryo Wash Buffer:

For a final volume of 1 L, mix:

1 L Nuclease-free water

6 g Sodium Chloride

2 mL 20% TritonX-100

Embryo Fixation Solution:

For a final volume of 10 mL, mix:

0.5 mL Nuclease-free water

0.5 mL 10X Phosphate Buffered Saline (PBS), RNase-free

4 mL 10% Ultra pure Formaldehyde

5 mL Heptane

PBT

Final composition is 0.1% (vol./vol.) Tween-20 in 1X PBS

For a final volume of 10 mL, mix:

10 mL 1X Phosphate Buffered Saline

10 µL Tween-20

Hybridization Buffer:

Final composition is 10% (vol./vol.) formamide in Hybridization Buffer

Hybridization Buffer should be mixed fresh for each experiment:

Due to viscosity of the solution, we recommend accounting for a 10% final volume excess in order to have enough Hybridization Buffer for all of your samples.

For a final volume of 1 mL, mix:

900 µL Stellaris RNA FISH Hybridization Buffer (LGC Biosearch Technologies Cat# SMF-HB1-10)

100 µL Deionized Formamide

NOTE: Do not freeze Hybridization Buffer.

WARNING! Formamide is a teratogen that is easily absorbed through the skin and should be used in a chemical fume hood.

WARNING! Be sure to let the formamide warm to room temperature before opening the bottle.

Wash Buffer A (10 mL):

Final composition is 10% (vol./vol.) formamide in Wash Buffer A

Mix and dilute Wash Buffer A fresh for each experiment:

For a final volume of 10 mL, mix:

2 mL Stellaris RNA FISH Wash Buffer A (LGC Biosearch Technologies Cat# SMF-WA1-60)

Add 7 mL Nuclease-free water

Add 1 mL Deionized Formamide

Mix well by vortexing gently.

Wash Buffer B:

Add Nuclease-free water to Wash Buffer B bottle upon first use.

Add 88 mL of Nuclease-free water to bottle (LGC Biosearch Technologies Cat# SMF-WB1-20) before use. Mix thoroughly.

Mounting media:

Prolong Diamond Mounting Medium from Life Technologies (#P36962)

Fixation Of *Cardiocondyla obscurior* Embryos:

Embryos were fixated by using the "slow-fixation method" (Laura Flórez, pers. comm.) and added prior to the modified Stellaris® RNA FISH protocol.

Additional steps ("Slow-fixation method"):

1) Collect embryos from random stock colonies and submerge them in a dissection dish containing PBT (0.3 %).
2) Visually classify embryos into their respective stage, according to the previously described embryogenesis (Chapter 5).
3) Transfer embryos with a pipette into an Eppendorf tube containing 4% paraformaldehyde in PBS (PFA).
4) Fix samples for at least 3d at 4 °C.

Beginning of the modified Stellaris® RNA FISH protocol (modified steps are highlighted):

a) removed

b) removed

c) Devitellinize the embryos in **200 µl** ~50% bleach for **5-10 minutes** by periodically **exchanging the solution** and gently stir.

d) Wash thoroughly to remove all traces of bleach, alternating washes between double distilled ddH_2O, or Nuclease-free water, which causes the embryos to clump together, and embryo wash buffer, which separates the clumps. Perform a final thorough wash in ddH_2O.

e) removed

f) removed

g) removed

h) Exchange solution with **500 µl** methanol, cap the vial and shake vigorously by hand for about 30 seconds, then place on the bench. The two phases will separate and the fixed, devitellinized embryos settle to the bottom in methanol. The upper phase of heptane should have remained, and all the burst vitelline membranes and non-devitellinized embryos will have remained in a cloudy layer at the interface.

i) removed

j) Rinse the embryos in fresh methanol by using a pipette. Repeat this step 3x.

k) Wash the embryos with **3 changes** (**500 µl**) of methanol. Embryos can then be stored in methanol at -20 °C for several years.

Hybridization of Embryos:

a) removed

b) Make a transition from methanol to PBT: 25%, 50%, 100% (rocking at room temperature on a roller platform for 5 minutes each).

c) Rock 3x 10 minutes with PBT.

d) Rock in 50:50 PBT:Wash Buffer A, 10 minutes.

e) Rock 2x 5 minutes with Wash Buffer A.

f) Remove as much Wash Buffer A as possible, add **250 µl** Hybridization buffer to each vial, and allow embryos to settle for 5 minutes.

g) (Replace with another **250 µl** Hybridization buffer, and) incubate in a 37 °C water bath for **1** hour.

h) Prepare Stellaris probe mixtures, diluting probe to 50 nM in 0.25 mL Hybridization buffer per vial.

i) Remove the Hybridization buffer from embryos, and add 0.25 mL probe mixture to each vial.

j) Incubate in the dark in a 37 °C water bath for ~14 hours **or overnight**.

k) Remove the probe mixtures, add **200 µl** pre-warmed (37 °C) Hybridization buffer, and incubate in the dark for 30 minutes at 37 °C.

l) Remove Hybridization buffer, and wash with **200 µl** pre-warmed (37°C) Wash Buffer A.

m) Wash 3x 15 minutes with **200 µl** pre-warmed (37°C) Wash Buffer A in the dark at 37°C.

n) Rock with **200 µl** Wash Buffer A for 15 minutes in the dark at room temperature.

o) Rock 3x 10 minutes with PBT in the dark at room temperature **and for 10 minutes in PBT + DAPI**.

p) Aliquot embryos to slides, and use an aspirator to thoroughly remove excess PBT, but without letting the embryos completely dry out.

q) Mount embryos under cover glass using Prolong Diamond Antifade with DAPI **or VECTASHIELD®, when already washed in PBT + DAPI**.

r) Dry slides flat in the dark at room temperature for 24 hours, then image immediately or store at -20°C.

10.3 SUPPLEMENTARY FIGURES

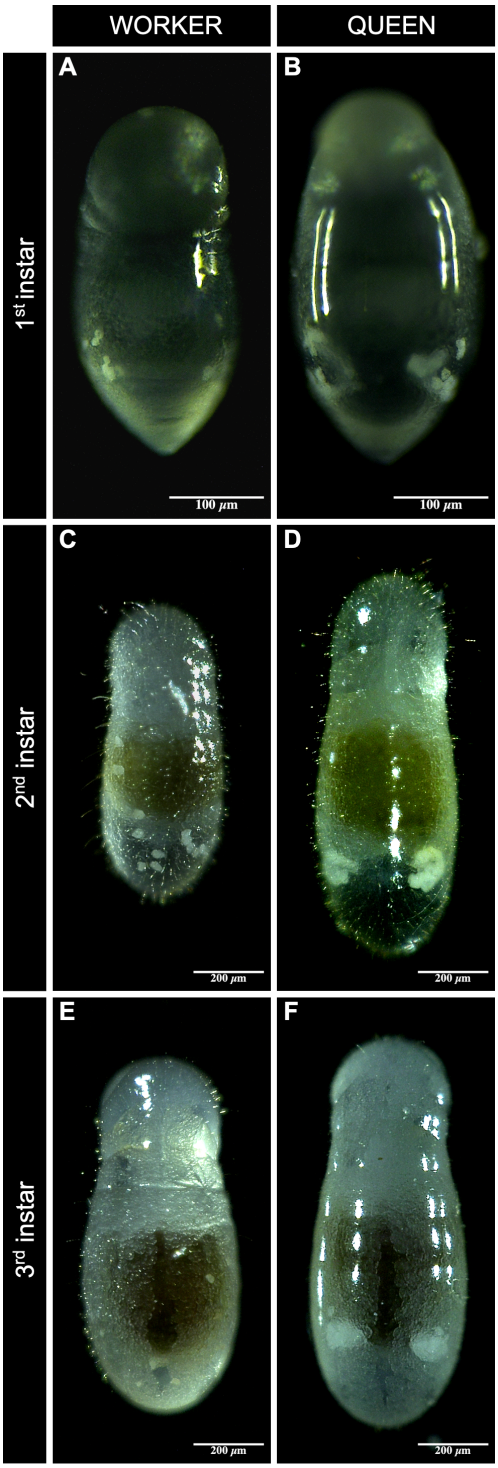

FIGURE S 1: Urate localization patterns.

Dorsal and ventral view of urate localization patterns in worker- and queen-destined larvae in the ant *C. obscurior*. Light microscope images of worker-destined larval instars (A, C & E) and queen-destined larval instars (B, D & F). (A, B) shows larvae in a dorsal orientation. Urate depots are visible as bilateral symmetrical clusters in queen-destined larvae.

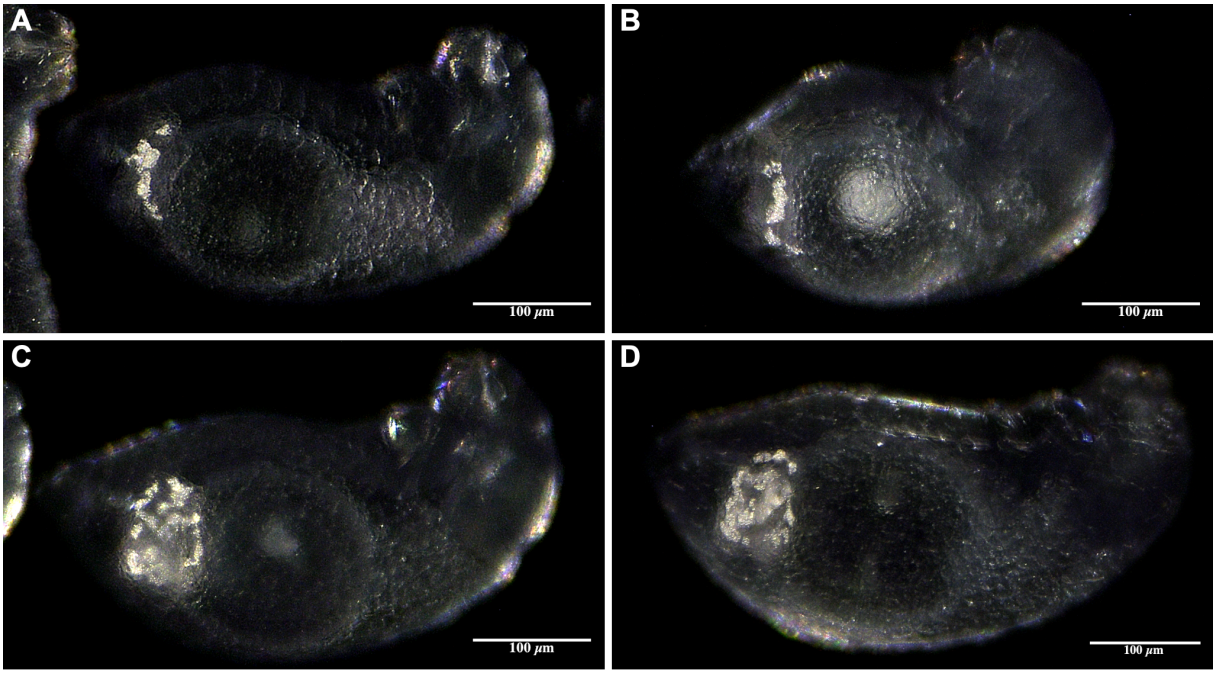

FIGURE S 2: Different types of urate localization patterns in queen-destined larvae.
(A, B) First instar larvae with pearl of strings-like urate depots. (C, D) First instar larvae with snail shell-like urate depots.

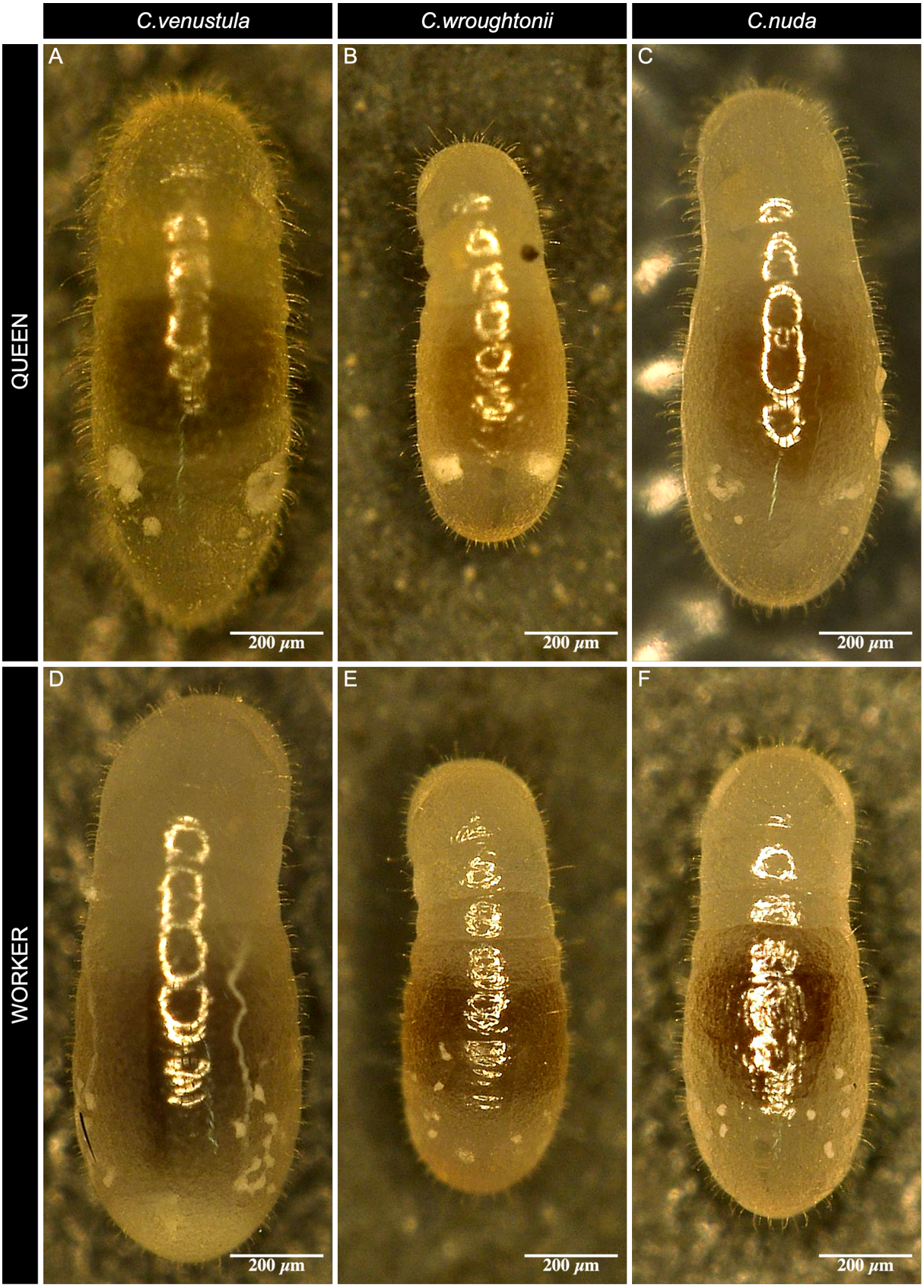

FIGURE S 3: Urate localization patterns distinguish queen- and worker-destined larvae in various *Cardiocondyla* species. Light microscope images of queen-destined larval instars (A, B, C) and worker-destined larval instars (D, E, F). (A) Queen larva of *C. venustula* (B) Queen larva of *C. wroughtonii*. (C) Queen larva of *C. nuda*. (D) Worker larva of *C. venustula*. (E) Worker larva of *C. wroughtonii*. (F) Worker larva of *C. nuda*. Ur = urate.

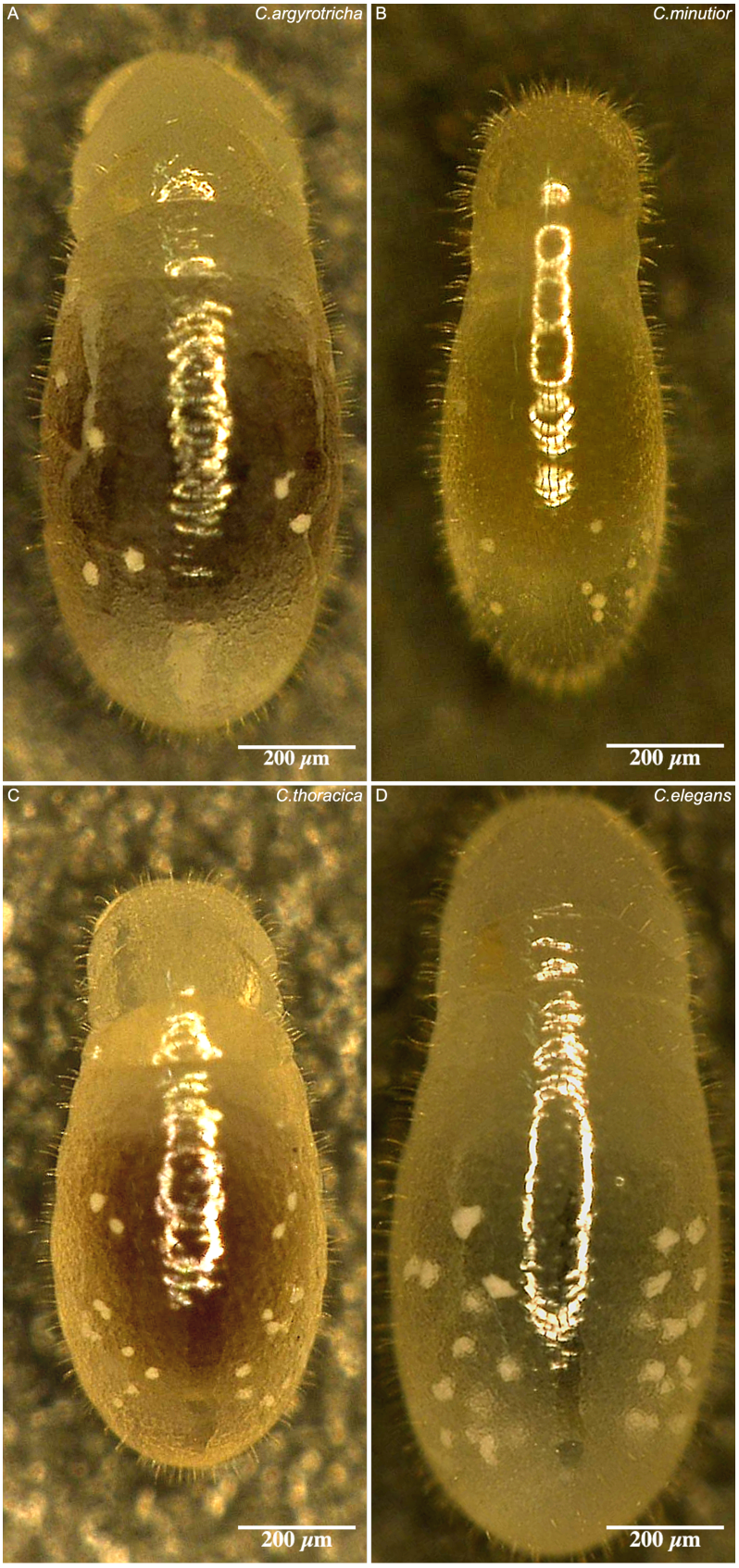

FIGURE S 4: Urate localization patterns in *Cardiocondyla* species without paired urate deposits.
Light microscope images of larval instars. (A) *C. argyrotricha*. (B) *C. minutior*. (C) *C. thoracica*. (D) *C. elegans*.

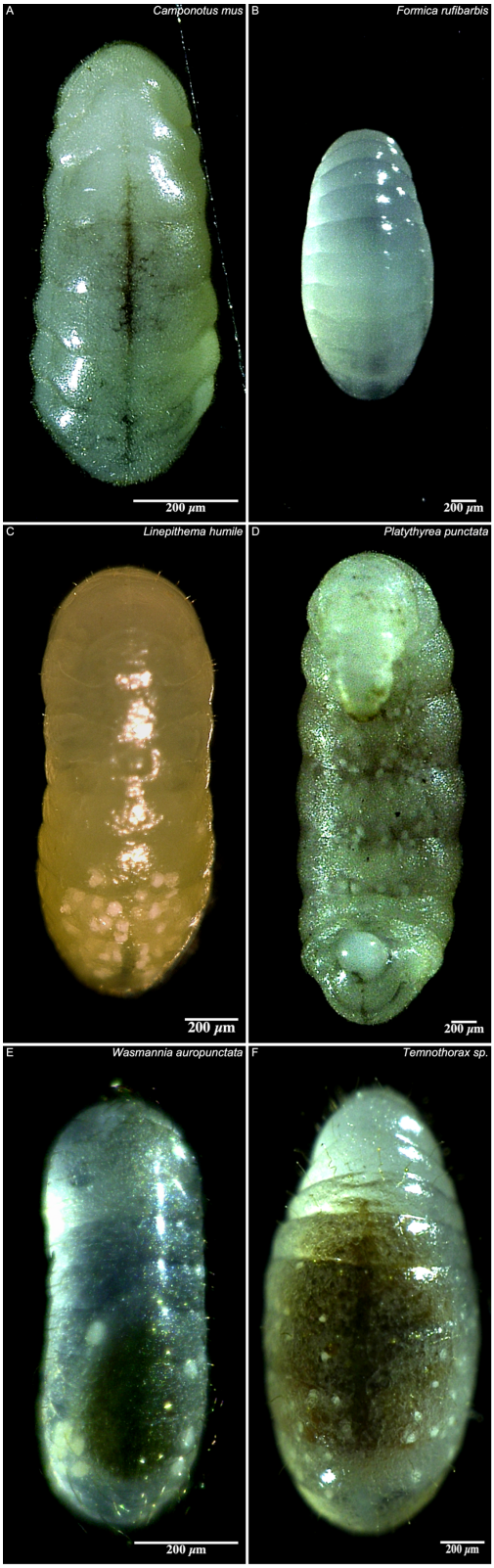

FIGURE S 5: Urate localization patterns in different species.

Light microscope images of larval instars. (A) *Camponotus mus* (Formicinae). (B) *Formica rufibarbis* (Formicinae). (C) *Linepithema humile* (Dolichoderinae). *Platythyrea punctata* (Ponerinae) (dorsal view). (E) *Wasmannia auropunctata* (Myrmicinae). (F) *Temnothorax sp.* (Myrmicinae). Both representatives of the Formicinae are missing visible urate localization patterns.

10.4 SUPPLEMENTARY STATISTIC

All electronic supplementary materials (ESM) used in this thesis are attached as a compact disc. This includes raw data and RMarkdown files for data handling.

11 REFERENCES

Abouheif, E., Favé, M.-J., Ibarrarán-Viniegra, A. S., Lesoway, M. P., Rafiqi, A. M., & Rajakumar, R. (2014). *Eco-Evo-Devo: The Time Has Come - Ecological Genomics: Ecology and the Evolution of Genes and Genomes* (C. R. Landry & N. Aubin-Horth (eds.); pp. 107–125). Springer Netherlands. https://doi.org/10.1007/978-94-007-7347-9_6

Aigouy, B., & Mirouse, V. (2013). ScientiFig: A tool to build publication-ready scientific figures. *Nature Methods*, *10*(11), 1048. https://doi.org/10.1038/nmeth.2692

Batra, S. W. (1966). Nests and social behavior of halictine bees of India (Hymenoptera: Halictidae). *The Indian Journal of Entomology*, *28*(375).

Becalska, A. N., & Gavis, E. R. (2009). Lighting up mRNA localization in *Drosophila* oogenesis. *Development*, *136*(15), 2493–2503. https://doi.org/10.1242/dev.032391

Boleli, I. C., Paulino-Simões, Z. L., & Bitondi, M. M. G. (1999). Cell death in ovarioles causes permanent sterility in *Frieseomelitta varia* worker bees. *Journal of Morphology*, *242*(3), 271–282. https://doi.org/10.1002/(SICI)1097-4687(199912)242:3<271::AID-JMOR6>3.0.CO;2-7

Boomsma, J. J., & Gawne, R. (2018). Superorganismality and caste differentiation as points of no return: how the major evolutionary transitions were lost in translation. *Biological Reviews*, *93*(1), 28–54. https://doi.org/10.1111/brv.12330

Boyle, M., & DiNardo, S. (1995). Specification, migration and assembly of the somatic cells of the *Drosophila* gonad. *Development (Cambridge, England)*, *121*(6), 1815–1825. http://www.ncbi.nlm.nih.gov/pubmed/7600996

Bressan, J. M. a., Benz, M., Oettler, J., Heinze, J. J., Hartenstein, V., & Sprecher, S. G. (2015). A map of brain neuropils and fiber systems in the ant *Cardiocondyla obscurior*. *Frontiers in Neuroanatomy*, *8*(February), 166. https://doi.org/10.3389/fnana.2014.00166

Brian, M. V. (1973). Caste control through worker attack in the ant *Myrmica*. *Insectes Sociaux*, *20*(2), 87–102. https://doi.org/10.1007/BF02223340

Campos-Ortega, J. A., & Hartenstein, V. (2013). *The embryonic development of Drosophila melanogaster*. Springer Science & Business Media.

Cardona, A., Saalfeld, S., Schindelin, J., Arganda-Carreras, I., Preibisch, S., Longair, M., Tomancak, P., Hartenstein, V., & Douglas, R. J. (2012). TrakEM2 software for neural circuit reconstruction. *PLoS ONE*, *7*(6). https://doi.org/10.1371/journal.pone.0038011

Chapman, R. F., Simpson, S. J., & Douglas, A. E. (2013). *The insects: structure and function* (5th ed.). New York: Cambridge University Press. https://doi.org/10.15713/ins.mmj.3

Chatterjee, S. S., Uppendahl, L. D., Chowdhury, M. a, Ip, P.-L., & Siegal, M. L. (2011). The female-specific *doublesex* isoform regulates pleiotropic transcription factors to pattern genital development in *Drosophila*. *Development (Cambridge, England)*, *138*(6), 1099–1109. https://doi.org/10.1242/dev.055731

Corona, M., Libbrecht, R., & Wheeler, D. E. (2016). Molecular mechanisms of phenotypic plasticity in social insects. *Current Opinion in Insect Science*, *13*(December 2015), 55–60. https://doi.org/10.1016/j.cois.2015.12.003

Corona, M., Libbrecht, R., Wurm, Y., Riba-Grognuz, O., Studer, R. A., & Keller, L. (2013). Vitellogenin Underwent Subfunctionalization to Acquire Caste and Behavioral Specific Expression in the Harvester Ant *Pogonomyrmex barbatus*. *PLoS Genetics*, *9*(8). https://doi.org/10.1371/journal.pgen.1003730

Costa-Leonardo, A. M., Laranjo, L. T., Janei, V., & Haifig, I. (2013). The fat body of termites: Functions and stored materials. *Journal of Insect Physiology*, *59*(6), 577–587. https://doi.org/10.1016/j.jinsphys.2013.03.009

Cremer, S., Suefuji, M., Schrempf, A., & Heinze, J. (2012). The dynamics of male-male competition in *Cardiocondyla obscurior* ants. *BMC Ecology*, *12*(1), 7. https://doi.org/10.1186/1472-6785-12-7

Cridge, A. G., Lovegrove, M. R., Skelly, J. G., Taylor, S. E., Petersen, G. E. L., Cameron, R. C., & Dearden, P. K. (2017). The honeybee as a model insect for developmental genetics. *Genesis*, *55*(5), 1–12. https://doi.org/10.1002/dvg.23019

Dallacqua, R. P., & Bitondi, M. M. G. (2014). Dimorphic ovary differentiation in honeybee (*Apis mellifera*) larvae involves caste-specific expression of homologs of *Ark* and *Buffy* cell death genes. *PLoS ONE*, *9*(5), 1–12. https://doi.org/10.1371/journal.pone.0098088

Dansereau, D. A., & Lasko, P. (2008). The development of germline stem cells in *Drosophila*. In *Methods in Molecular Biology* (Vol. 450). https://doi.org/10.1007/978-1-60327-214-8_1

De Menten, L., Cremer, S., Heinze, J., & Aron, S. (2005). Primary sex ratio adjustment by ant queens in response to local mate competition. *Animal Behaviour*, *69*(5), 1031–1035. https://doi.org/10.1016/j.anbehav.2004.09.005

De Souza, D. A., Kaftanoglu, O., De Jong, D., Page, R. E., Amdam, G. V., & Wang, Y. (2018). Differences in the morphology, physiology and gene expression of honey bee queens and workers reared in vitro versus in situ. *Biology Open*, *7*(11). https://doi.org/10.1242/bio.036616

DeFalco, T., Le Bras, S., & Van Doren, M. (2004). *Abdominal-B* is essential for proper sexually dimorphic development of the *Drosophila* gonad. *Mechanisms of Development*, *121*(11), 1323–1333. https://doi.org/10.1016/j.mod.2004.07.001

Deshmukh, R., Lakhe, D., & Kunte, K. (2020). Tissue-specific developmental regulation and isoform usage underlie the role of *doublesex* in sex differentiation and mimicry in *Papilio* swallowtails: Regulation of sex-limited traits by dsx. *Royal Society Open Science*, *7*(9). https://doi.org/10.1098/rsos.200792rsos200792

Dijkstra, M. B., Nash, D. R., & Boomsma, J. J. (2005). Self-restraint and sterility in workers of *Acromyrmex* and *Atta* leafcutter ants. *Insectes Sociaux*, *52*(1), 67–76. https://doi.org/10.1007/s00040-004-0775-8

Elliott, K. L., & Stay, B. (2007). Juvenile hormone synthesis as related to egg development in neotenic reproductives of the termite *Reticulitermes flavipes*, with observations on urates in the fat body. *General and Comparative Endocrinology*, *152*(1), 102–110. https://doi.org/10.1016/j.ygcen.2007.03.003

Ermer, V. M. (2020). *Gene knockdown with dsRNA in Cardiocondyla obscurior* (Bachlor's thesis). Regensburg.

Errbii, M., Keilwagen, J., Hoff, K. J., Steffen, R., Altmüller, J., Oettler, J., & Schrader, L. (2021). Transposable elements and introgression introduce genetic variation in the invasive ant *Cardiocondyla obscurior*. *Molecular Ecology*.

Foronda, D., Estrada, B., de Navas, L., & Sánchez-Herrero, E. (2006). Requirement of *abdominal-A* and *Abdominal-B* in the developing genitalia of *Drosophila* breaks the posterior downregulation rule. *Development (Cambridge, England)*, *133*(1), 117–127. https://doi.org/10.1242/dev.02231

Furtado, W. C. A., Azevedo, D. O., Martins, G. F., Zanuncio, J. C., & Serrão, J. E. (2013). Histochemistry and Ultrastructure of Urocytes in the Pupae of the Stingless Bee *Melipona quadrifasciata* (Hymenoptera: Meliponini). *Microscopy and Microanalysis*, *19*(06), 1502–1510. https://doi.org/10.1017/s1431927613013445

Ganin, M. (1869). *Über die Embryonalhülle der Hymenopteren- und Lepidopteren-Embryonen*. St.-Pétersbourg :Commissionnaires de l'Académie impériale des sciences,. https://www.biodiversitylibrary.org/item/16826

Gavis, E. R., Chatterjee, S., Ford, N. R., & Wolff, L. J. (2009). Dispensability of *nanos* mRNA localization for abdominal patterning but not for germ cell development*. Mech Dev.* (Vol. 125, Issue 609).

Ghosh, N., Bakshi, A., Khandelwal, R., Rajan, S. G., & Joshi, R. (2019). The Hox gene *Abdominal-B* uses DoublesexF as a cofactor to promote neuroblast apoptosis in the *Drosophila* central nervous system. *Development*

(Cambridge), *146*(16). https://doi.org/10.1242/dev.175158

Giehr, J., Senninger, L., Ruhland, K., & Heinze, J. (2020). Ant workers produce males in queenless parts of multi-nest colonies. *Scientific Reports*, *10*(1), 1–8. https://doi.org/10.1038/s41598-020-58830-w

Giehr, J., Wallner, J., Krüger, T., & Heinze, J. (2020). Body size and sperm quality in queen- and worker-produced ant males. *Journal of Evolutionary Biology*, *January*, 1–8. https://doi.org/10.1111/jeb.13616

Glastad, K. M., Graham, R. J., Ju, L., Roessler, J., Brady, C. M., & Berger, S. L. (2020). Epigenetic Regulator CoREST Controls Social Behavior in Ants. *Molecular Cell*, *77*(2), 338-351.e6. https://doi.org/10.1016/j.molcel.2019.10.012

Gösswald, K., & Bier, K. (1953). Untersuchungen zur Kastendetermination in der Gattung Formica. *Die Naturwissenschaften*, *40*(2), 38–39. https://doi.org/10.1007/BF00596426

Gotoh, A., Billen, J., Hashim, R., & Ito, F. (2016). Degeneration patterns of the worker spermatheca during morphogenesis in ants (Hymenoptera: Formicidae). *Evolution and Development*, *18*(2), 96–104. https://doi.org/10.1111/ede.12182

Goudie, F., & Oldroyd, B. P. (2018). The distribution of thelytoky, arrhenotoky and androgenesis among castes in the eusocial Hymenoptera. *Insectes Sociaux*, *65*(1), 5–16. https://doi.org/10.1007/s00040-017-0597-0

Gstöttl, C., Stoldt, M., Jongepier, E., Bornberg-Bauer, E., Feldmeyer, B., Heinze, J., & Foitzik, S. (2020). Comparative analyses of caste, sex, and developmental stage-specific transcriptomes in two *Temnothorax* ants. *Ecology and Evolution*, *January*, 1–11. https://doi.org/10.1002/ece3.6187

Hacker, J. (2019). *RNAi in Cardiocondyla obscurior* (Bachlor's thesis). Regensburg.

Haller, J. (2020). *RNAi-mediated Gene Knockdown in Cardiocondyla obscurior* (Bachlor's thesis). Regensburg.

Hamilton, W. D. (1964a). The genetical evolution of social behavior. I. *Journal of Theoretical Biology*, *7*, 1–16. https://doi.org/10.4324/9780203790427-4

Hamilton, W. D. (1964b). The genetical evolution of social behavior. II. *Journal of Theoretical Biology*, *7*, 17–52. https://doi.org/10.4324/9780203790427-5

Heinze, J. (2017). Life-history evolution in ants: the case of *Cardiocondyla*. *Proceedings of the Royal Society B: Biological Sciences*, *284*(1), e20161406. https://doi.org/10.1098/rspb.2016.1406

Heinze, J., Cremer, S., Eckl, N., & Schrempf, A. (2006). Stealthy invaders: The biology of *Cardiocondyla* tramp ants. *Insectes Sociaux*, *53*(1), 1–7. https://doi.org/10.1007/s00040-005-0847-4

Heinze, J., & Holldobler, B. (1993). Fighting for a harem of queens: Physiology of reproduction in *Cardiocondyla* male ants. *Proceedings of the National Academy of Sciences of the United States of America*, *90*(18), 8412–8414. https://doi.org/10.1073/pnas.90.18.8412

Heinze, J., Kühnholz, S., Schilder, K., & Hölldobler, B. (1993). Behavior of ergatoid males in the ant, *Cardiocondyla nuda*. *Insectes Sociaux*, *40*(3), 273–282. https://doi.org/10.1007/BF01242363

Hu, X. F., Ke, L., & Zeng, Z. J. (2019). Histomorphological study on embryogenesis of the honeybee *Apis cerana*. *Journal of Asia-Pacific Entomology*, *22*(3), 860–867. https://doi.org/10.1016/j.aspen.2019.07.002

Ito, F., & Ohkawara, K. (1994). Spermatheca size differentiation between queens and workers in primitive ants - Relationship with reproductive structure of colonies. *Naturwissenschaften*, *81*(3), 138–140. https://doi.org/10.1007/BF01131772

Jaffé, R., Kronauer, D. J. C., Kraus, F. B., Boomsma, J. J., & Moritz, R. F. A. (2007). Worker caste determination in the army ant *Eciton burchellii*. *Biology Letters*, *3*(5), 513–516. https://doi.org/10.1098/rsbl.2007.0257

Jaimes Nino, L., Heinze, J., & Oettler, J. (2021). Late-life fitness gains explain the absence of a selection shadow in ants Authors: Jaimes Nino LM, Heinze, J., Oettler, J Affiliation: Zoologie/Evolutionsbiologie, Universität

Regensburg. *BioRxiv*.

Jia, L. Y., Chen, L., Keller, L., Wang, J., Xiao, J. H., & Huang, D. W. (2018). *Doublesex* evolution is correlated with social complexity in ants. *Genome Biology and Evolution*, *10*(12), 3230–3242. https://doi.org/10.1093/gbe/evy250

Johnson, B. R., & Jasper, W. C. (2016). Complex patterns of differential expression in candidate master regulatory genes for social behavior in honey bees. *Behavioral Ecology and Sociobiology*, *70*(7), 1033–1043. https://doi.org/10.1007/s00265-016-2071-9

Kayukawa, T., Minakuchi, C., Namiki, T., Togawa, T., Yoshiyama, M., Kamimura, M., Mita, K., Imanishi, S., Kiuchi, M., Ishikawa, Y., & Shinoda, T. (2012). Transcriptional regulation of juvenile hormone-mediated induction of Krüppel homolog 1, a repressor of insect metamorphosis. *Proceedings of the National Academy of Sciences of the United States of America*, *109*(29), 11729–11734. https://doi.org/10.1073/pnas.1204951109

Keisman, E. L., Christiansen, A. E., Baker, B. S., Arias, A. M., Ashburner, M., Baker, B. S., Ridge, K. A., Belote, J. M., Baker, B. S., Brand, A. H., Perrimon, N., Bryant, P. J., Burtis, K. C., Coschigano, K. T., Baker, B. S., Wensink, P. C., Casares, F., Sanchez, L., Guerrero, I., … Nöthiger, R. (2001). The sex determination gene *doublesex* regulates the A/P organizer to direct sex-specific patterns of growth in the *Drosophila* genital imaginal disc. *Developmental Cell*, *1*(2), 215–225. https://doi.org/10.1016/S1534-5807(01)00027-2

Khila, A., & Abouheif, E. (2008). Reproductive constraint is a developmental mechanism that maintains social harmony in advanced ant societies. *Proceedings of the National Academy of Sciences*, *105*(46), 17884–17889. https://doi.org/10.1073/pnas.0807351105

Khila, A., & Abouheif, E. (2010). Evaluating the role of reproductive constraints in ant social evolution. *Philosophical Transactions of the Royal Society of London. Series B, Biological Sciences*, *365*(1540), 617–630. https://doi.org/10.1098/rstb.2009.0257

Khila, Abderrahman, & Abouheif, E. (2009). In situ hybridization on ant ovaries and embryos. *Cold Spring Harbor Protocols*, *4*(7). https://doi.org/10.1101/pdb.prot5250

Kijimoto, T., Moczek, A. P., & Andrews, J. (2012). Diversification of *doublesex* function underlies morph-, sex-, and species-specific development of beetle horns. *Proceedings of the National Academy of Sciences*, *109*(50), 20526–20531. https://doi.org/10.1073/pnas.1118589109

Klein, A., Schrader, L., Gil, R., Manzano-Marín, A., Flórez, L., Wheeler, D., Werren, J. H., Latorre, A., Heinze, J., Kaltenpoth, M., Moya, A., & Oettler, J. (2015). A novel intracellular mutualistic bacterium in the invasive ant *Cardiocondyla obscurior*. *The ISME Journal Advance Online Publication*. https://doi.org/10.1038/ismej.2015.119

Klein, A., Schultner, E., Lowak, H., Schrader, L., Heinze, J., Holman, L., & Oettler, J. (2016). Evolution of Social Insect Polyphenism Facilitated by the Sex Differentiation Cascade. *PLoS Genetics*, *12*(3). https://doi.org/10.1371/journal.pgen.1005952

Kuhn, A., Darras, H., & Aron, S. (2018). Phenotypic plasticity in an ant with strong caste-genotype association. *Biology Letters*, *14*(1). https://doi.org/10.1098/rsbl.2017.0705

Lécuyer, E., Parthasarathy, N., & Krause, H. M. (2008). Fluorescent In Situ Hybridization Protocols in *Drosophila* Embryos and Tissues. *Methods Mol Biol.*, *420*, 289–302. https://doi.org/10.1007/978-1-59745-583-1_18

Lee, Y. S., Nakahara, K., Pham, J. W., Kim, K., He, Z., Sontheimer, E. J., & Carthew, R. W. (2004). Distinct roles for *Drosophila* Dicer-1 and Dicer-2 in the siRNA/miRNA silencing pathways. *Cell*, *117*(1), 69–81. https://doi.org/10.1016/S0092-8674(04)00261-2

Lehmann, R. (2016). Germ Plasm Biogenesis-An Oskar-Centric Perspective. In *Current Topics in Developmental Biology* (1st ed., Vol. 116). Elsevier Inc. https://doi.org/10.1016/bs.ctdb.2015.11.024

Lerit, D. A., & Gavis, E. R. (2011). Transport of germ plasm on astral microtubules directs germ cell development in *Drosophila*. *Current Biology*, *21*(6), 439–448. https://doi.org/10.1016/j.cub.2011.01.073

Liang, L., Diehl-Jones, W., & Lasko, P. (1994). Localization of vasa protein to the *Drosophila* pole plasm is independent of its RNA-binding and helicase activities. *Development (Cambridge, England)*, *120*(5), 1201–1211.

Lillico-Ouachour, A., & Abouheif, E. (2017). Regulation, development, and evolution of caste ratios in the hyperdiverse ant genus *Pheidole*. *Current Opinion in Insect Science*, *19*, 43–51. https://doi.org/10.1016/j.cois.2016.11.003

Livak, K. J., & Schmittgen, T. D. (2001). Analysis of relative gene expression data using real-time quantitative PCR and. *Methods*, *25*, 402–408. https://doi.org/10.1006/meth.2001.1262

Locke, M. (1984). The Structure and Development of the Vacuolar System in the Fat Body of Insects. In R. C. King & H. Akai (Eds.), *Insect Ultrastructure: Volume 2* (pp. 151–197). Springer US. https://doi.org/10.1007/978-1-4613-2715-8_5

Lynch, J. A., & Desplan, C. (2010). Novel modes of localization and function of nanos in the wasp *Nasonia*. *Development*, *137*(22), 3813–3821. https://doi.org/10.1242/dev.054213

Manning, L., & Doe, C. Q. (2017). Immunofluorescent antibody staining of intact *Drosophila* larvae. *Nature Protocols*, *12*(1), 1–14. https://doi.org/10.1038/nprot.2016.162

Maori, E., Garbian, Y., Kunik, V., Mozes-Koch, R., Malka, O., Kalev, H., Sabath, N., Sela, I., & Shafir, S. (2019). A Transmissible RNA Pathway in Honey Bees. *Cell Reports*, *27*(7), 1949-1959.e6. https://doi.org/10.1016/j.celrep.2019.04.073

Miyazaki, S., Murakami, T., Kubo, T., Azuma, N., Higashi, S., & Miura, T. (2010). Ergatoid queen development in the ant *Myrmecina nipponica*: Modular and heterochronic regulation of caste differentiation. *Proceedings of the Royal Society B: Biological Sciences*, *277*(1690), 1953–1961. https://doi.org/10.1098/rspb.2010.0142

Mukherjee, N., & Mukherjee, C. (2021). Germ cell ribonucleoprotein granules in different clades of life: From insects to mammals. *Wiley Interdisciplinary Reviews: RNA*, *January*. https://doi.org/10.1002/wrna.1642

Mullen, J. R., & DiNardo, S. (1995). Establishing parasegments in *Drosophila* embryos: Roles of the odd-skipped and naked genes. In *Developmental Biology* (Vol. 169, Issue 1, pp. 295–308). https://doi.org/10.1006/dbio.1995.1145

Mutti, N. S., Dolezal, A. G., Wolschin, F., Mutti, J. S., Gill, K. S., & Amdam, G. V. (2011). IRS and tor nutrient-signaling pathways act via juvenile hormone to influence honey bee caste fate. *Journal of Experimental Biology*, *214*(23), 3977–3984. https://doi.org/10.1242/jeb.061499

Nakao, H., Matsumoto, T., Oba, Y., Niimi, T., & Yaginuma, T. (2008). Germ cell specification and early embryonic patterning in *Bombyx mori* as revealed by *nanos* orthologues. *Evolution and Development*, *10*(5), 546–554. https://doi.org/10.1111/j.1525-142X.2008.00270.x

Nijhout, H. F. (2003). Development and evolution of adaptive polyphenisms. *Evolution and Development*, *5*(1), 9–18. https://doi.org/10.1046/j.1525-142X.2003.03003.x

Oettler, J., Platschek, T., Schmidt, C., Rajakumar, R., Favé, M. J., Khila, A., Heinze, J., & Abouheif, E. (2018). Interruption points in the wing gene regulatory network underlying wing polyphenism evolved independently in male and female morphs in *Cardiocondyla* ants. *Journal of Experimental Zoology Part B: Molecular and Developmental Evolution*, *July*, 1–10. https://doi.org/10.1002/jez.b.22834

Oettler, J., & Schrempf, A. (2016). Fitness and aging in *Cardiocondyla obscurior* ant queens. *Current Opinion in Insect Science*, *16*, 58–63. https://doi.org/10.1016/j.cois.2016.05.010

Oettler, J., Suefuji, M., & Heinze, J. (2010). The evolution of alternative reproductive tactics in male *Cardiocondyla* ants. *Evolution*, *64*(11), 3310–3317. https://doi.org/10.1111/j.1558-5646.2010.01090.x

Okada, Y., Miyazaki, S., Miyakawa, H., Ishikawa, A., Tsuji, K., & Miura, T. (2010). Ovarian development and insulin-signaling pathways during reproductive differentiation in the queenless ponerine ant *Diacamma* sp. *Journal of Insect Physiology*, *56*(3), 288–295. https://doi.org/10.1016/j.jinsphys.2009.10.013

Oxley, P., & Chandra, V. (2018). Social regulation of insulin signaling and the evolution of eusociality in ants. *Science* **361** (6400), 398–402. https://doi.org/10.5281/ZENODO.1311222

Pan, L. X., Cheng, F. P., & Wang, Z. L. (2021). Caste-biased expression of *fem* and *Amdsx* Genes in *Apis mellifera ligustica* (Hymenoptera: Apidae). *Sociobiology*, *68*(2). https://doi.org/10.13102/SOCIOBIOLOGY.V68I2.5654

Park, K. S., Godt, D., & Kalderon, D. (2018). Dissection and staining of *Drosophila* pupal ovaries. *Journal of Visualized Experiments*, *2018*(133), 1–5. https://doi.org/10.3791/56779

Petralia, R. S., & Vinson, B. (1980). Internal anatomy of the fourth instar larva of the imported fire ant, *Solenopsis invicta Buren* (Hymenoptera: Formicidae). *Journal of Insect Morphology and Embryology*, *9*, 89–106.

Pontieri, L., Rajakumar, A., Matteen Rafiqi, A., Stenbak Larsen, R., Abouheif, E., & Zhang, G. (2020). From egg to adult: a developmental table of the ant *Monomorium pharaonis*. *BioRxiv*, 2020.12.22.423970. https://doi.org/10.1101/2020.12.22.423970

Potrikus, C. J., & Breznak, J. A. (1981). Gut bacteria recycle uric acid nitrogen in termites: A strategy for nutrient conservation. *Proceedings of the National Academy of Sciences*, *78*(7), 4601–4605. https://doi.org/10.1073/pnas.78.7.4601

Rafiqi, A. M., Lemke, S., & Schmidt-Ott, U. (2011). Megaselia abdita: Fixing and devitellinizing embryos. *Cold Spring Harbor Protocols*, *6*(4). https://doi.org/10.1101/pdb.prot5602

Rafiqi, A. M., Rajakumar, A., & Abouheif, E. (2020). Origin and elaboration of a major evolutionary transition in individuality. *Nature*, *585*(7824), 239–244. https://doi.org/10.1038/s41586-020-2653-6

Rajakumar, R., Koch, S., Couture, M., Favé, M. J., Lillico-Ouachour, A., Chen, T., De Blasis, G., Rajakumar, A., Ouellette, D., & Abouheif, E. (2018). Social regulation of a rudimentary organ generates complex worker-caste systems in ants. *Nature*, *562*(7728), 574–577. https://doi.org/10.1038/s41586-018-0613-1

Renault, A. D. (2012). *vasa* is expressed in somatic cells of the embryonic gonad in a sex-specific manner in *Drosophila melanogaster*. *Biology Open*, *1*(10), 1043–1048. https://doi.org/10.1242/bio.20121909

Richardson, B. E., & Lehmann, R. (2010). Mechanisms guiding primordial germ cell migration: Strategies from different organisms. *Nature Reviews Molecular Cell Biology*, *11*(1), 37–49. https://doi.org/10.1038/nrm2815

Robinett, C. C., Vaughan, A. G., Knapp, J. M., & Baker, B. S. (2010). Sex and the single cell. II. there is a time and place for sex. *PLoS Biology*, *8*(5). https://doi.org/10.1371/journal.pbio.1000365

Ronai, I., Vergoz, V., & Oldroyd, B. P. (2016). The Mechanistic, Genetic, and Evolutionary Basis of Worker Sterility in the Social Hymenoptera. *Advances in the Study of Behavior*, *48*, 251–317. https://doi.org/10.1016/bs.asb.2016.03.002

Sahut-Barnola, I., Godt, D., Laski, F. A., & Couderc, J. L. (1995). *Drosophila* ovary morphogenesis: Analysis of terminal filament formation and identification of a gene required for this process. In *Developmental Biology* (Vol. 170, Issue 1, pp. 127–135). https://doi.org/10.1006/dbio.1995.1201

Santos, A. C., & Lehmann, R. (2004). Germ cell specification and migration in *Drosophila* and beyond. *Current Biology*, *14*(14), 578–589. https://doi.org/10.1016/j.cub.2004.07.018

Sarikaya, D. P., Belay, A. A., Ahuja, A., Dorta, A., Green, D. A., & Extavour, C. G. (2012). The roles of cell size and cell number in determining ovariole number in *Drosophila*. *Developmental Biology*, *363*(1), 279–289. https://doi.org/10.1016/j.ydbio.2011.12.017

Schindelin, J., Arganda-Carreras, I., Frise, E., Kaynig, V., Longair, M., Pietzsch, T., Preibisch, S., Rueden, C., Saalfeld, S., Schmid, B., Tinevez, J.-Y., White, D. J., Hartenstein, V., Eliceiri, K., Tomancak, P., & Cardona, A. (2012). Fiji: an open-source platform for biological-image analysis. *Nature Methods*, *9*(7), 676–682. https://doi.org/10.1038/nmeth.2019

Schrader, L., Helantera, H., & Oettler, J. (2017). Accelerated evolution of developmentally biased genes in the tetraphenic ant *Cardiocondyla obscurior*. *Molecular Biology and Evolution*, *34*(3), 535–544. https://doi.org/10.1093/molbev/msw240

Schrader, L., Kim, J. W., Ence, D., Zimin, A., Klein, A., Wyschetzki, K., Weichselgartner, T., Kemena, C., Stökl, J., Schultner, E., Wurm, Y., Smith, C. D., Yandell, M., Heinze, J., Gadau, J., & Oettler, J. (2014). Transposable element islands facilitate adaptation to novel environments in an invasive species. *Nature Communications*, *5*, 5495. https://doi.org/10.1038/ncomms6495

Schrader, L., Simola, D. F., Heinze, J., & Oettler, J. (2015). Sphingolipids, transcription factors, and conserved toolkit genes: Developmental plasticity in the ant *Cardiocondyla obscurior*. *Molecular Biology and Evolution*, *32*(6), 1474–1486. https://doi.org/10.1093/molbev/msv039

Schrempf, A., & Heinze, J. (2006). Proximate mechanisms of male morph determination in the ant *Cardiocondyla obscurior*. *Evolution and Development*, *8*(3), 266–272. https://doi.org/10.1111/j.1525-142X.2006.00097.x

Schultner, E., Oettler, J., & Helanterä, H. (2017). The role of brood in eusocial hymenoptera. *The Quarterly Review of Biology*, *92*(1), 39–78. https://doi.org/10.1086/690840

Schultner, E., & Pulliainen, U. (2020). Brood recognition and discrimination in ants. *Insectes Sociaux*, *0123456789*. https://doi.org/10.1007/s00040-019-00747-3

Schultz, T. R. (2000). In search of ant ancestors. *Proceedings of the National Academy of Sciences of the United States of America*, *97*(26), 14028–14029. https://doi.org/10.1073/pnas.011513798

Slaidina, M., Banisch, T. U., Gupta, S., & Lehmann, R. (2020). A single-cell atlas of the developing *Drosophila* ovary identifies follicle stem cell progenitors. *Genes and Development*, *34*(3), 239–249. https://doi.org/10.1101/gad.330464.119

Snodgrass, R. E. (1935). *Principles of insect physiology*. McGraw-Hill Publishing Co., New York.

Strobl, F., Schmitz, A., & Stelzer, E. H. K. (2015). Live imaging of *Tribolium castaneum* embryonic development using light-sheet-based fluorescence microscopy. *Nature Protocols*, *10*(10), 1486–1507. https://doi.org/10.1038/nprot.2015.093

Suefuji, M., Cremer, S., Oettler, J., & Heinze, J. (2008). Queen number influences the timing of the sexual production in colonies of *Cardiocondyla* ants. *Biology Letters*, *4*(6), 670–673. https://doi.org/10.1098/rsbl.2008.0355

Sumner, S., Bell, E., & Taylor, D. (2018). A molecular concept of caste in insect societies. *Current Opinion in Insect Science*, *25*, 42–50. https://doi.org/10.1016/j.cois.2017.11.010

Tanaka, E. D., & Hartfelder, K. (2009). Sequence and expression pattern of the germ line marker vasa in honey bees and stingless bees. *Genetics and Molecular Biology*, *32*(3), 582–593. https://doi.org/10.1590/S1415-47572009005000043

Team, R. C. (2020). R: A language and environment for statistical computing. *R Foundation for Statistical Computing*. https://www.r-project.org/

Ting, X. (2013). Control of germline stem cell self-renewal and differentiation in the *Drosophila* ovary: Concerted actions of niche signals and intrinsic factors. *Wiley Interdisciplinary Reviews: Developmental Biology*, *2*(2), 261–273. https://doi.org/10.1002/wdev.60

Tomoyasu, Y., & Denell, R. E. (2004). Larval RNAi in *Tribolium* (Coleoptera) for analyzing adult development. *Development Genes and Evolution*, *214*(11), 575–578. https://doi.org/10.1007/s00427-004-0434-0

Trible, W., & Kronauer, D. J. C. (2017). Caste development and evolution in ants: it's all about size. *The Journal of Experimental Biology*, *220*(1), 53–62. https://doi.org/10.1242/jeb.145292

Tschinkel, W. R. (1987). Relationship between Ovariole Number and Spermathecal Sperm Count in Ant Queens: a New Allometry. *Annals of the Entomological Society of America*, *80*(2), 208–211.

https://doi.org/10.1093/aesa/80.2.208

Ün, Ç., Schultner, E., Manzano-Marín, A., Flórez, L. V., Seifert, B., Heinze, J., & Oettler, J. (2021). Cytoplasmic incompatibility between Old and New World populations of a tramp ant. *Evolution*, 1–17. https://doi.org/10.1111/evo.14261

Walsh, J. T., Warner, M. R., Kase, A., Cushing, B. J., & Linksvayer, T. A. (2018). Ant nurse workers exhibit behavioural and transcriptomic signatures of specialization on larval stage. *Animal Behaviour*, *141*, 161–169. https://doi.org/10.1016/j.anbehav.2018.05.015

Wang, W., & Yoder, J. H. (2012). Hox-mediated regulation of *doublesex* sculpts sex-specific abdomen morphology in *Drosophila*. *Developmental Dynamics*, *241*(6), 1076–1090. https://doi.org/10.1002/dvdy.23791

West-Eberhard, M. (1987). Flexible strategy and social evolution. *Animal Societies : Theories and Facts*, 35–51.

Wheeler, W. M. (1911). *The Ant-Colony As An Organism*. *3*, 307–325. https://doi.org/10.11603/1681-2778.2012.3.1988

Wilson, E. O. (1980). Caste and Division of Labor in Leaf-Cutter Ants - I. The overall pattern on *Atta sexdens*. *Behavioral Ecology and Sociobiology*, *7*(2), 143–156.

Yan, S. (2015). *Regulation of sexual dimorphism in the Drosophila melanogaster abdomen* (Issue Doctoral dissertation) [University of Alabama]. https://doi.org/10.1152/physrev.1998.78.1.1

Zara, F. J., & Caetano, F. H. (2004). Ultramorphology and histochemistry of fat body cells from last Instar larval of the *Pachycondyla* (=Neoponera) *villosa* (Fabricius) (Formicidae: Ponerinae). *Brazilian Journal of Biology*, *64*(3b), 725–735. https://doi.org/10.1590/S1519-69842004000400022

12 ACKNOWLEDGMENTS

First of all, I want to thank everyone who helped me complete my thesis. It's been a marathon and though one runs alone, every successful runner requires a support team. Without it I would have never made it through the finish line.

My gratitude goes to my supervisor Jan Oettler. Jan, we shared some exciting years! It's been a long journey, beginning with my master's internship in the CORE lab, continued as a WHK and then ending with my master's thesis. And after my rather moderate experience in Switzerland (who could have known?), I sat myself in the train and travelled all the way back to Regensburg where you had an open door for me, listened to me, comforted me, and instantly offered me a position in your lab (deep down I always knew that neurogenetics wasn't something for me, and let's be honest: ants are way cooler!!!). And for that I am deeply grateful!
We were so shocked when you fell ill, and we didn't know what was going on. And that right in the middle of a pandemic! It were some traumatic weeks. The uncertainty and helplessness left us in a state of shock. But you came back! And you fought your way back and have been fighting ever since. You never gave up and kept up the good spirit, even when things seemed hopeless. Your pure will of strength brought you where you are today, and this is really inspiring! Keep up the fight!
I was thrilled to have a supervisor like you who let me come up with my own ideas and left me the freedom to pursue them. I personally think this is what research should be all about. And look what has come out of it! We gained so much more knowledge about this little bugger we like so much. I hope that in the future we can share a glass of good Jamaican rum (I still got that bottle Eva and you brought back from Jamaica for my 30s birthday) and reminisce about the past years. From all my heart I wish you all the best for now and whatever your future holds.

A major thank you goes to Eva Schultner. You stepped up when Jan was incapacitated and led our group even though it must have been really tough on you. Thank you! And thank you for the shared time, be it long conversations over a Caipirinha (it must have been more than one though) at the beach of Guarujá or climbing sessions in Regensburg.

I would like to thank Jürgen Heinze for having me at his department for almost a decade now (with some minor break in between). I remember starting as a practical student during my bachelor and I was so fascinated by the ants that I wanted to continue working on them. And thank you for having my back when my contract ran out and the extension of the DFG wasn't approved yet. Thank you for

some memorable climbing trips. There's no better way to relax and take your mind of things whilst climbing a rock!

I would also like to thank my mentor Prof. Björn Brembs for always having an open door, giving me feedback, and showing interest in my work.

My gratitude goes to my second mentor Prof. Abderrahman Khila for taking his time explaining complicated procedures and being very enthusiastic about my work.

When you spent so much time at one place you get to know a lot of people and befriend them (if you're lucky). That's definitely the case with our department. I sometimes feel like I'm an old hand and part of the old guard ("Do you remember? Back in the day when we used to be in the old building?"), which in some ways I probably am. I have great memories of it and always felt welcome. That's why my sincere gratitude goes to all who make this department so special. To the TAs for keeping the place running and I could always have a nice chit chat with. To all my fellow PhD students for creating a nice and warm atmosphere. To Çiğdem and Mathilde for a memorable field trip to southern France. It always will be a cherished memory of mine! A great thank you goes to Çiğdem's mother for providing us with Turkish delights for our road trip. We definitely did not suffer hunger! And a warm thank you goes to Mathilde's family who were so welcoming, treated us like family and showed us all the delicacies southern France has to offer.
And even though it's all our nightmare to have to do a PhD during a pandemic, you all managed to do well and kept up the good spirit! I will surely miss you all and regret a little bit that we're not able to spend more time with each other in a COVID free environment. To all my colleagues with whom I spent so much time with in the past years, either having a drink, going on climbing trips (yes, our department is full with climbing enthusiasts) or just hanging out at work having a coffee or tea.

A warm thank you to my many, many students contributing to this thesis. You are the backbone of our research!

A special thanks goes to Sonja Dorfner for always being reachable and quick with answers. And for nice long conversations in her office that were not related to work.

My thanks go to the RIGeL PR-group for organizing the school trips, Boys/Girls Days and more recently the MINT-Haus. It was a great deal of fun and I enjoyed every minute of it. I really hope that it's work continues and inspires future generations of scientists.

A major thank you goes to the RIGeL management office with Kinga and Caroline. It was a great pleasure working with you two! Without you two RIGeL wouldn't be the same.

To my friends who had the patience to listen to my rants about work, life, or just simple things. Who were always there for me and motivated me when I felt down. And even though the Regensburg connection scattered all around Germany, Austria, Switzerland and the US, our home base always will be Ratisbona! The next ski trip is long overdue!
My friends in Kissing with Sarah, Tobi and Oskar deserve a big thank you for always being so welcoming. I am looking forward to being closer to you guys in the future!

The last paragraph is dedicated to my family.

Foremost I would like to thank my parents for supporting me in the past and are still today. I big thank you goes to my mother who was willing to read my thesis and correct it wherever necessary. My sister Kiki who helped me relax by sending pictures of our newest family members Tinker & Misty or just by visiting for a weekend and letting our Mongolian gerbil Chili and Pepper run around in a self-built parkour. Or by just eating donuts.

An meine Schwiegermutter Edith geht ein großes Dankeschön. Du hast mich in den vergangenen Jahren so viel unterstützt und liebevolle, nette und aufbauende Worte gefunden, dass ich meine Dankbarkeit gar nicht in Worte fassen kann. Bei dir bin ich immer willkommen, sei es um den Alltag zu vergessen oder einfach etwas Zeit auf deinem Balkon zu verbringen um der Hitze des Sommers zu entfliehen. Deine Besuche bei uns in Regensburg waren ebenfalls immer eine schöne Abwechslung zum Alltag und ich habe sie immer sehr genossen. Ich freue mich darauf mit dir und den Miezies Lola und Merlin Tür an Tür zu wohnen!

An großes Dankeschön geht an meinen Schwiegervater Jimmy und seiner Frau Angelika für die Unterstützung mit Nervennahrung und rotem Traubensaft. Das hat für die letzten Meter die nötige Energie gegeben!

The most important person I am mentioning last: my beautiful and wonderful wife Jenny. The past couple of years have been really though on you. On us both. And a huge part was definitely this thesis. It was like an all-consuming monster which sucked major parts out of us. I am so deeply grateful that

you stuck beside my side, gave me the butt-kick I needed when I drifted off and love me for who I am (even if I sometimes bring you to the brink of insanity, “Ja. Mhm. Ist das so?”).

Our marriage had a rough start. As newlyweds we were denied of our honeymoon due to the lockdown. And a year later we spent our first wedding anniversary still stuck in a pandemic. You always hear that the first year of marriage is hard but doing so under these circumstances was definitely a different level of hard. But we managed to pull through and our relationship is probably stronger than ever! It also proved that our relationship can and will withstand anything! The next 60 years (yes, I’m optimistic!) are going to be wonderful, love-filled, maybe not always easy, but exciting years!

After my experience in Switzerland and the time thereafter I would have never thought to find happiness again. But then I met you. Like in a classical love film I saw you and was dumbstruck by your appearance (and that was not only due to your blond hair at the time). I immediately knew that you were special. And there was undoubtedly electricity in the air, we both felt that in Kloster Schöntal. We had some initial difficulties but thanks to your dedication we are where we are now today. I won’t have it any other way. You are the love of my life, and I can’t wait what our future holds. But know this: as long as we are together, I have no fear (and I am a scaredy cat!). Because I love you.

After all this time?

Always.